Title
Brain-Mimetic Hydrogel Platform for Investigation of Glioblastoma Drug Resistance

Author
Xiao, Weikun

Publication Date
2019

Peer reviewed|Thesis/dissertation

UNIVERSITY OF CALIFORNIA

Los Angeles

Brain-Mimetic Hydrogel Platform for Investigation of Glioblastoma Drug Resistance

A dissertation submitted in partial satisfaction of the requirements for the degree of Doctor of Philosophy in Bioengineering

by

Weikun Xiao

2019

ABSTRACT OF THE DISSERTATION

Brain-Mimetic Hydrogel Platform

for Investigation of Glioblastoma Drug Resistance

by

Weikun Xiao
Doctor of Philosophy in Bioengineering
University of California, Los Angeles, 2019
Professor Stephanie Kristin Seidlits, Chair

Glioblastoma (GBM) is the most lethal and malignant cancer originating from the central nervous system. Even with intense treatment involving surgery and radio-chemotherapy, median survival after prognosis remains within 12 months, as GBM constantly develops resistance to common therapies. Many novel therapies developed for GBM have shown promising results in *in-vitro* studies, but unfortunately failed in actual clinical practices, partially because traditional model systems failed to recapitulate the microenvironment surrounding GBM tumors. Therefore, we posit that unique brain extracellular matrix (ECM) facilitates therapeutic resistance in GBM. To study this problem, we investigated ECM deposition in GBM patient samples and fabricated brain-mimetic, orthogonally tunable hydrogel system in which to culture patient-derived GBM cells in 3-dimensional manner. To validate our novel *ex-vivo* culture system, genomic sequencing and gene expression profiling were performed for comparison with traditional *in-vitro* culture and animal xenograft models. At the same

time, cell viability, proliferation and markers for cancer stem cell were assessed. Our model system was used to study the therapeutic response of GBM cells to commonly used therapeutics and to investigate resistance mechanisms. We found GBM cells displayed drug response kinetics comparable to *in-vivo* xenograft models. We also found novel molecular mechanisms describing how unique brain matrix facilitates therapeutic resistance through corresponding receptors in our 3D culture models. By utilizing novel engineered platforms to study drug resistance, we are able to uncover mechanisms that could not be observed through traditional methods.

The dissertation of Weikun Xiao is approved.

David A. Nathanson

Daniel T. Kamei

Michael Alan Teitell

Stephanie Kristin Seidlits, Committee Chair

University of California, Los Angeles

2019

Table of Content

List of Figures

Acknowledgement

Parts of this work are adapted or reprinted from 4 published or accepted papers.

Chapter 1 is adapted and reprinted from “Xiao, Weikun, Alireza Sohrabi, and Stephanie K Seidlits. 2017. “Integrating the Glioblastoma Microenvironment into Engineered Experimental Models.” *Future Science OA* 3 (3). Future Science Ltd London, UK: FSO189. doi:10.4155/fsoa-2016-0094.”

Chapters 2, 3 and 4 are adapted and reprinted from “Xiao, Weikun, Arshia Ehsanipour, Alireza Sohrabi, and Stephanie K Seidlits. 2018. “Hyaluronic-Acid Based Hydrogels for 3-Dimensional Culture of Patient-Derived Glioblastoma Cells.” *Journal of Visualized Experiments*, no. 138 (August): e58176. doi:10.3791/58176.” and “Xiao, Weikun, Rongyu Zhang, Alireza Sohrabi, Arshia Ehsanipour, Songping Sun, Jesse Liang, Christopher Walthers, Lisa Ta, David A Nathanson, and Stephanie K Seidlits. 2018. “Brain-Mimetic 3D Culture Platforms Allow Investigation of Cooperative Effects of Extracellular Matrix Features on Therapeutic Resistance in Glioblastoma.” *Cancer Research* 78 (5): 1358–70. doi:10.1158/0008-5472.CAN-17-2429.”

Chapter 5 is based on work “Weikun Xiao, Shanshan Wang, Rongyu Zhang, Alireza Sohrabi, Qi Yu, Sihan Liu, Arshia Ehsanipour, Jesse Liang, Rebecca D. Bierman, David A. Nathanson, Stephanie K. Seidlits. 2019. “Bioengineered scaffolds for 3D culture demonstrate extracellular matrix-mediated mechanisms of chemotherapy resistance in glioblastoma”. The manuscript is currently accepted for *Matrix Biology*.

Biographical Sketch

Professional Preparation

University of Illinois, Urbana-Champaign	Biochemistry	B.S., 2013
University of California, Los Angeles	Bioengineering	Ph.D., In Prog.

Appointments

2013-Now, Graduate Student Researcher, University of California

Publications

Xiao, W., Zhang, R., Sohrabi, A., Ehsanipour, A., Sun, S., Liang, J., Walthers, C., Ta, L., Nathanson, D.A. and Seidlits, S.K., 2018. Brain-mimetic 3D culture platforms allow investigation of cooperative effects of extracellular matrix features on therapeutic resistance in glioblastoma. *Cancer Research*, 78(5).

Xiao, W., Sohrabi, A. and Seidlits, S.K., 2017. Integrating the glioblastoma microenvironment into engineered experimental models. *Future science OA*, *3*(3), p.FSO189.

Xiao, W., Ehsanipour, A., Sohrabi, A., Seidlits, S. K..Hyaluronic-Acid Based Hydrogels for 3-Dimensional Culture of Patient-Derived Glioblastoma Cells. *Journal of Visual Experiment* e58176, In-press.

Lo, Y.H., Zhao, L., Gallagher-Jones, M., Rana, A., Lodico, J., **Xiao, W.**, Regan, B.C. and Miao, J., 2018. In situ coherent diffractive imaging. *Nature communications*, *9*(1), p.1826.

Tippana, R., **Xiao, W.** and Myong, S., 2014. G-quadruplex conformation and dynamics are determined by loop length and sequence. *Nucleic acids research*, *42*(12), pp.8106-8114.

Synergistic Activities

Teaching Associate, University of California, 2018

Course Developmental Teaching Assistant, University of California, 2017

Teaching Assistant, University of California, 2015 (course title: BE167L, Bioengineering Laboratory)

Awards and Recognitions

2014-2015 UCLA Nonresident Graduate Academic Doctoral Award

2016 NIH (NINDS) Travel Fellowship for 3D CNS Disease Modeling workshop

2018 UCLA DYF fellowship

Chapter 1

Introduction and Background

Glioblastoma

Glioblastoma (GBM) is the most lethal and malignant cancer originating from central nervous system (CNS)[1]. GBM is also referred as World Health Organization (WHO) grade IV glioma, the most aggressive form[1,2]. Unfortunately, median survival after diagnosis without therapy has remained within 6 months[3]. GBM constantly develops resistance to commonly used therapies, and the tumor's diffusive nature makes localized surgical procedures a mere method to delay the disease progress, as the tumors infiltration throughout the brain cannot be removed completely[1].

From gross level, GBM shows areas of necrosis and hemorrhage[1,2]. Microscopically, GBM migrates through brain parenchyma, spreads below the pial margin, surrounds neurons and vessels, and invades through white matter tracts and along vessels and other Scherer's structures[1]. Morphological pathology diagnosis of GBM involves diffuse infiltration, nuclear atypia, increased proliferation, necrotic cores, and microvascular proliferation[1,2]. All these complex characters formed the phenotypic and microscopic aspects of "multiforme" in GBM.

Origin of glioblastoma was traditionally believed to be from astrocyte, as GBM was classified as grade IV astrocytoma[1,2]. More recently, origin of GBM was just proposed potentially from glial progenitor cells[4]. Currently, others have proposed theories

indicating oligo progenitor cells (OPC) and neural stem cells (NPC, expressing nestin and SOX2) could be origin cells as well[4–6].

Typical treatments for newly diagnosed GBM involve intensive surgical resection, radiotherapy and chemotherapy using temozolomide. Unfortunately, even with the intensive therapies described above, median survival of GBM patients remained within 12-15 months[1,2,5].

Genetic subtypes and heterogeneity in GBM

Using The Cancer Genome Atlas (TCGA) network, researchers have found GBM frequently bear amplified genes such as epidermal growth factor receptor (EGFR), homozygous deleted genes such as CDKN2A/B, and mutated genes such as tumor suppressor p53 (TP53)[7]. Majorly altered signaling pathways in GBM have been identified as receptor tyrosine kinase (RTK)-Ras-phosphoinositide 3-kinase (PI3K) pathway, retinoblastoma suppressor (RB) pathway, and TP53 pathway[7]. The alterations of these pathways significantly drive tumor progression, proliferation and survival[7]. Around 18 years ago, researchers used combined activation of Ras and Akt in NPCs to successfully induced GBM formation in mice[4]. TCGA Network has also been used to classify GBM into proneural, classical, or mesenchymal subtypes based on their abnormalities in platelet-derived growth factor alpha (PDGFA), epidermal growth factor receptor (EGFR), and neurofibromatosis 1 (NF1) genes respectively, in which the mesenchymal subtype gives worst prognosis outcome, and interestingly, overall survival of patients bearing proneural subtype is not affected regardless of intensity of treatment[5].

Intratumoral heterogeneity contributes to genetic aspects of GBM. Existence of stem cells in GBM, or glioma stem cells (GSCs) was identified around 2004 when portions of GBM cells were isolated as CD133 positive, and those cells with tumor initiating capabilities were able to initiate a xenograft implantation in SCID-NOD mouse[8]. Besides CD133, other GSC markers like CD44, Nestin, Olig2 and SOX2 were identified in subsequent studies as CD133 markers might not be necessary markers for GSCs[6]. GSCs have capacity for of self-renewal and differentiation into different cell types to generate different cell populations[9]. Therefore, GSCs are key drivers that generate heterogeneity in GBM and believed to play key roles in therapeutic resistance in GBM, which will be described in later chapters. Recently, single-cell RNA sequencing technology revealed that a single solid GBM tumor contains different cell populations representing all categories of GBM subtypes[10]. More recently, anatomical heterogeneity of GBM was also identified through complicated genetic characterization of GBM tumors isolated from same patients but from different locations within the brains[11].

Microenvironment of Glioblastoma

Originating in the brain, GBM tumors closely interact with the unique microenvironment isolated behind the blood-brain barrier (BBB) that is distinct from that in peripheral tissues[12]. Interestingly, GBM rarely metastasizes outside of the brain, indicating a preference for the brain microenvironment[13]. The extracellular matrix (ECM) of the brain comprises around 20% of the brain[14]. The ECM of brain contains few fibrous proteins but high amounts of proteoglycans (PGs), glycosaminoglycans (GAGs), and glycoproteins[12,14]. Besides ECM, cell-cell interactions, tissue mechanics, and soluble factors (cytokines, growth factors, gases) also play various roles in microenvironment in

GBM. All these microenvironmental cues present a complex landscape which is altered in the presence of GBM tumors to support tumor invasion and treatment resistance[15](**Figure 1.1, Figure 1.2**).

Figure 1.1

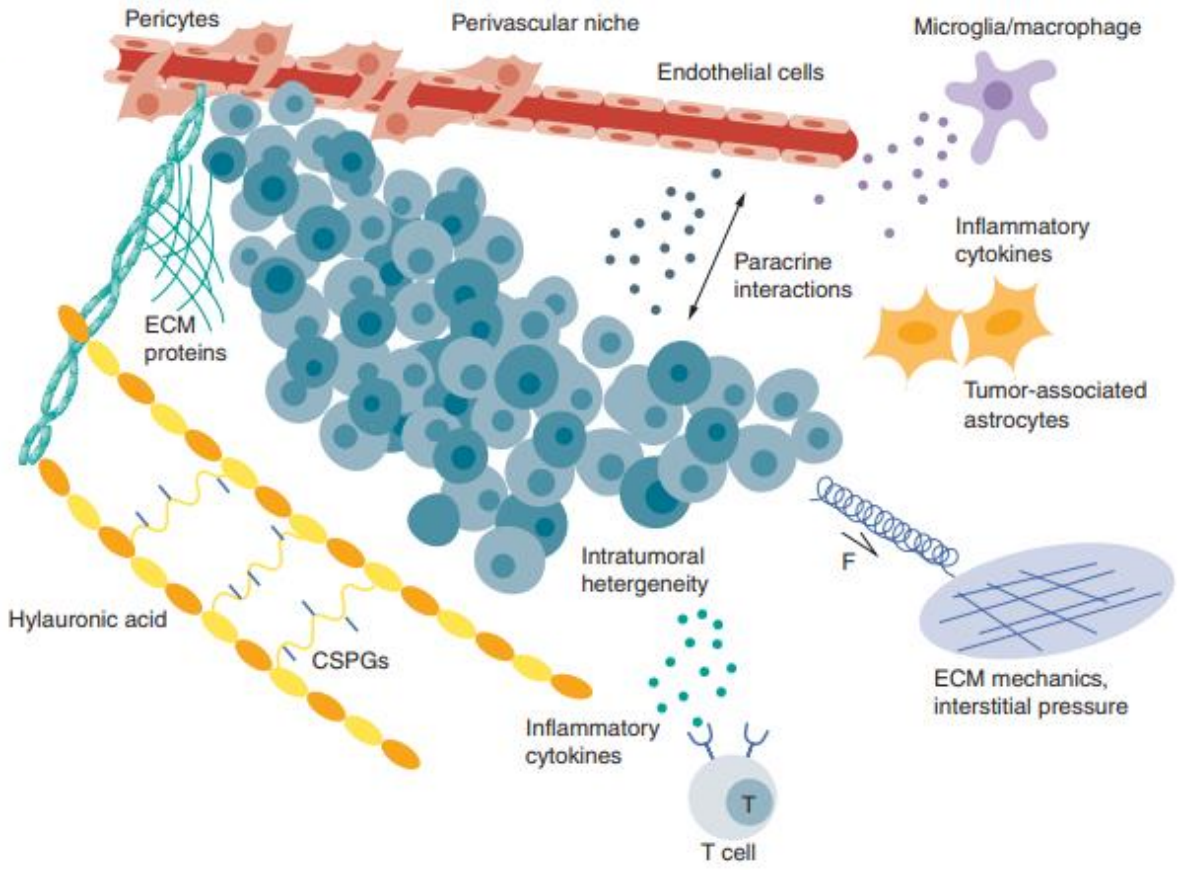

Figure 1.1. GBM microenvironment at the tissue scale. HA, glycosaminoglycans, proteoglycans and proteins in the ECM relay mechanical and biochemical cues to tumor cells. An increase in interstitial pressure in the tumors also contributes to the mechanical microenvironment. GBM tumors are made up of a heterogeneous mixture of cells with different phenotypes, including stem-like cells. Other tumor-supportive cells in the microenvironment include those in the perivascular niche (endothelial cells and pericytes), astrocytes and immune cells (microglia/macrophages and T cells). The figure is adapted from Xiao et al[16].

Figure 1.2

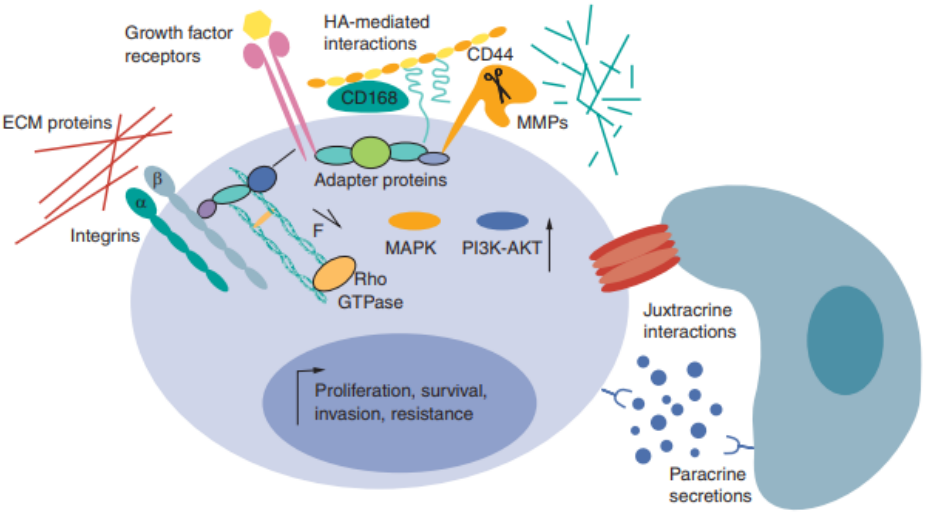

Figure 1.2. Microenvironmental features at the level of single GBM cells. Adhesion to ECM proteins through integrins relay biochemical and mechanical cues through the actin cytoskeleton and intracellular signaling pathways, including Rho-GTPase. CD44 and CD168, mediate interactions with HA in the surrounding ECM. Growth factor binding activates receptors, including tyrosine kinases that upregulate oncogenic MAPK and PI3K/AKT pathways. Growth factor receptors, HA receptors and integrins interact through membrane-associated adapter proteins to amplify oncogenic pathways through feedback loops. Membrane-bound MMPs anchor to CD44 to facilitate ECM degradation and cell invasion. Cell–cell interactions occur directly through gap or cadherin mediated adherens junctions (juxtracrine interactions) and indirectly through secreted soluble factors (paracrine interactions). Together, GBM cells integrate these microenvironmental cues, resulting in upregulation of genes promoting survival, proliferation and treatment resistance. The figure is adapted from Xiao et al[16].

Hyaluronic acid (HA) is negatively charged, nonsulfated, and unbranched GAG. HA contains repeating unit of D-glucuronic acid and N-acetyl-D-glucosamine monomers, which is highly abundant in the brain[12,14]. In normal brain, high-molecular-weight (HMW) HA larger than 10^6 Da, can act as the organizational center of the ECM. HA can interact with proteins and PGs through small adapter/linker proteins such as HA binding proteins (HABPs)[17]. This network of interaction can create a hydrogel-like mesh[17]. HA is frequently upregulated in GBM tumors, and elevated HA around GBM tumor is reported to facilitate progression, invasion, proliferation and resistance to therapeutics in GBM[12,14,18–22]. Catabolic and anabolic enzymes of HA like HA synthase and hyaluronidase, respectively, and other cell surface HA receptors are also observed to be overexpressed in GBM and to contribute to hyper aggression in GBM[23–25]. Notably, HA interacts with GBM cells through CD44 and CD168 in which signaling pathways of PI3K-Akt and MAPK-ERK are upregulated, resulting in increased apoptosis resistance and migratory capacity[18,26,27]. So far, the complex mechanisms driving HA-mediated drug resistance are not fully understood, but various studies have proved that HA-CD44 interactions are essential to protect the GBM cells from drug induced apoptosis[18,20,22,28].

Besides HA, ECM proteins are abundant around GBM. Cell attachment to ECM proteins is most commonly mediated by integrin receptors, which undergo heterodimerization of α and β subunit upon binding to Arginine-Glycine-Aspartate (RGD) motif on ECM molecules[27,29,30]. Many integrins, like β_1, β_3, β_5, and α_V, are over-expressed by GBM cells[31–33]. Increased deposition of many ECM proteins, including vitronectin, fibronectin, tenascin-C, and type IV collagen (a basement membrane component concentrated near blood vessels), has been documented, and this elevated presence directly correlates

with poor prognosis and invasion[31,33]. For example, GBM cell migration along microvasculature is potentially facilitated through interactions between integrin $\alpha_3\beta_1$ type IV collagen or laminin[34,35].

Elevated glycoproteins, chondroitin sulfate (CS), and heparan sulfate (HS) proteoglycans (PGs) were also observed around GBM tumors[14,36]. These glycosylated proteins facilitate a wide range of functions from cell migration to tumor growth[36]. For example, HS is able to sequester growth factors including EGF, PDGF-A, and transforming growth factor β (TGF-β) to facilitate the activation of the oncogenic tyrosine kinase receptors[36–38]. Versican, an HSPG, interacts with TGF- β to promote tumor migration[36]. Usually, PGs function through cooperative interaction with other ECM proteins. For example, GBM cleaves the CSPG brevican and the cleaved segments associate with fibronectin to further promote GBM invasion[39]. So far, only few studies focused on functional effects of PGs in GBM progress[36]. In fact, it's likely that complex interactions among PGs, GAGs, and many other ECM proteins together dictate GBM physiology.

Bioactive soluble factors are abundant in GBM microenvironment. Over-expressions of TGF-β, TGF-α, EGF, VEGF, and tumor necrosis factor α (TNF-α) can promote survival and proliferation of GBM cells[40,41]. Therefore, therapies against TGF, EGF, and VEGF have all been evaluated in clinical trials. Among those soluble factors, EGF and PDGF interactions with GBM draw interest to the field. More than 50% and 11% of GBM tumor bear amplification/mutation of the EGFR and PDGFR, respectively[42]. Interactions between PDGF-A and its corresponding receptors trigger an autocrine loop that promotes GBM proliferation and survival[42]. EGFR activation through EGF can

upregulate oncogenic pathways like Pi3K-Akt and MAPK to significantly promote tumor progression[40,43,44]. Pharmacological inhibition of EGFR through small molecules often resulted in failure, as a switch of tyrosine kinase dependency from EGFR to PDGFR was observed in in laboratory research[42]. Similar cooperative effects have been observed as EGF and TGF participate in an autocrine loop, resulting in amplified EGFR signaling and promoted GBM invasion[40,43,44]. At the same time, EGFR and PDGFR can also interact with ECM receptors to promote tumor progression. For example, CD44 was observed to associate with EGFR to augment MAPK-ERK and PI3k-Akt activation[27,45]. Besides growth factors, disordered profiles of inflammatory cytokines in GBM microenvironment contributes to tumor progression. TGF-β can indirectly promote GBM growth by stimulating the production of PDGF, intensify angiogenesis by upregulating VEGF, and increase GBM invasion by enhancing matrix-metalloprotease (MMP) expression[41,46–49]. In the aspect immunomodulation, TGF-β inhibits cytotoxic T cell-mediated tumor clearance and promote infiltrative anti-inflammatory, M2-type macrophage infiltration to the tumor area, which can further promote tumor growth[49,50]. On the other hand, TNF-α can activate a toll-like receptor 4 (TLR4) dependent pathways to elevate Akt and HIF-1α expression in GBM[51]. Moreover, TNF-α mediates enhancement of tumor angiogenesis through increasing the production of VEGF and FGF-2[52].

Besides HMW HA mentioned previously, low-molecular-weight (LMW) HA acts as important soluble factors in GBM microenvironment[21]. LMW HA can activate TLRs on immune cells to induce proinflammatory events[53]. As an example, LMW HA interacts with TLR4 in macrophages to elevate TNF-α[21,54]. In GBM, LMW-HA can be generated

by catalytical cleavage through hyaluronidase expressed by the tumor cells[55]. Although some researches showed a clear correlation of HA degradation and tumor metastasis at lymph node in breast cancer, the link in GBM remains unclear[56].

Besides degradation of HA, degradation of other adhesive ECMs can be mediated by ECM-degrading enzymes expressed by GBM. ECM degradation paves the way for GBM invasion and angiogenesis[57,58]. In GBMs, MMP-2 and MMP-9 overexpression has been correlated with poor prognosis[59,60]. Substrates of MMP-2 includes several brain ECM proteins like collagen, fibronectin, laminin, osteonectin, and vitronectin[57]. MMP-2 also has a strong affinity towards type IV collagen[57]. It's been reported that inhibition of MMP-2 or MMP-9 could decrease glioma invasion and proliferation in experimental models[32,59]. Besides direct degradation abilities, MMP-2 has also been found to co-localizes with integrin $\alpha v\beta_3$ to enhance cell migration near blood vessels[61]. Cooperation between CD44 and MMP-9 has also been observed to increase HA matrix degradation [62]. Besides MMPs and hyaluronidases, plasminogen activators and a dis-integrin and metalloproteinase (ADAM) proteins on GBM cell surface have been observed to degrade ECM[45]. These ECM degradation enzymes were linked to higher tumor invasion and increased angiogenesis[62,63].

As in other physiological systems, throughout the brain, cells sense and respond to micron-scale gradients of mechanical rigidity in 3D environment[64]. Several cell surface receptors including integrins, G-protein-coupled receptors (GPCR), stretch-activated ion channels and CD44 are known to transduce mechanical signals[29,30,65,66]. A number of studies have confirmed integrins transduce mechanical signals through Rho-family GTPases, focal adhesion kinase (FAK)-Pi3k-Akt, and ERK/MAPK pathways, as the

individual pathways are known to be upregulated in migrating cells, and these receptors are anchored to the actin cytoskeleton[29,30,66,67]. Upon sensing the mechanical stimuli, the receptors trigger release of actin-bound transcriptional factors and directly couple to the nuclear membrane[68]. Tumors were also reported to change their surrounding microenvironment in mechanical stiffness. For example, in GBM, an integrin-mediated positive feedback loop was identified, where migrating cells stiffen their surrounding matrix, in turn increasing their own cell motility[29,30]. Many researchers have pointed out that GBM tumor tissues are stiffer than healthy brain. In one study, compressive moduli of xenografted GBM tumors were reported to be 20-times stiffer than normal mouse brain[69]. In clinical cases, researchers used ultrasound-based shear wave elastography and found GBM tumors have around twice the Young's moduli of surrounding normal brain tissue[70].

The local interstitial fluid pressure rises as the GBM grows[71,72]. Cerebral spinal fluid is reported to accumulate in GBM tumor, resulting in a sharp gradient of increased interstitial pressure between the tumor and healthy tissue[71,73]. Researches have reported that increased interstitial fluid pressure would transduce similar mechanical signal that influences GBM progression in a way similar to ECM stiffening[74]. The abnormal deposition of ECM may contribute to increased uptake and sequestration of fluid ion which results in increased interstitial fluid pressure[12,36,62]. Recently, some studies confirmed the role of increased interstitial pressure in increased GBM growth and invasion via C-X-C motif chemokine ligand 12 (CXCL12)-CXCR4 and HA-CD44 interactions[75].

Intercellular interactions between GBM cells (homo-cellular) or between GBM cells and other cells in the brain (hetero-cellular) have important roles in GBM pathology. Direct homocellular interactions through gap junction (connexin-43) was reported to protect GBM cells from temozolomide-induced apoptosis[76]. Cadherins also mediate homotypic interactions between GBM cells[16]. However, reports on the functions of cadherins in the GBM have been conflicting. While some found that GBM cells lacking N-cadherin-based adherens junctions have higher invasive potential[77,78], other researchers found GBM upregulates N-cadherins, which does not affect the degree of invasion[79]. More recent studies indicated that N-cadherin-based interactions may activate the canonical Wnt pathway which promotes GBM invasion and therapeutic resistance[80]. Homotypical interactions through connexin-46 are essential for self-renewal and maintenance of GSC[81,82]. N-cadherin can also increase GSC invasion through cooperation with integrin α6[83].

Neovascularization is one of the hallmarks of cancer. Formation of vessels satisfies high nutritional and oxygen demands[84]. GBM tumor can utilize several mechanisms including angiogenesis through sprouting of new vessels, vascular co-option through tumor hijacking of normal vessels, and vascular mimicry through formation of vessels-like structures by tumor cells[84]. Just like other tumors, GBM tumor overexpresses VEGF, which can recruit pericytes and endothelial cells that leads to formation of new vessels[40,49]. GBM cells also directly interacts with pericytes to modify contractile activity of pericytes through Cdc42 and actin-based extensions. More interestingly, GBM cells have been reported to trans-differentiate into endothelial cells or pericytes to create new vessels[85,86].

Vessels in GBM pathology not only provide nutrition and oxygen, but also help maintain GSC capabilities including induction of tumor initiation and therapeutic resistance[87–89]. Studies have confirmed GSCs can interact with the surfaces of existing blood vessels to facilitate their invasion in the brain parenchyma[90]. Laminin-α2 is abundantly embedded in the perivascular area, integrin α5 on GBM is reported to interact with laminin-α2 to activate downstream cascades that is important for GSC maintenance and proliferation[91,92]. Since GBM grows extremely fast, insufficient delivery of oxygen can create hypoxic niche[93]. This hypoxic gradient can induce GBM far from blood vessels to upregulate transcriptional activities of hypoxia induced factor (HIF) which subsequently induces expression of Oct4, Sox2, LOX and CXCR4[53,94]. All these proteins are responsible for GSC maintenance and invasion. At the same time, VEGF and PDGF-B are also downstream targets of HIF, which supports angiogenesis to counter the oxygen insufficiency and promotes GBM growth[95].

Blood brain barrier (BBB) strictly separates circulation of blood from the brain, through which the permeability is highly selective. In GBM however, the BBB is compromised or “leaky”[90]. Some studies indicate GBM can secret soluble factors to disrupt BBB or directly displaces astrocyte from the vascular surface[35]. Accumulation of these leaky sites contribute to increased interstitial fluid pressure as well[72]. In a co-culture system which includes GBM and astrocyte, researchers found GBM and astrocytes mutually promote survival. Astrocytes are more prone to inflammatory phenotypes, and they can express several factors that facilitate GSC invasion[96,97].

In the immune-microenvironment of GBM, microglia in normal CNS acts as macrophage-like immune cells. In GBM tumors, monocyte-derived macrophages can

cross the leaky BBB[98]. Microglia and macrophageassociate with GBM to provide an immunosuppressive environment that facilitates GBM progression[98]. Recruitment of microglia and macrophages is mediated by tumor-expressed CXCL12[99]. In turn, TGF-β and MMPs can be produced by reactive microglia, promoting GBM cell invasion and proliferation[63,100].

Together, various components in the microenvironment surrounding GBM work closely to affect GBM progressions. Therefore, *in vitro* and *in vivo* methods to culture GBM are crucial to determining the outcome of experiments and scientific conclusions.

Currently used experimental models to GBM

Several *in vitro* and *in vivo* models are currently used to study GBM physiology and evaluate the therapeutic efficacy of potential clinical strategies. The advantages and disadvantages across different culture methods are listed in **Figure 1.3**.

Figure 1.3

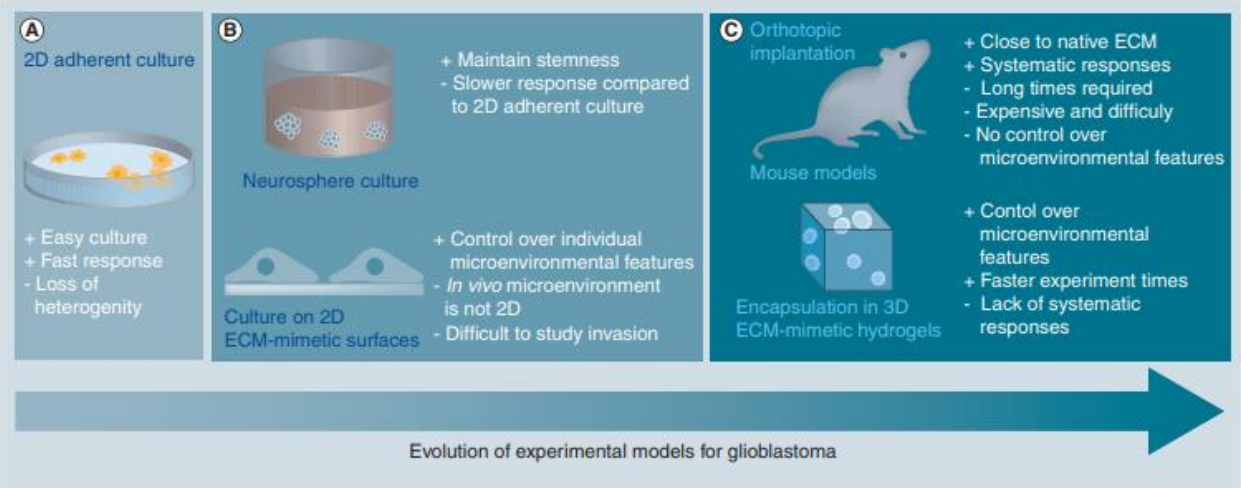

Figure 1.3. Advancements in experimental models of glioblastoma tumors. (A) 2D monolayer cultures on protein-coated plastic or glass. (B) Suspension culture of patient-derived neurospheres (top) and 2D culture on biomimetic materials (bottom). (C) Orthotopic transplantation of patient-derived cells into mice (top) and 3D culture of glioblastoma cells in biomaterial microenvironments (bottom). The figure is adapted from Xiao et al[16].

2D culture models

To study GBM physiology, researchers have used 2D monolayer cultures of cells that were derived clonally from tumors isolated from patients since 1960s[101]. Among numbers of GBM lines, U87MG has been very widely used to collect data for scientific conclusions[102]. Although extensive data were collected using these lines, it's hard to interpret their clinical relevance given occurrence of mutations and phenotypic drift generated since the isolation of the original cells, and apparently inadequate representation of the heterogeneity seen in clinical cases of GBM.

Serum-based, usually fetal bovine serum, monolayer cultures have been widely used to evaluate effects of various agents on GBM cells. Serums isolated from animals usually contain various ECM proteins and soluble factors that aid in cell adhesion to culture substrate (usually polyethylene plastic dishes) and promote proliferation of the cultured cells. Unfortunately, GBM cell cultures reliant on serum-containing medium have many disadvantages. Serum induces selection of cells with specific characteristics which eliminates the heterogeneity of subsequent passages[103]. Significant phenotypic and genetic changes can be observed in cultured cells[103,104]. At last, serums used in the experiment are usually from animals like bovine, which suffers greatly from batch to batch differences, affecting reproducibility[105]. These effects may partially explain why many treatments that are successful *in vitro* but fail in clinical models are.

Substrates for monolayer cultures can be coated with ECM proteins to facilitate cell adhesion and serve the purpose of studying specific ECM-cell interactions in GBM. However, adsorption to glass or plastic substrates causes denaturation of the coated

protein, making the *in vivo* relevance of experimental results difficult to discern, as native structural integrity of the protein is destroyed. Moreover, addition of single ECM protein does not capture all components in the ECM microenvironment. To solve this problem, Matrigel has been very widely used as a “mixture” of ECM proteins. Basic components of Matrigel were derived from the basement membrane of Englbreth-Holm-Swarm mouse sarcomas, which roughly contain 60% laminin, 30% type IV collagen and 8% entactin, along with several small molecule growth factors like EGF, TGF-β and PDGF, whose roles in the ECM were introduced in previous sections. However, Matrigel was not originally designed to mimic brain ECM, and the mixture was more relevant to matrix environment of peripheral cancers. Therefore, it does not accurately reflect GBM matrix microenvironment, and apparently all relative components are non-customizable, which poses difficultly in studying individual effect of single ECM component. At last, Matrigel also suffers from lot-to-lot variability, and derivation from non-human sources are also major concerns[16].

Gliomasphere (GS) suspensions

Recently, development of methods for GBM cell isolation and culture that can generate data with better relevance to clinical outcomes[103,106]. In order to maintain GSC-like and patient-specific behaviors, tumor cells are carefully dissociated from freshly isolated patient biopsies and cultured in suspension as clonally dividing GS in serum-free, animal free (xeno-free) medium that is supplemented with EGF and bFGF-2[103]. It has been reported that GS cultures derived from human GBM tumors better preserve the genotypic, phenotypic and some *in vivo* characteristics of the original patient[103]. Additionally, GS cultures provide a semi-3D environment in which the GBM cells can

deposit ECM to create their own unique microenvironment[107]. To date, GS cultures have enabled many significant findings, including characterizing the GSC microenvironmental niches and mechanisms of some treatment resistance in a clinically relevant aspect[108].

Despite improvement over monolayer culture, GS cultures do not adequately capture all aspects of GBM tumors. On one hand, GS culture is highly enriched with GSC, while heterogeneity aspect of the tumor is harmed as the population with low self-renewal capabilities are lost[81,103,109]. On the other hand, GS formation is in fact an *in vitro* phenomenon. In contrast, GSCs *in vivo* typically reside in a perivascular niche where they experience a different microenvironment that is absent in the GS suspension culture[87].

It is notable to mention one study where researchers generated a 3D GBM organoids that reached several millimeters in diameter (much larger than typical GS which are on the order of around 150μm). As a result, hypoxic gradients were present in the organoid, inducing significant phenotypic differences in cells located in the periphery or at the core of the “bulk tumor”. Heterogeneity of GBM is conserved in this model when researchers observed the GBM cells at “core” displayed stronger radiation resistance. It’s more promising that orthotopically transplanted organoids in mice displayed some histological features better resembling clinical GBM tumors than did GS-cultured cells. However, disadvantages of the organoid are also obvious: organoids culture takes months to form large spheres, and long term culture may cause more genetic mutations that deviate from original patient biopsy.[110]

In vivo animal models

Animal models provide better opportunities to take more microenvironmental influences into account than *in vitro* models. For example, animal models provide GBM interactions with stromal cells, vasculature, and the immune system, each of which significantly contributes to GBM physiology. Therefore, *in vivo* animal models have provided the most clinically relevant experimental results to date. Mouse models of GBM are commonly used in orthotopic xenograft of patient derived GBM gliomaspheres, syngenetic transplants of mouse GBM cells, and genetically engineering mouse models (GEM). [104]

Orthotopic xenografts of patient-derived GBM GS into immunodeficient mice have been regarded as standard model for human GBM, particularly for evaluating the efficacy of potential therapies[103,104]. Recapitulation of the invasive phenotype, histopathological features and genetic markers of the original patients are among the major achievements of intracranial implantation of patient-derived gliomaspheres[103,107]. However, disadvantages such as loss of heterogeneity and phenotypic/genetic drift over long periods of culture also apply to the orthotopic xenografts. Meanwhile, immune-deficient mice cannot provide adaptive immune response[104]. As a result, important immunological events such as interactions between T cells and GBM tumors are absent[111].

In order to preserve patient specific genomic aberrations that result in distinct therapeutic responses, in the spirit of personalized medicine, researchers have recently developed “AVATAR” models of GBM patients, which involve direct orthotropic injection

of fresh tumor cells from patients into NOD-SCID mice (mice with homozygous for the severe combined immune deficiency spontaneous mutation of Prkdc^{scid}) within 12h of tissue dissection[112,113]. This method eliminates the ex-vivo procedure that involves the generation of passages in gliomasphere culture conditions. Studies have confirmed AVATAR mice model can maintain genomic characteristics, subtype profile and histopathology of parental GBM better than patient derived gliomaspheres. More promisingly, GBM formation and invasion in AVATAR mice were observed to directly correlate with patient outcomes. Potentially, AVATAR models may enable identification of patient-specific biomarkers and important genomic alterations that will more accurately predict clinical prognosis and treatment response. Despite significantly improved fidelity of AVATAR models to both clinical and scientific outcome, the immune system of NOD-SCID mice is compromised, and other microenvironment factors in mouse model are still very different from those in human system, as described in the previous paragraphs.[112,113]

Syngeneic transplantation of mouse GBM cells into species-matched mice allows preservation of the interactions between GBM and the immunesystem[104,111]. For example, mouse models based on C57/B16 mice served as “gold standard” for studying immune cell-tumor interactions and therapeutic vaccines[111,114]. In recent years, several successful cases have shown strong potential of using immunotherapy to treat cancer, and at the same time some immunotherapy strategies have been investigated in clinical trials[115]. However, it is obvious that a better model is urgently needed to replace the syngeneic transplantation with a model replace human physiology.

Implantation of purified and “mature” GBM cells into animals cannot allow researchers to investigate how a tumor has initiated and developed. To solve this problem, GEM model have been developed in which the role of specific gene mutations in tumor initiation and progression can be investigated[116,117]. Moreover, targeted gene manipulations through mutations, silencing and overexpression can be performed with temporal control. GEM models also utilize immunocompetent mice, providing sufficient environment to study immune events that are involved in tumor initiation. Nevertheless, the GEM model is still a non-human model, and extensive understanding of roles of many cancer genes is needed to make GEM model a faithful model for human cancer[116,117]. Additionally, a major disadvantage of GEM model is the inability to control tumor and the timing of tumor initiation. As a result, reproducibility is harmed.

Bioengineered platforms to model GBM

Although mouse models enable the study of GBM inside an environment of living host, the financial cost, time, reproducibility and complexity of performing *in vivo* experiments pose strong drawbacks. While *in vitro* culture systems have solved the above issues, traditional *in vitro* systems often fail to deliver clinically relevant results, because of the absence of a proper microenvironment. Therefore, researchers have been actively developing advanced culture systems to accurately mimic the physical and biochemical aspects of the native GBM microenvironment at ex vivo level.

The majority of the biomimetic culture platforms developed to date involve hydrogel biomaterials that exhibit tissue-like water content and mechanical properties and

support culture of cells in 3D manner. These platforms can be fabricated through ECM derived biomolecules.

Adherent 2D culture models

In an engineered 2D culture system, cells are cultured on the materials exhibiting stiffness closer to that of native brain and/or modified with ECM biomolecules using methods that provide better control and preservation of their native state other than simple adsorption. Polyacrylamide based hydrogels were used in many studies, in which the materials can be readily modified to present varying mechanical properties, topographical structures and bioactive molecules[118–122]. Generally, the GBM oncology field believes that cells residing in or near GBM tumors experience stronger mechanical forces due to increased interstitial fluid pressure or stiffening of ECM as described above[72,118]. To investigate the effects of these mechanical cues, researchers have cultured GBM cells on 2D substrates made with silicone rubber, polyacrylamide, or HA along with varied mechanical properties. It has been reported that more rigid substrates increased GBM cell migration, actin stress fiber formation and focal adhesion maturation[119]. Some studies have reported stiffened substrates increased migration capabilities and proliferation for some cells[118,121,123,124]. However, conflicting data were reported in different studies. The inconsistencies might be raised from lack of orthogonal control to keep biochemical composition unchanged while modulating the stiffness. It is worth noticing the participation of CD44 in mechano-sensing. Studies have shown CD44 mediates the increased migration speed in GBM cells cultured in stiffer substrate[30]. Another study indicated physical topography and confinement of cells facilitate a response that is similar to substrate mechanics[120]. In detail, culture of

immortalized GBM cell lines in confined, micron scale channels or on substrates with aligned nano-fibers significantly increased GBM cell polarity and migration speed[125,126]. The result above was further confirmed with U373mg cells when the researchers decoupled the engineering environment stiffness and confinement. They found that more confined chamber alone could increase migration speed regardless of stiffness[125,126].

Chemical modifications can be applied to non-bioactive 2D substrates such as polyacrylamide and poly-ethylene glycol (PEG) to add bioactive ECM derived peptides or whole protein that can interact with the GBM cells without being denatured as the methods of conjugation are not mere adsorption. Meanwhile, biomaterials conjugated with various bioactive molecules can be used better to mimic the complex *in vivo* environment. In particular, HA-based hydrogels with covalently attached peptides or proteins were used to investigate the interaction between CD44 and integrin on GBM cell behaviors[30,118,127,128]. Increasing in GBM migration speed was seen when HA was incorporated into the 2D substrates in U87mg and U373mg cells[128]. ECM can also be attached to substrates fabricated from core-shell nanofibers which provide control of mechanics and topography. “Core” part in the nano-fibers controls substrate stiffness, and the “shell” can be coated with biochemical molecules. In one example, nanofibers with poly-caprolactone cores were modified with collagen, HA or Matrigel shells to achieve an orthogonal control[125]. In the system above, motility of patient derived GBM cells OSU-2 on HA shell nanofibers was slower than those with shells containing integrin-binding sites.

3D culture models

Compared to 2D cultures, 3D constructs can provide more physiologically relevant features. For example, the punctate focal adhesions that are “common” observation in 2D cultures are not even seen in 3D cultures or whole tissue[30,118,121,129,130]. Moreover, 3D culture can stimulate pore-size dependent events like nutritional diffusion and GBM invasion into the ECM[123,128]. Microenvironmental landscape directly influences diffusion of nutrients, metabolic waste and oxygen in 3D stage. In the aspect for GBM, cells experience hypoxic conditions that further increase malignant properties[130]. Therefore, it is not surprising that 3D culture systems better preserve features of hypoxia-induced metabolism, treatment response and GSC phenotype[131–133]. At the same time, GBM invasion is also affected by the ability of cells to navigate through pores, degrade and remodel the scaffold[134,135]. Encapsulation of GBM cells within a 3D hydrogel microenvironment through using the highly biocompatible crosslinking chemistries is very common. Given that cell-cell and cell-ECM interactions in GBM are highly complex, ex vivo culture platforms in which individual aspects of the microenvironment can be isolated experimentally, which allow researchers to “tease apart” these entangled effects in a simplified context. The old ways to fabricate 3D scaffolds from microporous, solid plastics, such as poly(lactide-coglycolide) and solid plastics, these materials require that cells be seeded top and enter scaffolds either passively by gravity or actively by migrations[88,132]. In contrast, hydrogels are more relevant to the native brain microenvironment in water content and mechanical properties. Hydrogels are preferred material to study GBM physiology because they can be formed using gentle and aqueous chemistries to encapsulate live cells to ensure viability. Hydrogels can also provide long term insoluble cues from native ECM components through bioconjugation,

and apparently hydrogel allows observation of 3D cell migration and matrix remodeling. At last, optical transparency of the hydrogel culture allows facile imaging of live cells living in 3D culture system.[133]

Hydrogels can be formed by covalent or physical (mono-covalent) crosslinking of hydrophilic polymer chains into insoluble networks using a variety of chemical methods. Functional groups with complementary moiety or initiation activators are required in covalent crosslinking of hydrogel. Condensation, Michael-type addition and Diels Alder reactions are commonly used to fabricate hydrogels for 3D cell culture, because these crosslinking reactions can proceed readily under physiological conditions. Producing water as a by-product, biocompatible hydrogels are often formed via condensation reactions between amines and carboxylic acid[136,137]. Many other biocompatible hydrogels are crosslinked via Michael addition in which a thiol and acrylate/vinyl sulfone readily react to form thioester linkages[128,133,138].

Photochemistry has been widely popular in 3D culture fabrication since the reaction would not occur until exposure to light with specific wavelength, so photochemistry allows precise spatial and temporal controls. When modeling GBM, photochemical patterning has been attractive strategy for creating microenvironment with gradient features. Often, hydrogels are crosslinked through chain-growth polymerization of acrylates[131,139]. More recently, researchers favored thiol-ene photoreaction (formation of linkage between thiol and norbornene groups) over other methods[140,141]. The thiol-ene reactions proceed by step-growth polymerization, which produces hydrogels with more defined networks and fewer defects than those produced by chain-growth polymerization[142]. UV activated radical initiator, Irgacure 2959 has been commonly used

for fabrication of biocompatible hydrogels due to its water solubility and biocompatibility. Alternatives to Irgacure 2959 include phenyl-2,4,6-trimethylbenzoylphosphinate, with higher water solubility and more efficient photoactivation than Irgacure 2959[143].

Besides condensation reaction and photochemistry, which form permanent covalent linages, noncovalent crosslinks are typically formed via temperature or pH-induced segregation of polymer regions based on hydrophobicity or ionic interactions. Usually, resultant hydrogels are often weaker than those formed by covalent crosslinks, but noncovalent gelation methods are usually more biocompatible due to mild reactions involved in hydrogel formation[144]. Noncovalently crosslinked hydrogels commonly used for 3D culture include laminin-I based Matrigel and type I collagen, which forms hydrogel at physiological temperature[138,145]. Another popular use of noncovalent hydrogel is through alginate solution, which undergoes gelation only at presence of calcium ions[146].

Influences of stiffness in 3D culture

As introduced in previous sections, GBM behavior is regulated by mechanical properties of the surrounding microenvironment. To investigate this effect ex vivo, researchers have worked to control the mechanical properties of 3D scaffolds (**Figure 1.4**). In general, mechanical strength of hydrogel scaffolds increases with increased backbone polymer content or crosslinking density. In gel formation methods involving Michael type addition reaction, changing the molar ratio of thiol/vinyl sulfone groups can be used to alter the density of crosslinks and thus the mechanical properties. In photo-crosslinked hydrogel, by increasing the number of reactive groups, light exposure time or initiator

concentration will yield higher mechanical moduli. In a similar manner, increasing the calcium concentration will result in stiffer alginate-based hydrogels.

Figure 1.4

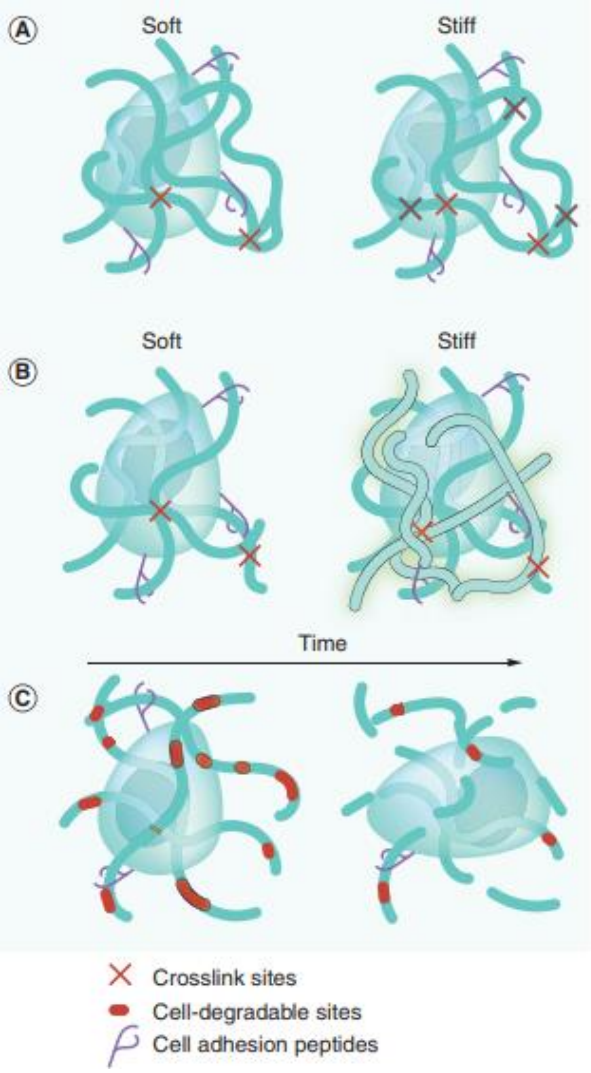

Figure 1.4

Controlling biochemical and physical properties in 3D hydrogel biomaterials. Mechanical properties can be tuned by (A) altering crosslink density or (B) base polymer concentration, both of which affect hydrogel pore size and diffusion of soluble factors through scaffolds. (C) Incorporation of degradable polymers, such as matrix metalloprotease or hyaluronidase-susceptible sites, facilitates cell migration and degrades scaffolds over time. The figure is adapted from Xiao et al[16].

In contrast to 2D cultures, GBM cells cultured in 3D matrices displayed higher migration speed with decreased scaffold stiffness[123,128,144]. Interestingly, conflicting conclusions have been reported on how mechanical environment affects MMP expression. As an example, U87mg GBM cells cultured in HA-based hydrogels with higher stiffness both increased and decreased MMP-9 secretion in different studies[131,141]. For proliferation, discrepancies on mechanical influences are reported in 2D and 3D constructs[123,139,141]. Many of these discrepancies could be caused by inability to decouple the effects of mechanical features from other biochemical aspects in extracellular matrix cues. Bioactive molecules such as HA and collagen can be used as based hydrogel to affect both biochemical and mechanical parameters. To decouple the biochemical and mechanical properties, researchers can change initiator concentration instead of polymer concentration. It is worth noting that changes in stiffness will cause drastic changes in pore size of the polymer, which can greatly affect GBM migration physically, a possible reason for discrepancies generated in previous studies.

Biochemical interactions in 3D culture

In order to mimic the biochemical composition of the native brain and GBM tumor microenvironment, 3D hydrogel scaffolds have been fabricated from a variety of ECM derived biopolymers, including chitosan, HA, chondroitin sulfate polysaccharides and collagen/gelatin proteins[122,131,136,139,141,145,147]. As the ECM in the CNS contains high amounts of GAGs and very few fibrous proteins such as collagen I, many researchers have been using hydrogels with HA backbones to mimic native brain[16]. In these hydrogels, GBM cells increased migration speed with increased amounts of HA and/or chondroitin sulfate GAGs[128,134,137]. In addition, high HA content is reported to decrease

GBM proliferation and increase the expression of genes associated with tumor progressions, including HA synthase, hyaluronidase, MMPs, VEGF, and HIF1[131,139,145]. At last, cultures of multiple patient-derived GBM lines in 3D HA hydrogels better induce resistance to radiation and chemotherapy, which is also observed in clinical cases[133]. Facilitation of cell adhesion can be enabled through using gelatin that contains sites for integrin attachment[131,139]. Increased gelatin concentration in HA-based hydrogels upregulated MMP-9, VEGF, HIF1 and fibronectin expression, and downregulation of MMP-2 by U87mg was cells[131,139]. Collagen I based hydrogel can form spontaneous hydrogel through fibrillogenesis, requiring no functional chemical modification[16]. Hybrid scaffolds of HA and collagen I have also been used to investigate the effects of HA on migration of a few patient derived GBM gliomasphere lines[138,145]. As an example, interpenetrating networks-where hydrogels of collagen I hydrogels were infused with thiol modified HA, in which disulfide bond would enable self-crosslinking. These hydrogels were used to evaluate effects of HA content and found that adhesion and migration speed of GBM cells degreased with higher HA concentration[138]. In contrast, a newer study found that addition of HA to collagen I hydrogels facilitates GBM cell invasion/migration[145]. Although high molecular weight HA (>250kDa) was used in both studies, the backbone HA in the latter study was not modified or crosslinked chemically but used as simple coating to collagen I fibers. Collagen I is not typically present in the brain, hydrogels fabricated through this method better resemble to peripheral tissues than brain[14]. Moreover, hydrogel bond dependent 3D structure can be disrupted through chemical modification of carboxylic group on the glucuronic acid on HA backbone[148]. Since the 3D structure of HMW HA is at least partially responsible for its ability to induce

cell responses different from LMW HA does, it is highly likely that the high degree of modification used in the former study altered biochemical function of HA[138,149]. The latter study reported that expression of CD44 and CD168 was increased with higher HA content, implying that HA receptor interactions were enhanced. At last, the latter study cultured GBM cells as spherical aggregation instead of dissociated single cells. The "microtissues" are more reflective of the native GBM microenvironment because it permits direct cell-cell contacts and collective migration of cells from a core tumor[138,148].

Biocompatible PEG and alginate hydrogels have been used as blank substrate, and active biomolecules are added to them[140,141,146,150]. Proteins and peptides containing cysteine can be added to those polymers through Michael-type addition[132,151]. Using this method, controlled quantity of molecules and crosslinking density can be added with precision[151]. Multi-arm, branched PEG macromers can yield more defined networks than linear PEGs, as the integrity of 3D structure does not rely on polymer entanglement[151]. In photochemistry, for example, acrylate-modified biomolecules can be mixed into PEG-acrylate solutions prior to photoinitiation that completes hydrogel formation[143,147]. Besides whole proteins like fibronectin, ECM-derived adhesive peptides, such as those containing the ubiquitous integrin binding RGD sequence, are commonly used[30,127,128,140,141,150]. Although integrin binding peptides may not have the comprehensive effects of their full-length counterparts, they can pinpoint effects of matrix interactions with specific subsets of integrin. Moreover, it is generally easier to control their functional presentation within hydrogel matrices. Incorporation of RGD peptides would increase GBM cell adhesion[128]. Conjugation of RGD into alginate hydrogel has been shown to protect GBM cells from toxin induced apoptosis[150]. Other

ECM derived adhesive peptides such as elastin could increase invasion and the production of MMP-2 and MMP-12 in multiple GBM lines[136]. Small protein factors such as growth factors and other cytokines can be incorporated into scaffold microenvironments through simple diffusion of solubilized factors, direct chemical conjugation or non-covalent tethering to the hydrogel matrix. Interestingly, addition of soluble EGF to 3D collagen hydrogel cultures could increase migration of U87mg[131,139], while opposite effect was seen in 2D cultures with collagen substrates[152]. In the native ECM, noncovalent interactions of diffusible growth factors with heparins can create a bioactive concentration gradient of cytokines[40]. Hydrogel scaffolds have been modified with heparin to mimic this phenomenon in engineered culture environments[153].

Cell-cell interactions in 3D culture

In order to investigate the interactions of GBM cells with other cell types, which are present in the *in vivo* microenvironment, including astrocytes, microglia/macro- phages and endothelial cells – researchers have worked to develop coculture models to study the effects of both paracrine signaling and direct cell–cell contacts. While several previous studies have studied the effects of cell-produced factors of nontumor cells on GBM cells cultured on 2D substrates using conditioned media, these experiments are unfortunately unable to provide information about crosstalk between cell types. To solve these problems researchers have been using Transwell and Boyden chamber assays to investigate crosstalk through paracrine signaling but cannot easily determine effects of direct cell-cell interactions or those with secondary structures, such as blood vessels, an important component in BBB[96,154,155]. In the native GBM microenvironment, cells interact with each other in 3D through direct contacts and diffusing paracrine factors, and

therefore a 3D model is necessary to recapitulate these interactions. To study the angiogenic effects of GBM cells, a transformed endothelial cell line (HUVEC) was cultured on dextran beads first and then embedded into a 3D fibrin hydrogel scaffold[156]. Culture of transformed GBM lines on the surface of HUVEC-embedded, fibrin hydrogels increased angiogenesis[156]. However, obviously, this method did not allow for direct contact of GBM and endothelial cells in three dimensions. A more recent study used coculture of transformed GBM lines with an immortalized astrocyte line within 3D spheroids to show how the presence of astrocytes protected GBM cells from temozolomide-mediated apoptosis[157]. Segall and coworkers have developed a method for 3D coculture of GBM and microglia/macrophage immortalized lines, where cell mixtures are embedded into a Matrigel scaffold through which both effects of paracrine and juxtracrine interactions on GBM cell invasion can be investigated[158]. However, no studies on patient-derived cell lines have been used so far with co-culture system. One challenge to developing cocultures with patient-derived lines is that serum, a necessary compound to support co-cultured cell type like HUVEC, cannot be used without altering GBM cell phenotype[103]. Moreover, co-cultures with immune cells and astrocytes can also be difficult to interpret, as culture conditions may promote inflammatory phenotypes that are not reflective of their GBM-associated counterparts *in vivo*[159]. Therefore, identification of co-culture medium that can maintain GSC signatures and survival of both cell types remains challenge. As an alternative to true cocultures, synthetic peptides that mimic juxtracrine receptors, such as N-cadherin, are incorporated into biomaterials[159]. Despite the fact that this method cannot be used to characterize dynamic crosstalk between live cells, it provides a simpler method to investigate the

isolated effects of cell–cell contacts. More recently, ‘Organ-on-chip’ astrocyte–endothelial cell cocultures that model the *in vivo* BBB may also be promising novel model to study the interactions of GBM tumors with vasculature structures[160,161].

Brief introduction of known intracellular mechanisms of GBM drug resistance

In previous section, how microenvironment facilitates therapeutic response is briefly introduced. While our understanding to microenvironment-mediated resistance is shallow, numerous studies have focused on how GBM utilizes intracellular mechanisms to avoid being eliminated by therapeutics. Generally, drug resistance is categorized as either acquired or intrinsic[162]. Acquired drug resistance occurs after a tumor responded to the treatment initially, and intrinsic resistance refers to a tumor shows no respond to the therapy at the onset of the treatment[162]. Obviously for GBM, intrinsic and acquired resistances share common foundations.

Drug efflux mechanisms

First important mechanism is the active efflux of a broad range of anticancer drugs through cellular membrane by multi drug resistance proteins[162–165]. The efflux proteins can transport the drugs in ATP-independent or dependent manners[163]. The ATP-dependent proteins consist of ATP-binding cassette (ABC) transporter family, which includes p-glycoproteins and breast cancer resistant protein (BCRP)[164]. Overexpression of P-gp, the protein encoded by gene MDR1, is mostly considered as cause of anticancer drug resistance[20]. For example, actions of P-gp in conjunction of Bcrp1 are considered partially responsible for erlotinib resistance[162]. P-gp also attributes to chemoresistance of doxorubicin and vincristine[164]. Besides overexpression of efflux

pumps on GBM cells, another important contributor of efflux transporter mediated mechanism is the BBB[163]. Since long time ago, the BBB is considered as diffusion barrier that impedes the influx of most compounds from the blood to the brain[163]. Tight junctions between the endothelial cells of the brain capillaries offer low permeability[163]. Therefore, there is negligible level of paracellular transport of substance under physiological conditions. As a result, only passive diffusion, receptor mediated transcytosis or action of passive carrier system can uptake the drug that treats GBM[163]. Moreover, researchers found abundant expression of ABC family proteins such as P-gp and MRP that actively efflux drugs and limit accumulation of the drugs as described in above texts[163]. Therefore, the BBB remain as critical role in preventing drugs from penetrating into the brain system.

Damage repair

Most commonly used chemotherapies act through damaging the DNA of GBM cells like TMZ. TMZ is an alkylating agent whose action is to add methyl group at O6 position of DNA[166]. In most cases of GBM, failure of DNA repair will initiate apoptosis program in the cells. However, O6-methylgranine methyl transferase (MGMT) in GBM can actively remove the DNA adduct caused by alkylating agent, resulting in treatment resistance[162,166]. As a result, methylation of the MGMT promoter has been extensively studied as predictor for treatment outcome[162,166]. Therefore, mRNA expression and histological analysis would be valuable prognostic markers for GBM patient.

While induction of apoptosis is the ultimate goal of alkylating agent. Loss of DNA mismatch repair (MMR) has been proved to be another cause of alkylating agent

resistance[167]. Loss of MMR can cause the drug resistance directly by impairing the ability of the cell to detect DNA damage and activate apoptosis, and at the same time the rate of mutation is increased. Resistance to variety of drugs including procarbazine, TMZ, busulfan, cisplatin and carboplatin[162,166]. Therefore, it is challenging to assess the clinical significance of the presence of deficient cells in tumors and to discover drugs that retain activity against MMR deficient cells.

Glioma stem cells

As introduced in previous sections, intratumoral heterogeneity of GBM involves large population of GSCs that promote therapeutic resistance. In summary, these GSC populations are identified to express high levels of ABC transporters such as P-gp and ABCG2 which contributes to effective efflux of drugs[168,169]. GSCs also share common properties with normal stem cells, such as extended propagation and self-renewal capabilities that promote long lifespan and ability to differentiate into other tumor cell types which may effectively survive from certain kinds of therapies and later contributes to tumor recurrence[169,170]. This clonal evolution paradigm is most accepted theory for GBM recurrence when only the responsive populations got eliminated by certain drugs[165].

Alternate receptor dependency in targeted therapies

More than 50% of GBM bear EGFR amplification which drives many aspects of GBM progression[171,172]. Showing promising success in breast and lung cancer, EGFR targeting drugs like erlotinib were considered promising therapies for GBM[173,174]. Unfortunately, failure of erlotinib was shown in experiments and clinically[175]. Several

mechanisms were discovered to indicate the intracellular mechanisms of resistance lay at multiple level. In genetic aspect, Nathanson et al. proved amplified EGFR genes play “hide and seek” with the treatment, as the tumor does not express/depend on EGFR signaling[172]. At expression level, GBM was shown to switch receptor dependency from EGFR to PDGFR in the presence of erlotinib[176]. Finally, at signaling level, mutation/loss of PTEN directly relieves the regulatory “brake” of downstream signaling of EGFR activation, rendering complete drug resistance against erlotinib[175]. All these mechanisms show plasticity and versatility of strategies utilized by GBM, making single target therapy ineffective against GBM.

Resistance to Apoptosis

While induction of apoptosis is the major goal of nearly all GBM therapies, GBM has several abilities to prevent initiation of apoptosis. B cell lymphoma-2 (Bcl-2) is commonly discussed anti-apoptotic protein that is highly expressed in treatment resistant GBM cancers[177]. Overexpression of Bcl-2 and Bcl-XL are observed in most GBM cells[177]. Around 20 years ago, the truncated version of EGFR (EGFRvIII, expressed by more than half of GBM bearing EGFR mutation) was proved to inhibit DNA damaging induced apoptosis through elevation of Bcl-Xl expression[177,178]. Bcl family pro-survival and anti-apoptotic signaling also includes PI3k-Akt, Stat3/5 and MAPK/ERK1/2 pathways, where all these pathways maybe activated through microenvironment as described above[165].

Brief Conclusion

In GBM, a highly complex and sophisticated extracellular system dynamically affects equally complex internal cellular decisions in therapeutic response. Therefore, solving the mysteries of how ECM renders therapeutic resistance requires a translational culture system that can systemically investigate effects of ECM to GBM. In the next chapters, investigation of GBM extracellular system in clinical and in-vivo systems and construction of brain-mimetic HA-based system with orthogonal tunability will be described in detail.

Chapter 2

Characterization of GBM matrix microenvironment

My research has focused on GBM extracellular matrix, especially adhesion proteins that contains “RGD” motif and matrix hyaluronan. This chapter describes investigation of the presence of fibronectin, vitronectin, laminin and hyaluronic acid histologically in both patient and animal models. Each of these ECM components likely plays a role in progression in GBM and other types of cancer[12,16]. Previous research has indicated that fibronectin, vitronectin and laminin, which contain RGD motifs, interact with integrin receptors on GBM to activate multiple pathways that promote tumor progression[14,91,179,180]. The purpose of these experiments was to immuno-histologically visualize ECM deposition of these proteins and macromolecules along with corresponding receptors CD44 and integrins in GBM patients and xenograft animal models. These results provide crucial information for establishing engineered microenvironment in the next chapters.

Materials and methods:

Both patient samples and *in vivo* (mouse xenograft with patient-derived GBM cells) experimental samples were used in the investigation. Clinical samples were generously provided by Dr. William Yong from Brain Tumor Tissue Resource (BTTR) in UCLA. Regular GBM samples were collected from clinical biopsy samples. Tissue micro array (TMA) samples prepared from 39 GBM patients and 19 lower grade CNS cancer samples (grade I-III astrocytoma, grade I-III oligodendroglioma, meningioma and pituitary gland cancer) were provided. All samples were paraffin-embedded and

sectioned at 5µm thickness. Mouse xenograft samples were provided by Nathanson lab at UCLA. All studies were approved by the UCLA Institutional Animal Care and Use Committee (IACUC). For intracranial xenografts, GBM cells (GBM39, a GBM cell line derived from a patient, in this chapter) with constitutive expression of Gaussia Luciferase were injected into the right striatum of female nod-SCID-mice. Tumor burden was monitored through bioluminescence bi-weekly via IVIS 200 instrument imaging. Mice were euthanized when moribund (loss of 20%-30% body weight from tumor implantation in addition to symptoms such as neurological defects, paralysis, hydrocephalus and hunching. In subcutaneous xenograft experiments, 1E6 cells/100µL were injected into subcutaneously into the right dorsal flank of mice. Animals were euthanized once subcutaneous tumors grew large enough to impede movement. All extracted tissues were embedded in paraffin and sectioned at 5µm.

All prepared slides were deparaffined in 100% xylene for 5 minutes followed by a 5-step alcohol gradient (100% ethanol to de-ionized water). Later, antigen retrieval was performed in citrate buffer pH 6 at 98^{o}C for 20 mins followed by 10 mins pepsin treatment at 37^{o}C. All samples were washed in washing buffer (tris buffered saline (TBS) and 0.1% tween-20 added for non-receptor staining) 3 times for 3 mins each followed by 1hr blocking in 5% normal goat serum and 1% bovine serum albumin in washing buffer. All slides were then incubated with primary antibodies (or biotinylated HA binding protein (HABP)) overnight at 4^{o}C. The next day, primary antibodies were washed away and samples were incubated with corresponding secondary antibodies or Vectastain ABC kit and 3,3'-diaminobenzidine (DAB) substrate were used after 3 washes after primary antibody incubation. All sections were rinsed in tap water and

performed with dehydration through alcohol gradients. At last, all slides were mounted in toluene mounting solution with cover glass. All images were taken with Zeiss Axio-Observer using Zen software.

Staining results:

First, we observed strong positive DAB staining of various ECM components in patient biopsy samples (**Figure 2.1**). Except for laminin, staining of the targets distributed throughout ECM and the tumor cells. In the case of laminin, expression was mostly seen in micro-vessels, as laminin is the major component of vessels[14]. Abundant expression of CD44 and Integrin beta 1 was seen in the tumor area in all cases. Interestingly, integrin beta 3 was not observed in tumor area, even though numbers of reports indicated overexpression of integrin beta 3 and its implication in tumor progression in GBM[32].

Second, to investigate how the 4 ECM components changes with tumor progression, we assessed the TMA array staining semi-quantitatively using a scoring system as described previously[181]. As expected HA, laminin and vitronectin expression scoring in GBM was significantly higher than lower grade CNS cancer samples. Interestingly all types of cancer had fibronectin (**Figure 2.2**).

Thirdly, knowing the presence and possible implications of the ECM molecules, we assessed the expression of the ECM molecules in intracranial/subcutaneous xenograft models in which patient-derived GBM cells (GBM39) were implanted. In orthotopic xenograft model, fibronectin, laminin and vitronectin were deposited in the extracellular regions and expressed inside the tumor cells (**Figure 2.3**). However, in the case of

subcutaneously implanted tumors, we mainly observed staining located inside the cytoplasm (only tumor areas were preserved for intracranial cases) (**Figure 2.4**). HA presence was seen surrounding and within intracranially xenografted tumors. In contrast, in the case of subcutaneously implanted GBM 39, HA deposition was only found within tumors, and not surrounding tissue (**Figure 2.3, Figure 2.4**).

Figure 2.1

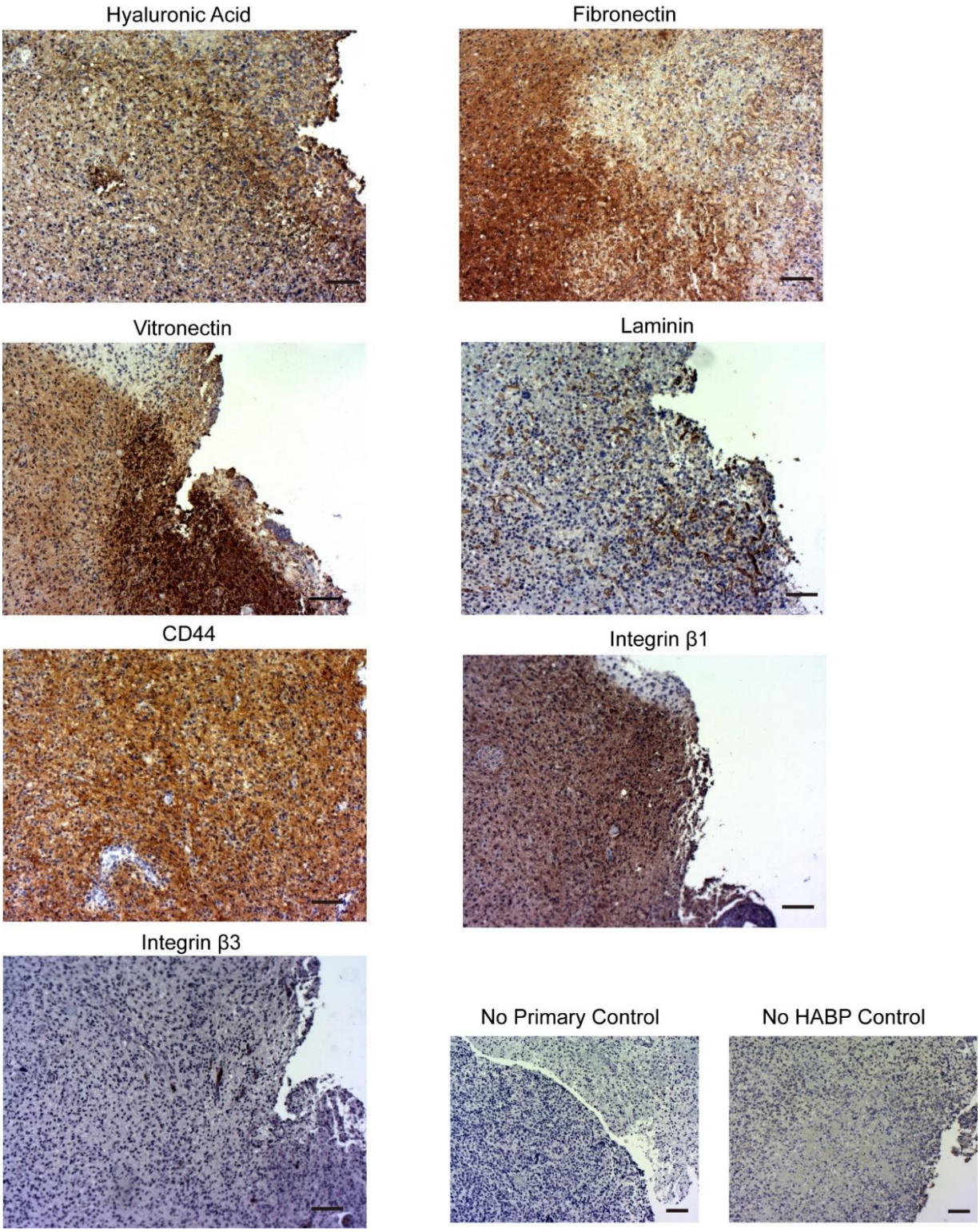

Figure 2.1. ECM molecules and receptors are abundantly present in the GBM clinical samples. Representative images of immune-staining of various ECM targets of clinical GBM samples (brown, positive stain; dark blue, hematoxylin). Scale bar= 100µm.

Figure 2.2

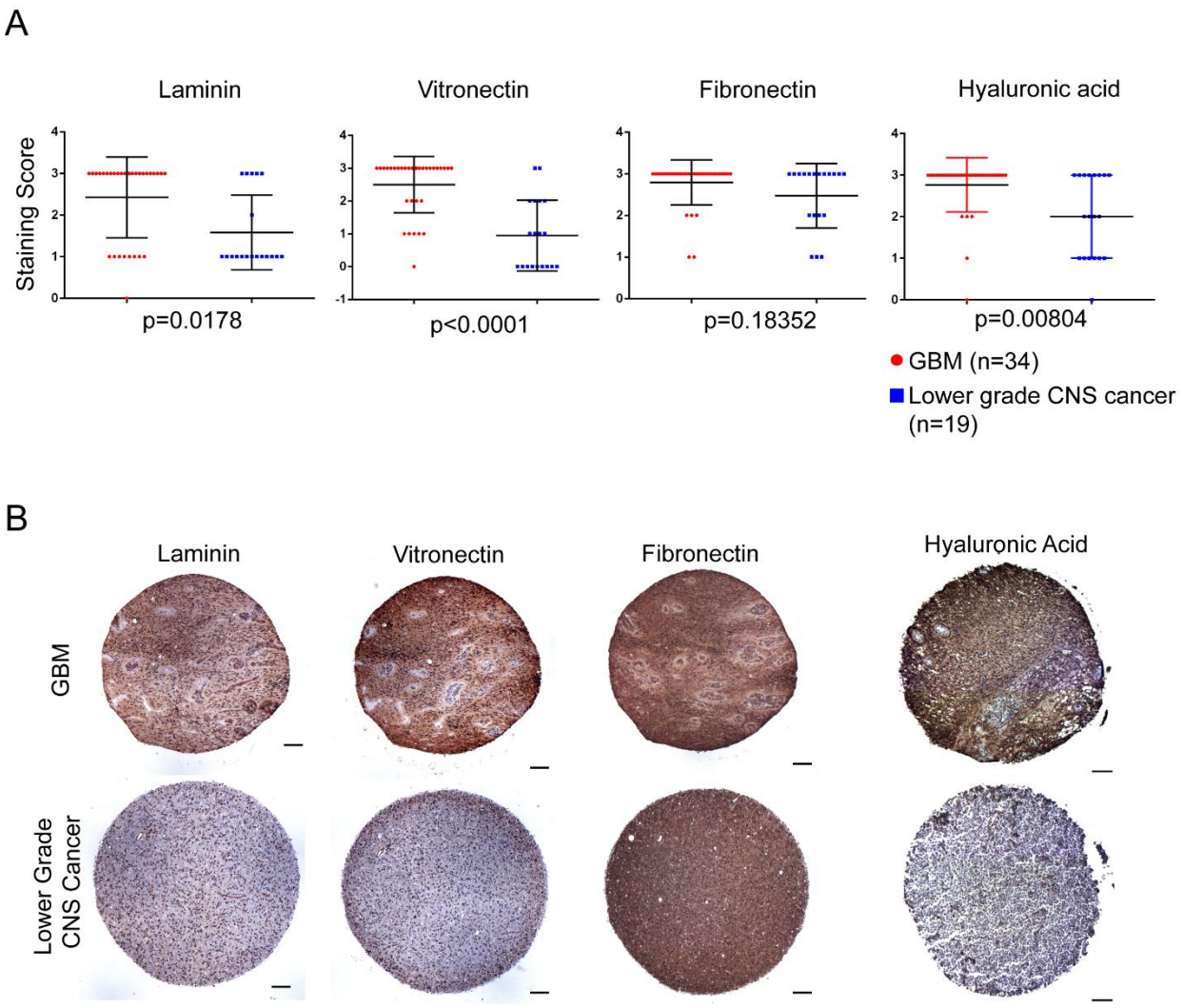

Figure 2.2. Some ECM components are significantly more expressed in GBM than other CNS cancers. A) Semi-quantitative scoring of IHC staining of TMA array samples from 34 GBM patients and 19 patients with lower grade CNS tumor. p value was calculated through Mann-Whitney U test. B) Representative images of IHC staining TMA slides. Brown, positive stain; dark blue, hematoxylin. Scale bar= 100µm.

Figure 2.3

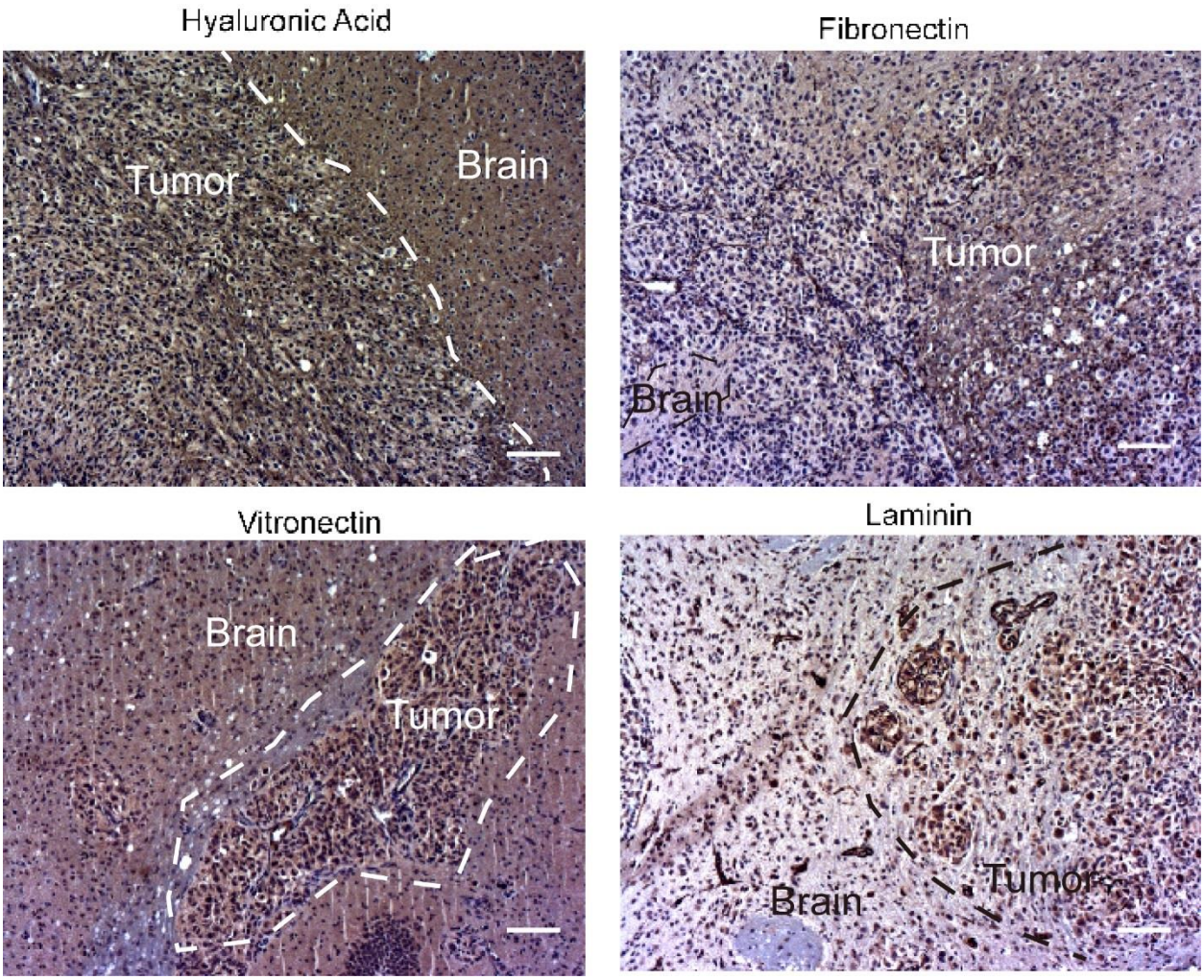

Figure 2.3. Representative ECM staining on intracranially implanted GBM39 samples. Brown, positive stain; dark blue, hematoxylin. Scale bar= 100μm.

Figure 2.4

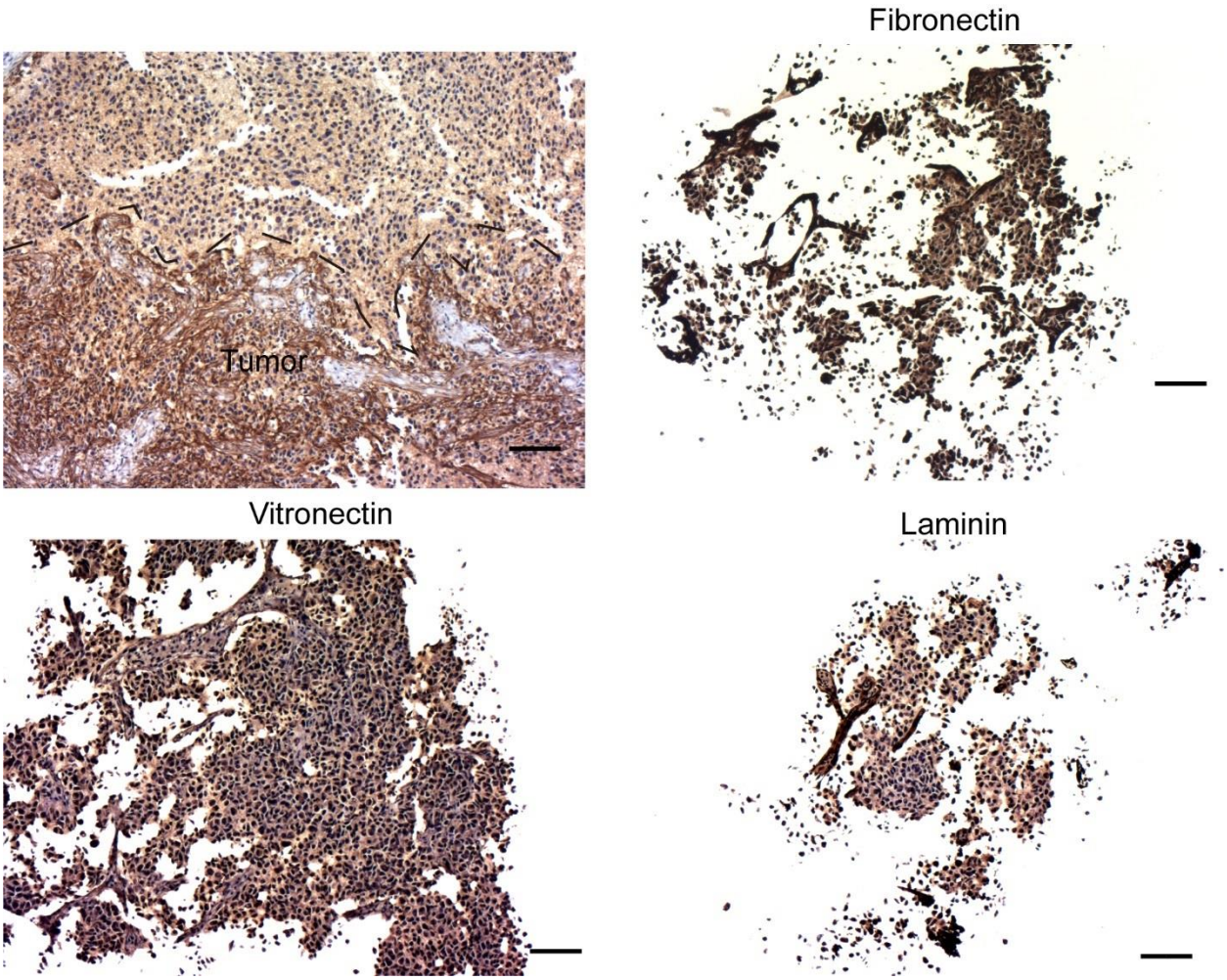

Figure 2.4. Representative ECM staining on subcutaneously implanted GBM39 samples. Brown, positive stain; dark blue, hematoxylin. Scale bar= 100µm.

Discussion and implications:

Our small-scale study confirmed several things. First of all, we confirmed that our selected set of ECM molecules are expressed at tumor locations. From the quantitative TMA analysis, the results indicated HA and the adhesive ECM proteins may contribute to tumor progression and worse prognosis outcome, consistent with previous studies[91,179,180], and these ECM proteins will potentially facilitates GBM progression. From the animal experiment, we found mouse brain provided a relatively ideal microenvironment for implanted cells, as presence of the ECM molecules could be observed around the tumor areas, indicating that trafficking mechanisms involving the cargo proteins are fully functional[182]. However, subcutaneously implanted GBM cells only “internally” expressed the adhesive ECM proteins, indicating lack of transportation mechanism to “deposit” the molecules to surrounding matrix. More interestingly, brain could provide matrix HA that is considered high molecular weight compared to low molecular weight HA fragments expressed by tumor itself [21,183]. More specifically, high molecular weight HA (500–1,000 kDa), which is found in abundance in native brain, suppresses the immune response, but 200 kDa HA stimulates cytokine production[184]. High molecular weight HA has also been reported to activate receptor tyrosine kinases (RTKs) more efficiently than HA with lower molecular weight chains[185]. Although some HA was detected in subcutaneously implanted GBM tumors, it is thought that tumors contain high amounts of low molecular weight of HA, which contribute to tumor growth and angiogenesis[21].

Together, the results above indicate that it is necessary to look for a specialized experimental model to include HA and adhesive molecules which could interact with

CD44 and integrins respectively. Moreover, it would be more interesting to compare GBM drug response between intracranially and subcutaneously implanted GBM cells, as the striking difference in ECM deposition pattern was observed.

Chapter 3

Construction of brain-mimetic hydrogel culture system

Based on knowledge that the specific set of ECM proteins like HA should be included in a new experimental model from previous chapters, we constructed a brain-mimetic, HA-based hydrogel 3D culture system that allows for independent control of HA concentration, mimetic adhesive peptide attachment and stiffness. In this chapter, method of material preparation, hydrogel fabrication and cell encapsulation for 3D culture will be introduced. Characterization of physical parameters including diffusion coefficient and Young's modulus will be presented. Validation of platform including viability and proliferation of encapsulated, patient-derived GBM cells will be shown. At last, immunostaining showing deposition of ECM inside hydrogel environment will be demonstrated.

Fabrication of HA-based hydrogel

The first step of hydrogel fabrication involves functionalization of carboxylate groups of HA polymer chain with thiol groups. To thiolate the carboxylate groups, sodium hyaluronate (HA, 700 kDa, LifeCore Biomedical, Chaska MN USA) was dissolved to 10 mg/mL in distilled, deionized water (diH_2O) until fully dissolved in around 2hrs. Here, the molar ratios are reported with respect to HA carboxyl groups. 1-ethyl-3-[3-dimethylaminopropyl] carbodiimide (EDC) was dissolved in diH_2O and immediately added to HA solution at the appropriate molar ratio (0.25 EDC:HA). N-hydroxysuccinimide (NHS) was then added to the HA solution (0.13 NHS:HA) in the similar way. Reaction solution was stirred at room temperature for 45 minutes while the

pH was maintained at 5.5. Cystamine dihydrochloride (Sigma-Aldrich, St. Louis, MO USA) was added (0.25 cystamine:HA), and the pH was adjusted to 6.25, and the reaction continued at room temperature overnight. Next day, dithiothreitol (DTT, Sigma-Aldrich) at pH 8.5 in diH_2O was added in excess (4x greater than amount of cystamine) and the solution stirred for at least 1 hour to cleave cystamine disulfides and yield thiolated HA. The reaction was quenched by change the pH of the reaction mixture to 4. The product was dialyzed against diH_2O (adjusted to pH 4 with 1M NaCl) for 3 days (MWCO 14 kDa). Purified HA-thiol was filtered through a 0.22 µm vacuum driven filter, lyophilized, and stored at -20°C in desiccated chamber. HA thiolation was confirmed using H^+-NMR spectroscopy and an Ellman's assay for free thiols as described previously[186].

ECM adhesive peptide was obtained from GenScript (Piscataway, NJ USA) with customized sequence NH_2-GCGYGRGDSP-COOH. To prepare solutions prior gelation, RGD peptide or free L-cysteine (Sigma-Aldrich) was dissolved in PBS at 2.8 mM and was mixed with 20 kDa, 4-arm PEG-maleimide (Laysan Bio, Inc. Arab AL USA) for 15 minutes at room temperature at final concentration of 280 µM. The modified PEG-mal solution was used to mix with dissociated GBM cells at a concentration of 1,000k/ mL. Thiolated HA was dissolved at 13.3 mg/ml in 20 mM HEPES buffer (pH 10), and the pH was adjusted to 6.8. A total of 40µL of the HA-thiol solution was mixed at a 3:1 volume ratio with 5 mg/ml or 40 mg/ml 20 kDa, 4-arm PEG-thiol (Laysan Bio). PEG-maleimide was then added in equal volume and hydrogels (80 µL per gel) were formed in silicone rubber molds (Grace BioLabs, Bend, OR, USA).

Physical characterization of hydrogel:

Mechanical characterization: Linear compressive modulus of hydrogels was tested at room temperature using an Instron 5564 material testing device attached to a 2.5 N load cell (Instron, Norwood, MA USA). Each hydrogel sample was compressed at a constant strain rate of 1 mm/min to at least 40% strain. BlueHill 2 software version 2.2.348 was used to acquire the data. Compressive testing was performed in at least quintuplicate per treatment group. Data were analyzed with Matlab software version R2015a 8.5.0.197613 (Mathworks, Natick, MA USA) to calculate Young's modulus from the linear portion of the slope of each stress-strain curve using the formula:

$E(Pa) = \sigma/\varepsilon$

where stress σ = force/surface area, and strain $\varepsilon = \Delta L/L_o$ (probe displacement of the hydrogel/the original height of the hydrogel).

Diffusion through hydrogels: Hydrogels were incubated with solution of 1 mg/ml dextran-fluorescein isothiocyanate (FITC) (20 kDa, 70kDa, and 150kDa) in phosphate-buffered saline at pH 7.4 for 3 days at 37 °C. After this period hydrogels were placed in PBS and 100 µl of the sample solutions was collected every 30 min for the duration of 4 hours. A final sample was collected at 24th hr. Fluorescence intensity (excitation at 490nm and emission at 525 nm) of each sample was read using plate reader (Biorad Synergy II, Hercules, CA USA) and then correlated to fluorescein concentration using a standard curve constructed by using known fluorescein concentrations.

$$\frac{M_t}{M_{inf}} = 2\left[\frac{D_e t}{\pi x^2}\right]^{1/2}$$

Effective diffusion coefficients (D_e) were calculated using Fick`s diffusion law, Where M_t is the mass of solute at time t, M_{inf} is mass of the solute in solution, D_e is the diffusion coefficient, t is time and x is the depth of the hydrogel as previously described[187].

Validation of cell behaviors:

GBM cell culture: Primary GBM cell lines GBM39, HK301, GBM6 and HK423 were used. HK301 and HK423 cells were generously provided by Dr. Harley Kornblum at UCLA. HK301 and HK423 lines were collected in April 2010 and October 2013, respectively, with strict adherence to UCLA Institutional Review Board protocol 10-000655[188]. GBM39 and GBM6 was collected in span of 1999–2006[106]. HK301 and HK423 cells were used between passages 15 and 25. GBM39 cells were used at fewer than 15 passages. All cell lines were authenticated previously by short-tandem repeat analysis [189]. Cell cultures routinely tested negative for mycoplasma contamination (Life Technologies, C7028). Cells (50,000/mL) were cultured in DMEM/F12 with 1xG21 (Gemini Bio), 1% penicillin/streptomycin (1x), 50 ng/ml EGF (Peprotech), 20 ng/mL FGF-2 (Peprotech), and 25 µg/mL heparin (Sigma-Aldrich). When gliomaspheres reached around 200 µm in diameter, they were dissociated into single cells in 1mL of TrypLE Express and filtered through 70-µm cell strainer. For hydrogel cultures, dissociated cells were resuspended in peptide-modified PEG-maleimide at 1 million cells/mL prior to mixing the HA-thiol/PEG-thiol to initiate crosslinking. The medium was replaced 4 days later.

Proliferation assay: Hydrogel cultures with encapsulated cells were placed in 1mL of Tryple Express at 37 °C for 5 min, then reaction was quenched with 4 mL of PBS

containing 1% BSA. The cell suspension solution was slowly passed through 20 G needle 10 times and then a 70 µm cell strainer to obtain single cells for flow cytometry. Gliomasphere culture was treated similar but not with 20G needle to disrupt the aggregations. 10µM of EdU (Abcam, Cambridge UK) was added to culture medium for 2.5 hours at 37 °C before cell extraction. Extracted single cells were fixed in 4% PFA for 15 min., then washed with 3 ml of 1% BSA in PBS. Fixed cells were permeabilized in 0.1% saponin and 1%BSA in PBS for 15 min., followed by incubation with 100 mM sodium ascorbate, 2 mM $CuSO_4$ and 1 µM Alexa Fluor 647 conjugated with azide (Life Technologies) in PBS for 30 min. at room temperature. Finally, cells were washed with 3mL of 0.1% saponin and 1%BSA in PBS and resuspended in 500µL of the washing buffer. Data were collected using Fortessa LSRII flow cytometer (BD Biosciences, Franklin Lakes, NJ USA) with proper and uniformed single cell gating methods.

Examination of cell viability: 24 hours after encapsulation, hydrogel cultures were soaked in prepared live/dead assay solution (Life Technologies L3224) for 30 mins at room temperature. Hydrogel cultures were then placed on rectangular coverglasses and imaged using Leica SP5 confocal microscopy.

Cryopreservation of hydrogel cultures for ECM staining: Hydrogel GBM cultures were fixed in 4% paraformlaldehyde (PFA) overnight at 4 °C. The next day, 4% PFA was replaced by 5% (w/v) sucrose in PBS 1 hr, followed by three 30 min. washes with 20% sucrose in PBS sufficient to immerse the whole gel, and finally 20% sucrose in PBS overnight. Hydrogels were embedded in 20% sucrose in O.C.T. at 4 °C for at least3 hrs. Frozen blocks were Cryo-sectioned at 18 µm by UCLA Tissue Pathology Core Laboratory (TPCL). Gliomasphere cultures were fixed and sectioned for staining in the same manner.

For hydrogel samples preserved in paraffin, paraffin embedded samples were sectioned at 10μm by UCLA TPCL.

RNA extraction and sequencing: Total RNA of hydrogel cultured cells and gliomaspheres were extracted using RNeasy extraction kit (Qiagen) following manufacture suggested protocol. Total RNA sample was sequenced by UCLA Technology Center for Genomics & Bioinformatics (TCGB) core facility. Libraries for RNA-Seq were prepared with Nugen Universal Plus Kit. The workflow consisted of mRNA enrichment, cDNA generation, and end repair to generate blunt ends, A-tailing, adaptor ligation and PCR amplification. Different adaptors were used for multiplexing samples in one lane. The data was sequenced on Illumina HiSeq 3000 for a pair-end 150bp run. Data quality check was done on Illumina SAV. Demultiplexing was performed with Illumina Bcl2fastq2 v 2.17 program. The reads were mapped to the latest UCSC transcript set using Bowtie2 version 2.1.0[190] and the gene expression level was estimated using RSEM v1.2.15[191]. TMM (trimmed mean of M-values) was used to normalize the gene expression. Gene Set Enrichment Analysis (GSEA) 3.0 was used to analyze the normalized TMM values from the gene expression profile RSEM data performed on GS024 and GS025. All signals were analyzed based on gene sets from h.all.v6.2 symbols and HuGene 2.0 chip set from broad institute. Gel and xenograft conditions were compared to gliomasphere conditions. The GeneSet permutation was selected as the method for calculation of statistical values to evaluate the significance of GeneSet enrichment between culture conditions.

Gel fabrication and characterization results:

High molecular weight (HMW) HA (~700 kDa), which induces CD44 clustering to achieve distinct biological effects from its low molecular weight counterparts[184], was used to best mimic the native brain ECM. HA was modified with thiol groups to enable crosslinking via maleimide groups on polyethylene glycol (PEG) macromers. Thiol groups were conjugated to approximately 5% of HA disaccharides through modification of carboxylates on N-glucuronic acid **(Figure 3.1)**. Using the fabrication methods described above **(Figure 3.2)**, hydrogels encapsulating single GBM cells can be formed rapidly within seconds **(Figure 3.3)**.

Hydrogel mechanical properties were also selected to best mimic native brain, which exhibits a linear compressive modulus around 1 kPa and a shear elastic modulus around 200 Pa as previously described[159,192,193]. The concentration of HA was altered independently of stiffness by substituting bioinert/biocompatible PEG-thiol for HA-thiol to maintain a constant total polymer content and molar ratio of thiols to maleimide groups for crosslinking (**Figure 3.2**). **Figure 3.4** demonstrates that increasing total PEG concentration from 0.5% (w/v) to 1% (w/v) yields hydrogels that are twice as stiff—around 1 kPa and 2 kPa linear compressive moduli, respectively—while keeping HA concentration constant at around 0.5% (w/v). In addition, HA concentration was lowered to 0.1% (w/v) while maintaining a linear compressive modulus of 1 kPa (981Pa).

Figure 3.1

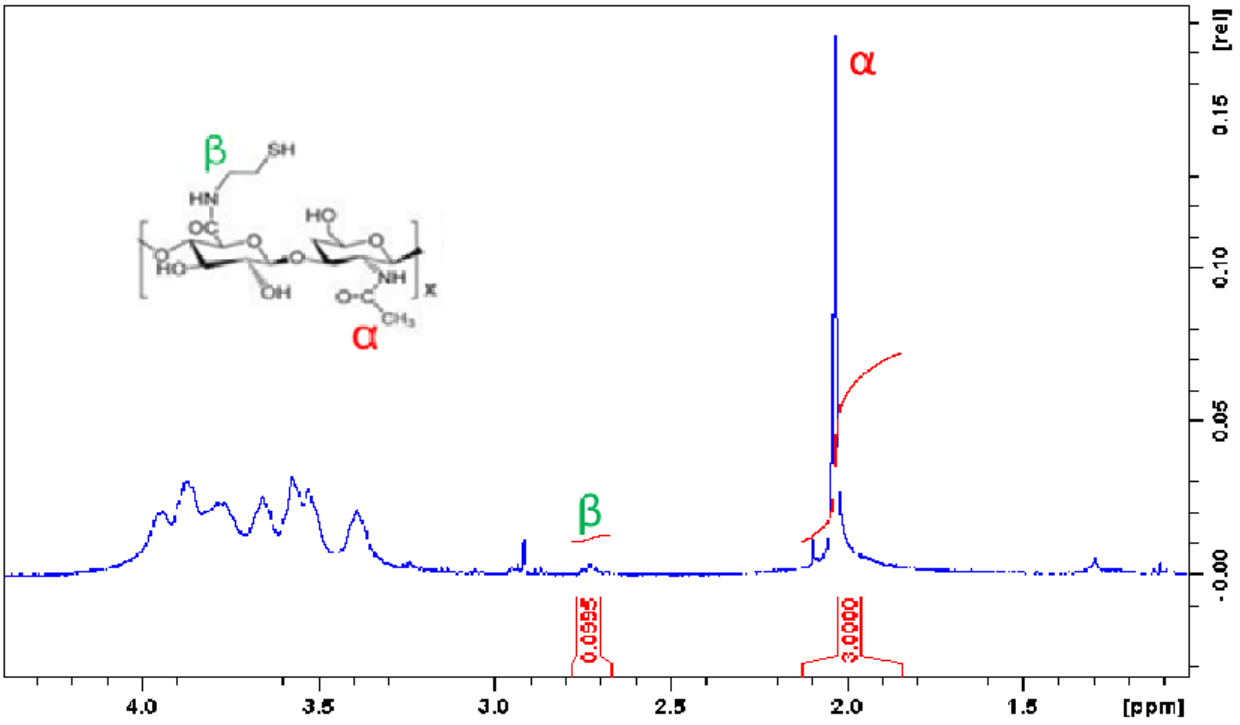

Figure 3.1. Successfully thiolated HA probed by proton-NMR. Representative proton-NMR spectrum of thiolation, indicating that approximately 5% of glucuronic acid groups on HA have been modified with a thiol.

Figure 3.2

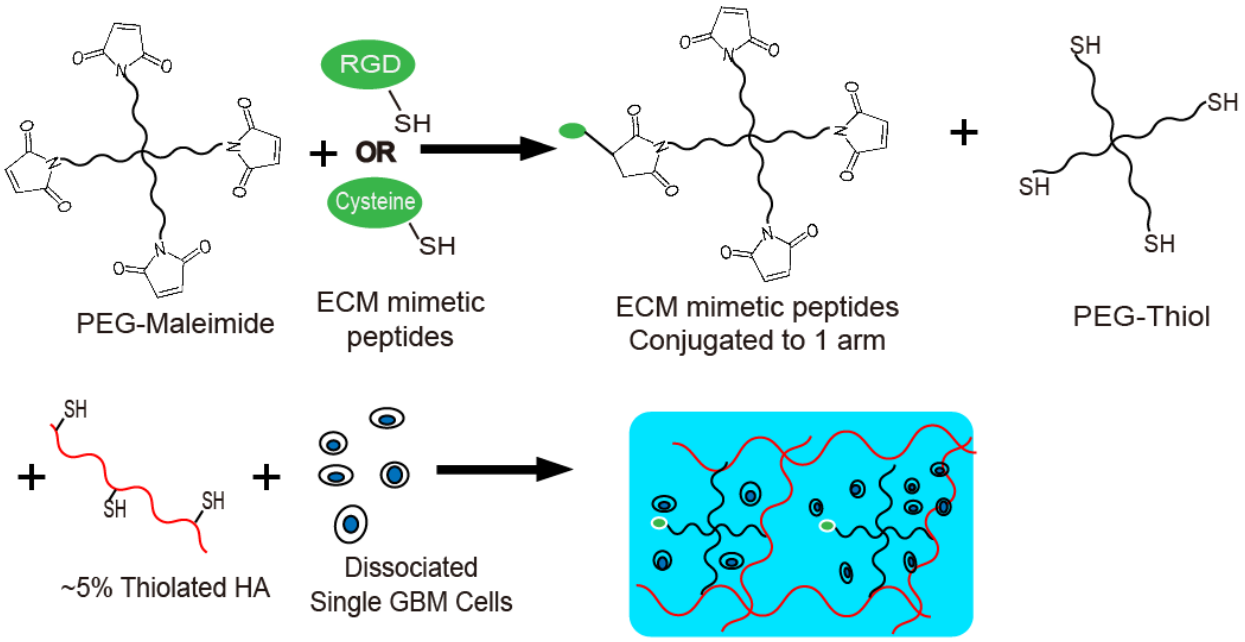

Figure 3.2. Fabrication of HA based hydrogel. Schematic of hydrogel encapsulation of GBM cells for 3D culture. Cysteine-bearing peptides were first conjugated to PEG maleimide. Single GBM cells were resuspended in PEG maleimide-peptide before mixing with PEG thiol and 5% thiolated HA. Molar ratio of thiol to maleimide was maintained at approximately 1.1 to 1.

Figure 3.3

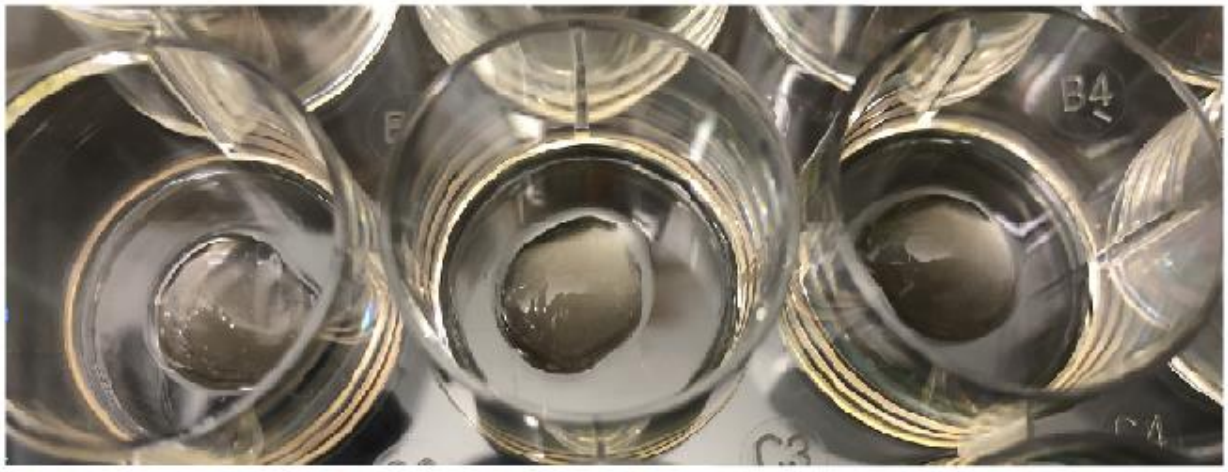

Figure 3.3. Example photograph images of fabricated 80 µL gels in 12-well plates. After crosslinking, hydrogels were swollen in cell culture medium.

Figure 3.4

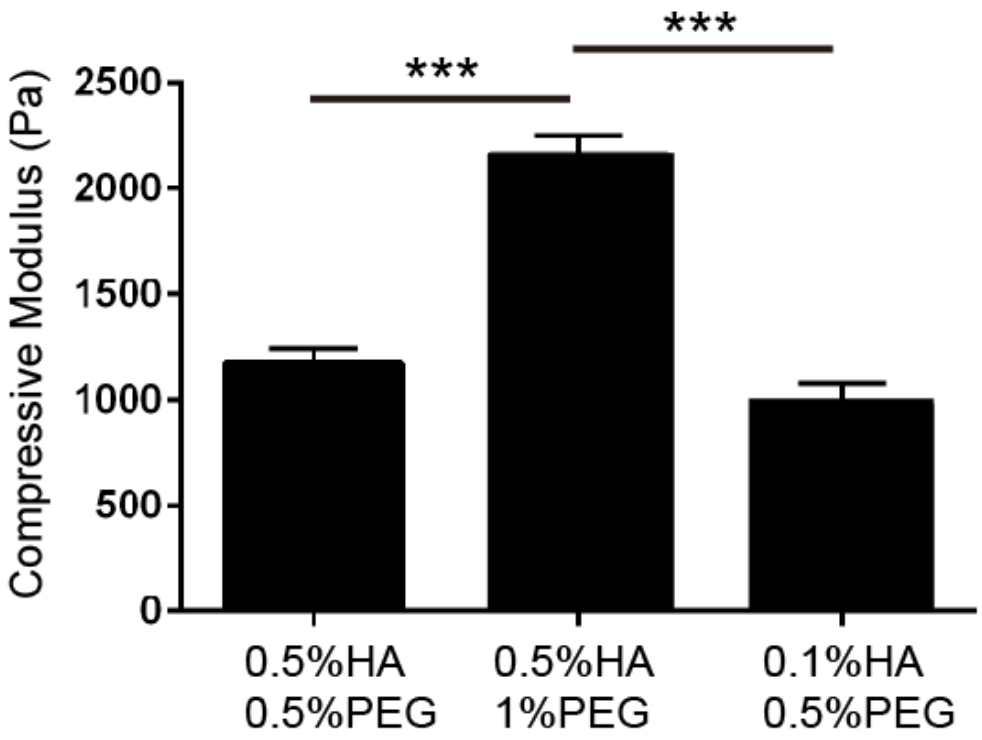

Figure 3.4 Linear compressive moduli of hydrogels indicate orthogonal tunability of hydrogel system. Percentages indicate weight to volume ratios (w/v). Error bars, SEM (n=3, average from 3 independent repeats). Statistics: one-way ANOVA with Tukey test for multiple comparisons was performed (***, $p<0.001$).

As higher compressive moduli were achieved by increasing total polymer content, there remained a possibility that diffusion of key molecules, such as erlotinib and growth factors, would vary between softer and stiffer hydrogels, resulting in unequal drug/biochemical penetration. To evaluate this possibility, diffusion of fluorescent dye-labeled dextrans of varying molecular weights through hydrogels was quantified (**Figure 3.5**). For 20 kDa and 70 kDa dextrans, effective speed to diffuse through the 1 kPa and 2 kPa hydrogels were statistically equivalent. For all hydrogel formulations, diffusive equilibrium (i.e., M_t/M_{inf} reaching 1) was reached by around 7 hours for 20 kDa and around 11 hours for 70 kDa dextrans. An upper size limit was found at 150 kDa, which did not diffuse into any of the hydrogels (data not shown). This result indicates that the hydrodynamic radius of 150 kDa dextran is larger than the hydrogel mesh size. Our results confirm that availability and penetration of nutrients, FGF-2 and EGF (<15 kDa), and erlotinib (around 300 Da), was equivalent for all hydrogel cultures investigated.

To verify maintenance of viability and proliferation of hydrogel encapsulated GBBM cells, a live/dead assay performed 24 hours after cell encapsulation confirmed that the majority of cells remained viable in all hydrogel conditions (**Figure 3.6**). Using an EDU-based assay to quantify numbers of actively proliferating cells, we found that approximately 20% more HK301 cells entered S-phase within a 2.5 hours period when cultured in 3D than when cultured as gliomaspheres ($P < 0.05$; **Figure 3.7**). We also confirmed that variations in HA content or compressive modulus had no significant effects on cell proliferation.

Figure 3.5

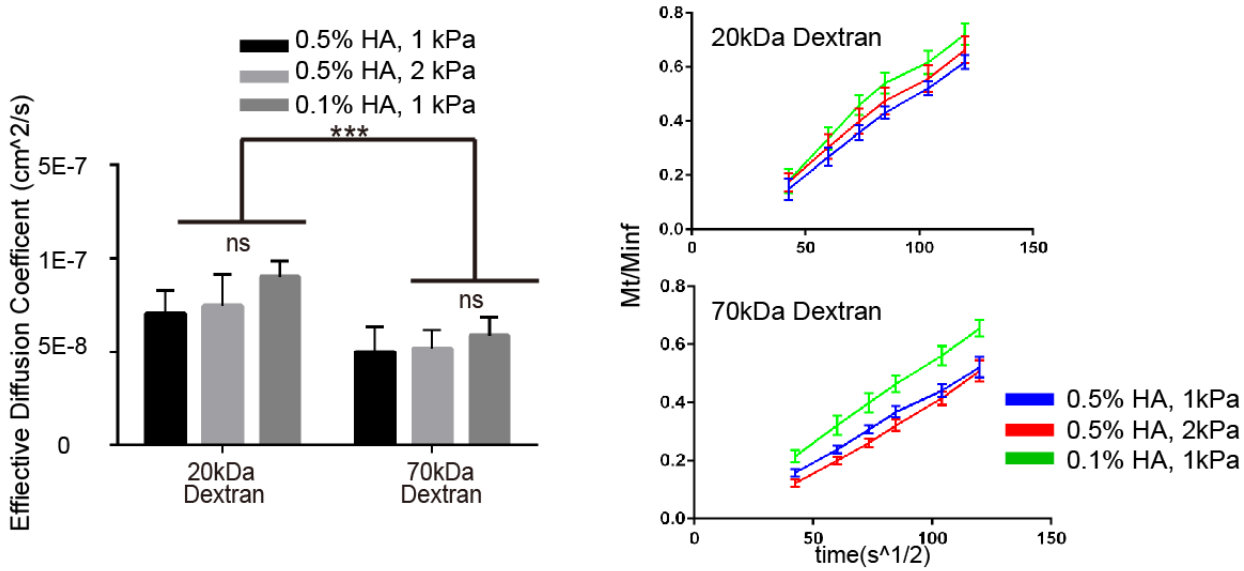

Figure 3.5. Diffusion coefficients of different hydrogel formulations are same. Left panel, effective diffusion coefficients (cm^2/s) for 20 kDa and 70 kDa dextrans, respectively, through 3 different hydrogels. Statistics: Two-way ANOVA with Tukey test for multiple comparisons was performed (***, $P < 0.001$). Error bars, SEM (n= 3). Right panel, diffusion over time of dextran through HA hydrogels. M_t/M_{inf} is defined as the ratio of dextran released at a specific time (M_t) to the total amount of dextran released at infinite time (M_{inf}). M_t/M_{inf} is plotted against the square root of time ($s^{1/2}$) so that the slope indicates diffusion rate. HA percentage indicates volume to weight percentage (w/v). ns, nonsignificant.

Figure 3.6

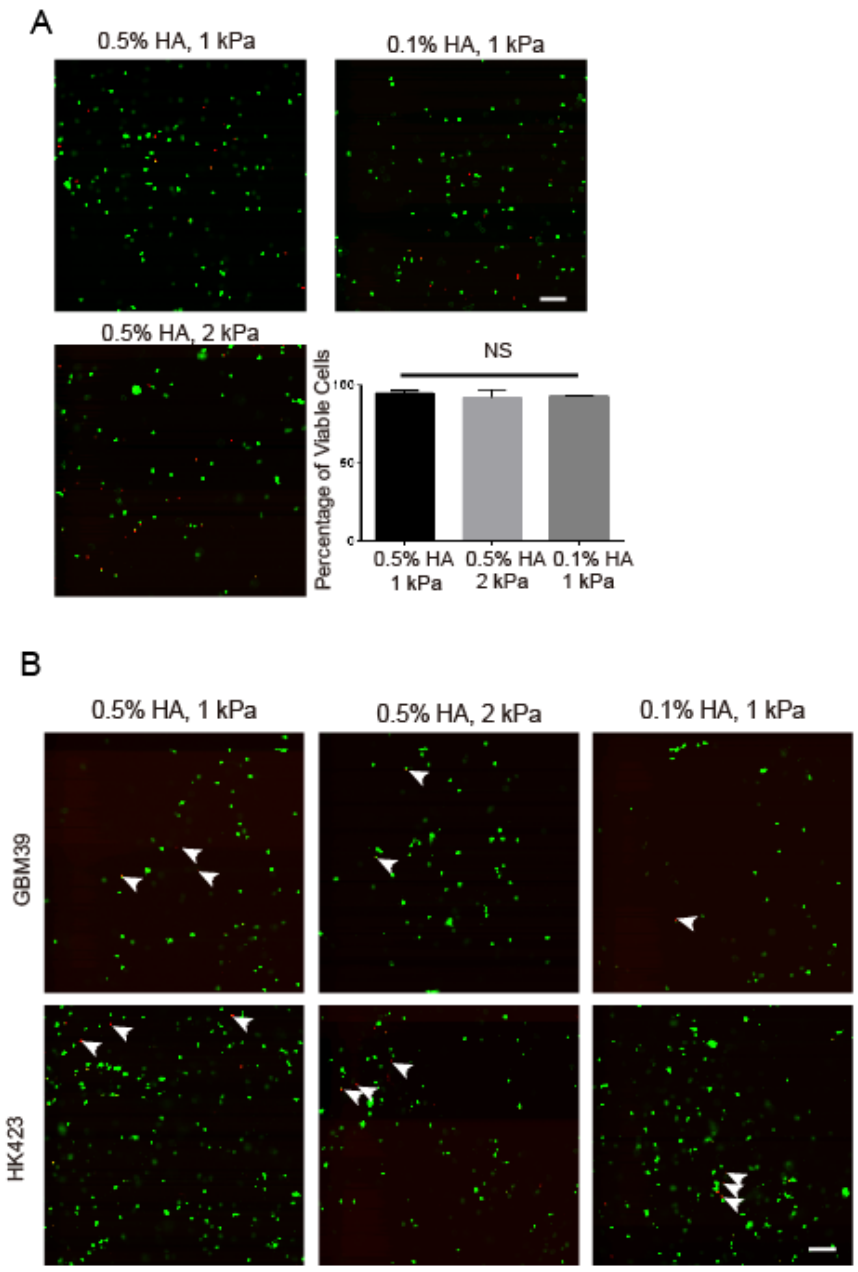

Figure 3.6. High viability of encapsulated GBM cells. A) Representative confocal microscopy images showing live (green) and dead (red) cells 24 hours after hydrogel encapsulation of HK301 cells. Scale bar, 100 µm. Quantification of the percentage of viable cells (HK301) 24 hours after encapsulation is shown on the lower right. Error bar, SEM (n=3). One-way ANOVA with Tukey multiplicity test was performed. NS, nonsignificant. B) Representative confocal microscopy images showing live (green) and dead (red) cells 24 hours after hydrogel encapsulation of GBM39 and HK423 cells. Scale bar, 100 µm. Arrows indicate dead cells.

Figure 3.7

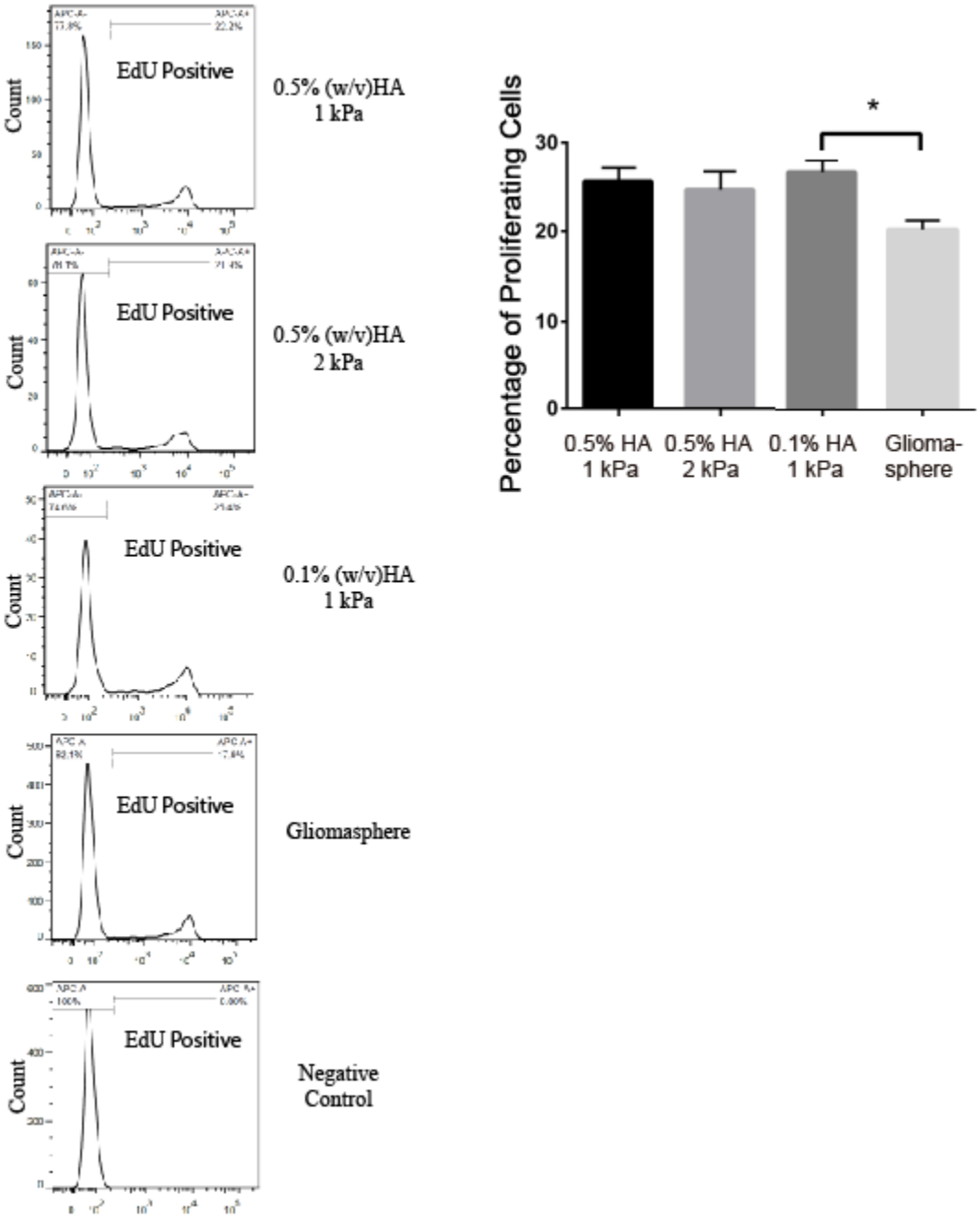

Figure 3.7. High proliferation rate in encapsulated GBM cells. Left panel, representative results of proliferation rate measured using flow cytometry. GBM cells (HK301) were incubated with 1 μM EdU (5-ethynyl-2′-deoxyuridine) for 2.5 h on the fourth day after encapsulation or passaging. A click-reaction was used to conjugate fluorescent dye to

incorporated EdU. Right panel, summarized data of proliferation of HK301 cells. N=3. Statistics: one-way ANOVA with Tukey test for multiple comparisons was performed (*, $P < 0.05$).

To make direct observation of the biochemical effect of hydrogel to encapsulated GBM cells, we surprisingly found GBM cells displayed invasive morphology only in high HA content (0.5% w/v HA) hydrogel incorporated with RGD mimetic peptide (**Figure 3.8A**). This result indicated possible cooperative effect of HA and adhesive ECM molecules to mediate GBM cell morphologies. Effect of RGD incorporation was further confirmed when cells abolished invasive morphology upon addition of cilengitide to the culture medium to competitively replace the engagement between integrin and RGD segment incorporated in nonsoluble phase of the hydrogel, which transduce a force equivalent to stiffness of the hydrogel through integrin binding (**Figure 3.8B**).

We then performed immunostaining of HA receptor CD44. The result indicated culture in hydrogels with high HA (0.5% w/v) induced higher CD44 expression compared with culture in hydrogels with low HA (0.1% w/v) or gliomaspheres (**Figure 3.9**). These results are consistent with murine xenograft results, which will be discussed in future chapters. In a long-term culture (2.5 weeks) experiment with 3 cell lines, we found differential “intra-tumoral” expression of CD44 in hydrogel (0.5% w/v HA) cultured samples (**Figure 3.10**). The result indicated hydrogel culture may restore a heterogeneity stage to cells in a tumor bulk.

Figure 3.8

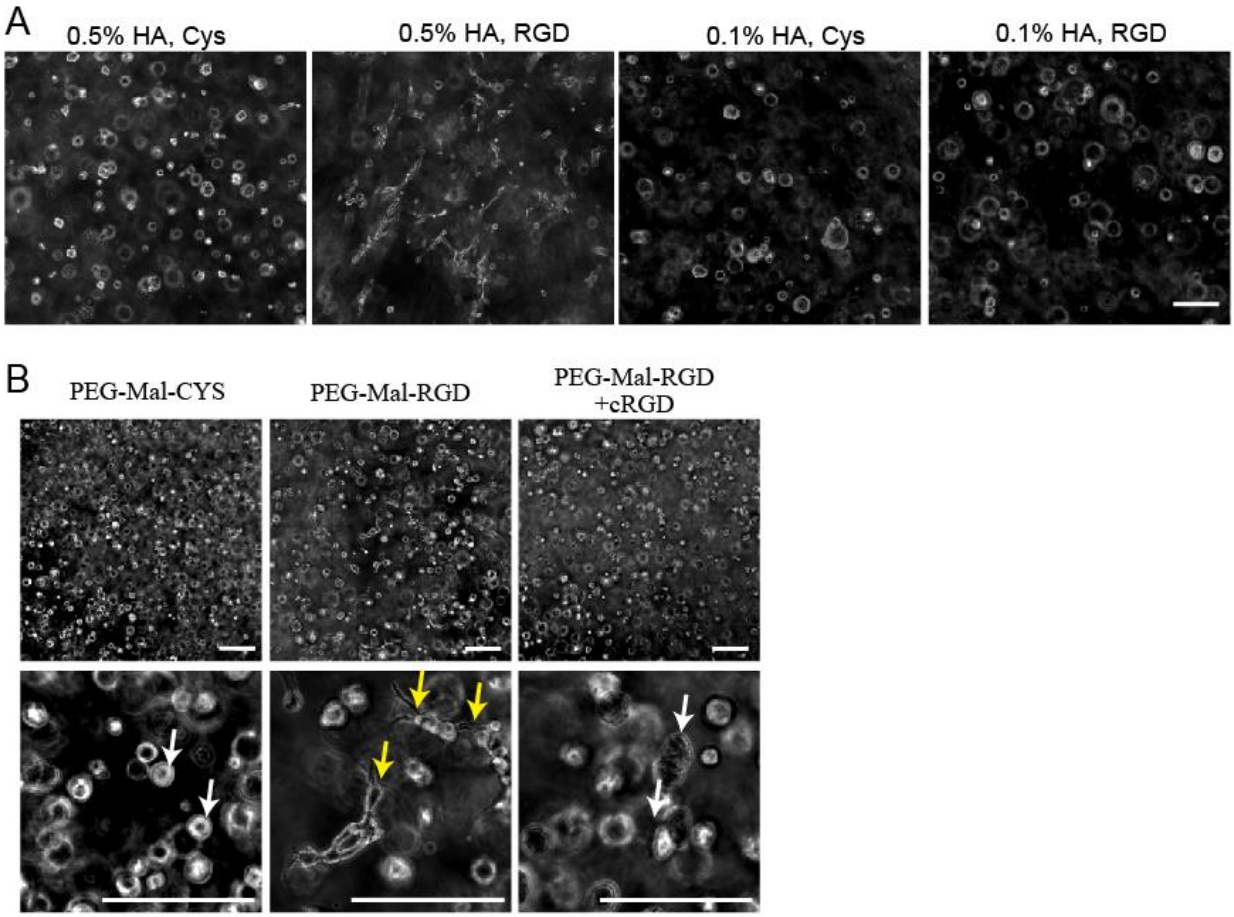

Figure 3.8. HA content and RGD incorporation cooperatively influence morphology of encapsulated GBM cells. A) Representative phase contrast images of hydrogel-cultured cells 8 days after encapsulation. Percentage indicates weight volume (w/v). B) Representative phase contrast images of 0.5% (w/v) HA hydrogel-cultured cells under varying conditions for 8 days after encapsulation. Yellow arrows indicate cells with an invasive morphology, and white arrows indicate cells with spherical morphology. cRGD group was treated with 50μM cilengitide 24hr prior to imaging. Scale bars= 200μm.

Figure 3.9

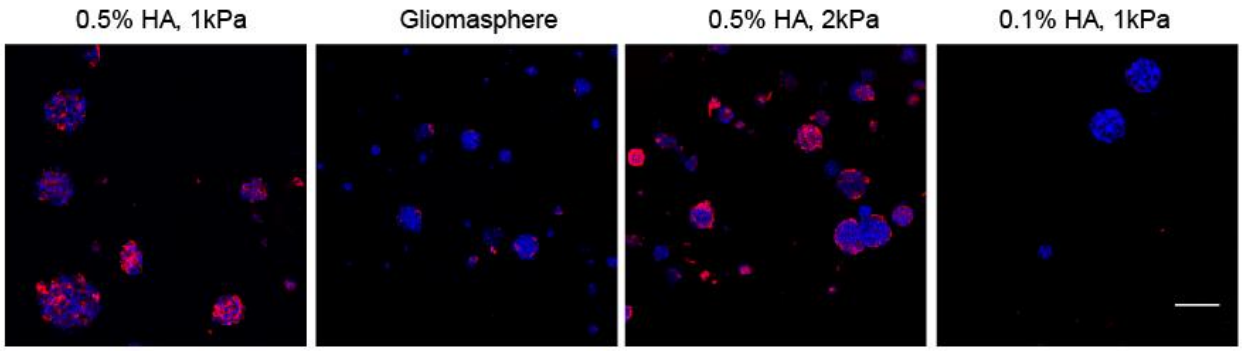

Figure 3.9. Expression of CD44 is ECM dependent in encapsulated HK301. Representative images of immunofluorescence staining for CD44 (red) in cryosectioned hydrogel and gliomasphere cultures of HK301 cells. Scale bar, 100 µm. HA percentage indicates volume to weight percentage (% w/v).

Figure 3.10

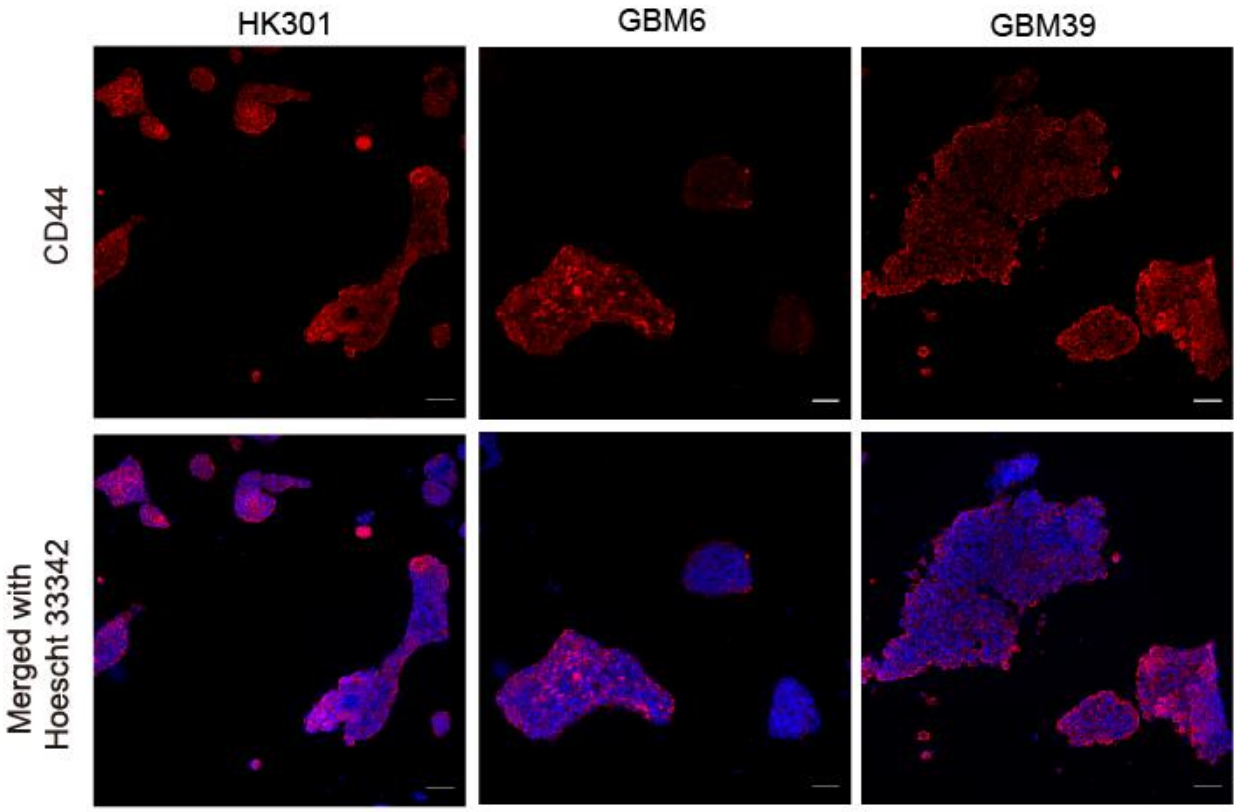

Figure 3.10. Intratumoral differential expression of CD44 is observed in HA hydrogel cultured samples. Representative images of immunofluorescence staining for CD44 (red) in cryosectioned hydrogel cultures of HK301, GBM6 and GBM39 cells 2.5 weeks after encapsulation. Scale bar, 100 µm.

A more exciting features of hydrogel 3D culture is that the tumor cells can change their surrounding matrix microenvironment. Therefore, deposition of ECM was investigated. We found GBM cells were able to express and deposit various ECM proteins relating to GBM progression as introduced in previous chapters through both DAB and fluorescence-based staining (**Figure 3.11, Figure 3.12, Figure 3.13**). In a closer look to different cell lines, we also found differential intratumoral expression of ECM proteins (**Figure 3.12, Figure 3.13**), as some ECM proteins were preferentially located at edge or core of the “tumor bulks” instead of a uniform distribution, which further implied possibility of heterogeneity restored by hydrogel culture. At last, orthogonal tuning of hydrogel by RGD incorporation also resulted in increased expression of ECM proteins such as vitronectin (**Figure 3.14**). This result indicates GBM cells may alter ECM expression in different matrix environments.

All these results suggested possible alterations of global gene expressions caused by ECM components in our 3D hydrogel. Therefore, RNA sequencing quantifying global gene expression was performed. In comparison among intracranial xenograft, gliomasphere and hydrogel cultures, we performed a principal component analysis that captures more than 95% variation between samples (**Figure 3.15**) and found that gliomasphere culture caused significant expression drift. However, hydrogel culture restored some features of xenograft that were lost in gliomaspheres. While several ECM related genes were revealed in differential expression analysis (**Figure 3.16** left panel), many gene sets related to cellular fate such as hypoxia induced events, TNF and epithelial mesenchymal transition (EMT) are more enriched in xenograft/hydrogel culture when compared to gliomasphere cultures (**Figure 3.16** right panel).

Figure 3.11

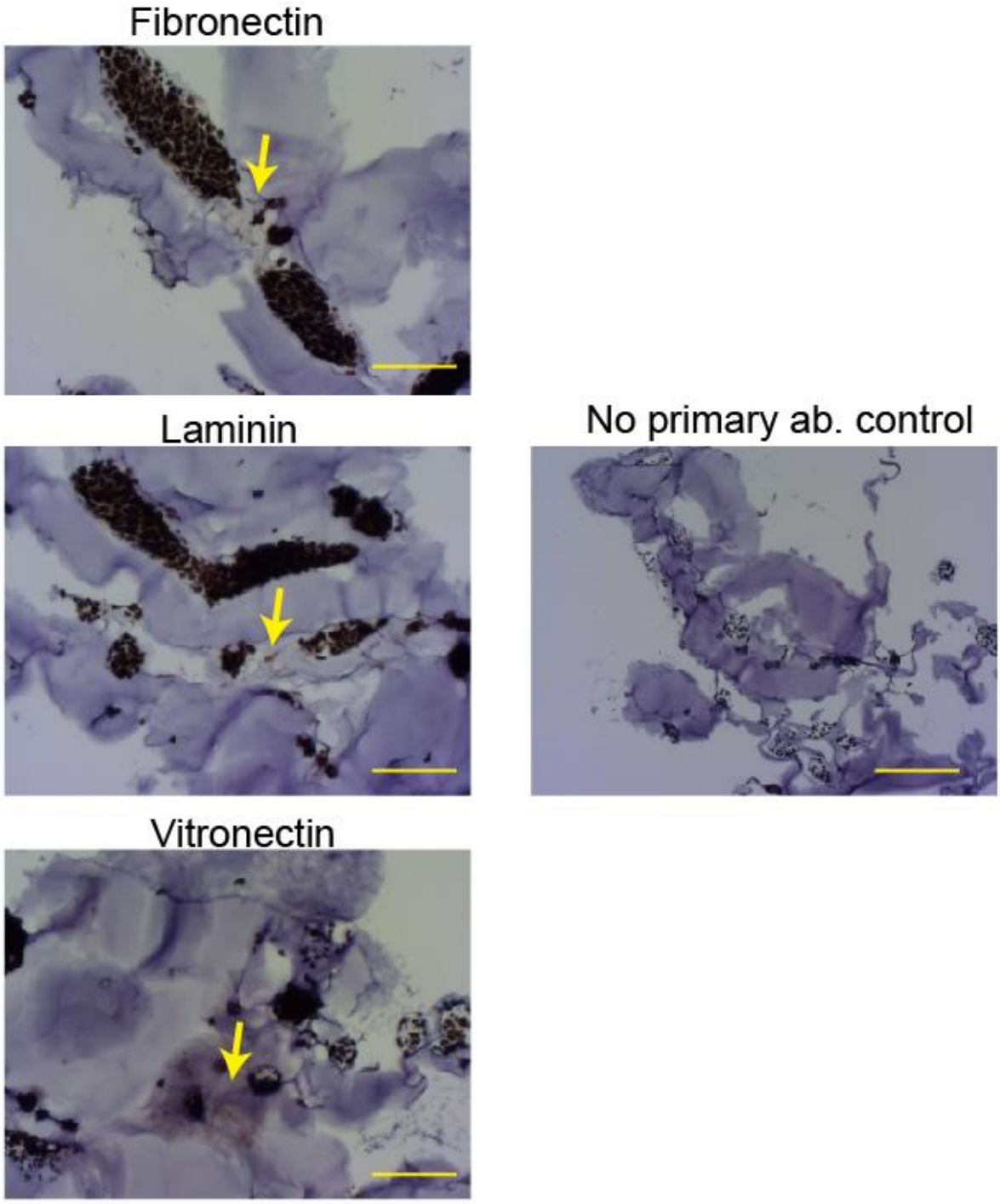

Figure 3.11. Deposition of ECM proteins in encapsulated GBM6. Representative DAB staining images of 0.5% (w/v) HA cultured GBM6 cells (2 weeks after encapsulation) embedded in paraffin. Arrows indicates deposition of ECM proteins (brown) in extracellular regions. Scale bar, 100µm.

Figure 3.12

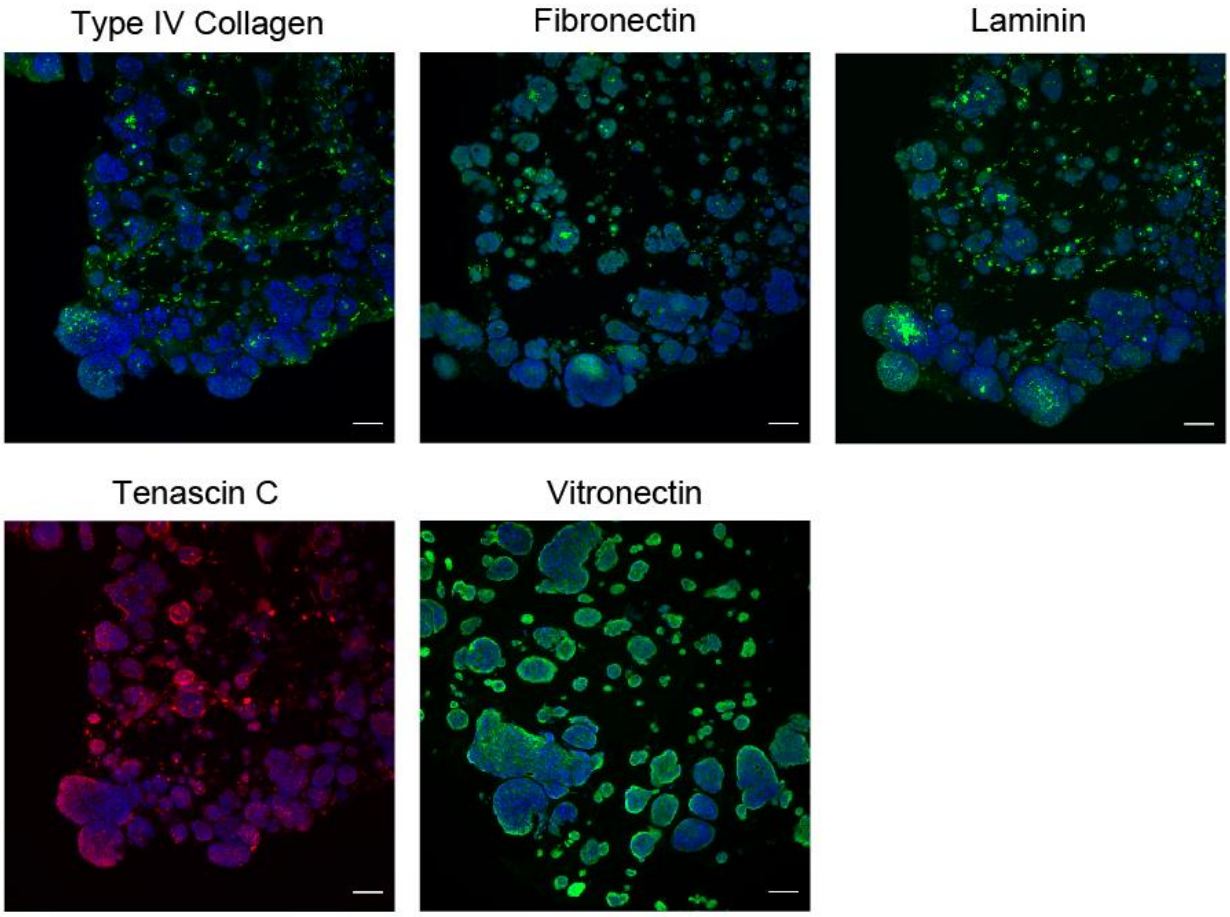

Figure 3.12. Deposition of ECM proteins in encapsulated HK301 cells. Representative images of immunofluorescence staining for ECM proteins (green or red) in cryosectioned hydrogel cultures of HK301 cells (2 months after encapsulation). Scale bar, 100 µm.

Figure 3.13

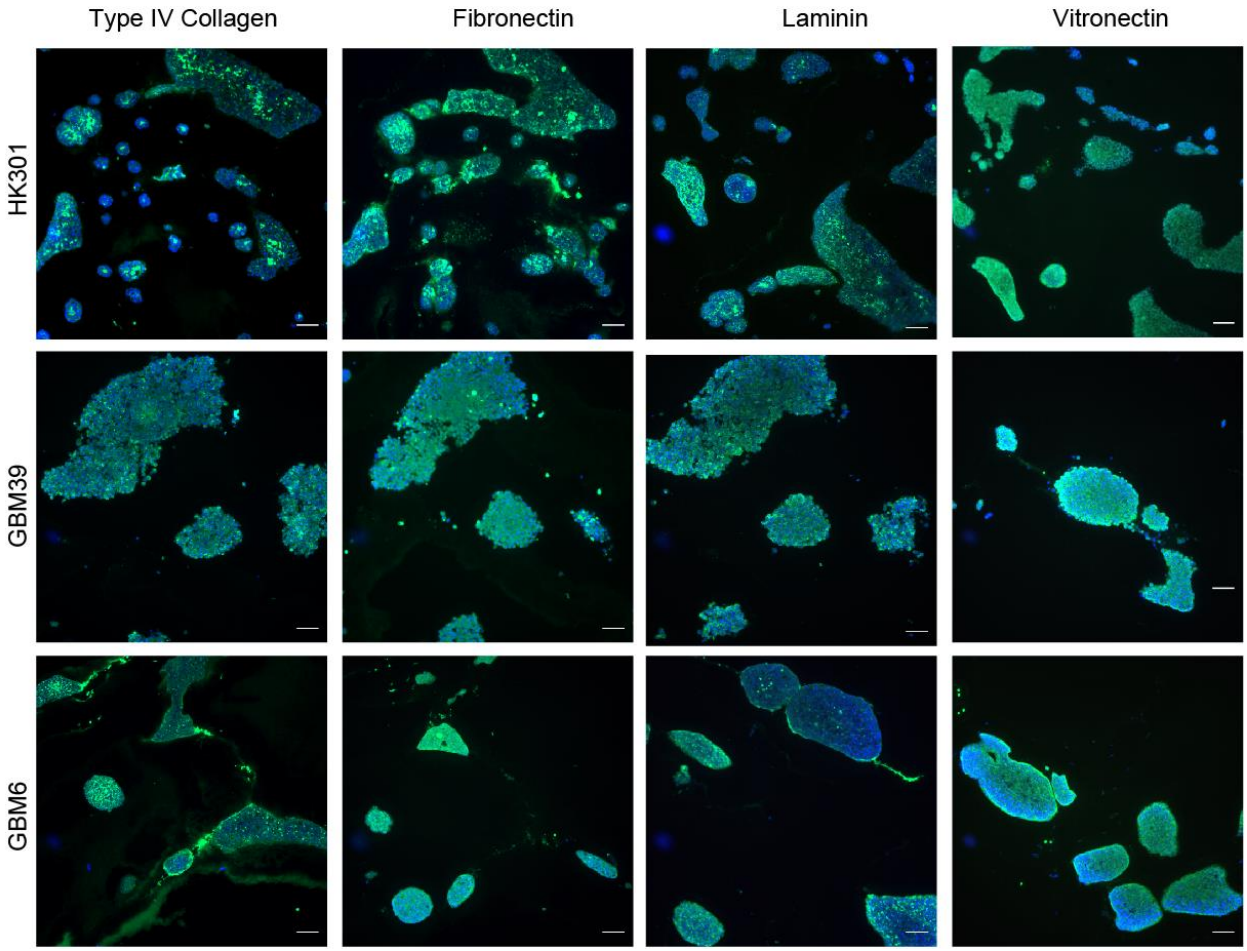

Figure 3.13. Differential expression and deposition of ECM proteins in encapsulated HK301, GBM39 and GBM6 cells. Representative images of immunofluorescence staining for ECM proteins (green) in cryosectioned hydrogel cultures of GBM cells (2.5 weeks after encapsulation). Scale bar, 100 μm.

Figure 3.14

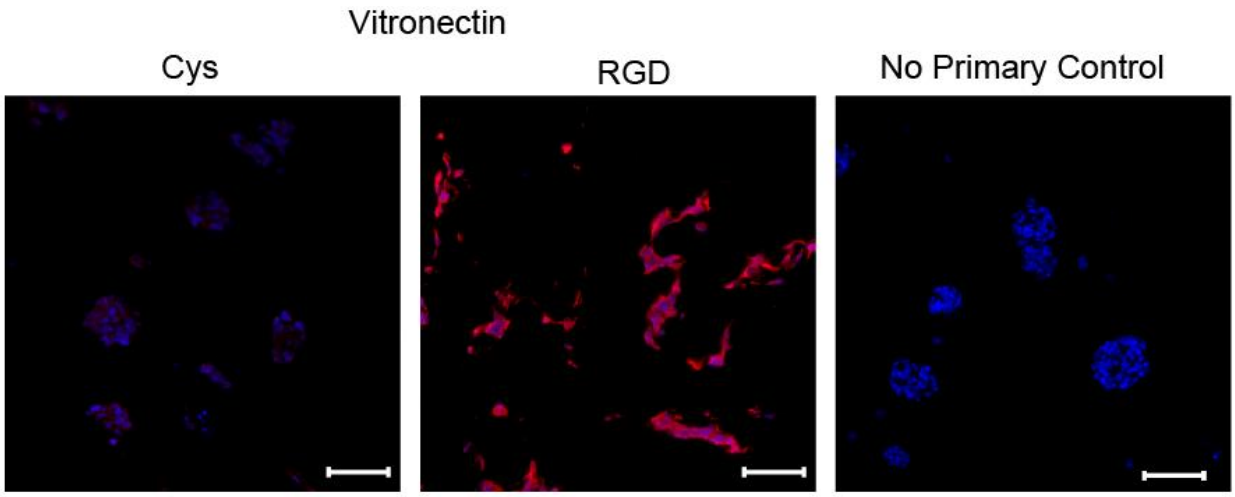

Figure 3.14. Differential expression and deposition of vitronectin in encapsulated HK423 cells. Representative images of immunofluorescence staining for vitronectin (red) in HK423 cultured in cryosectioned hydrogels incorporated with cysteine or RGD peptide for 8 days. Scale bar, 100 μm.

Figure 3.15

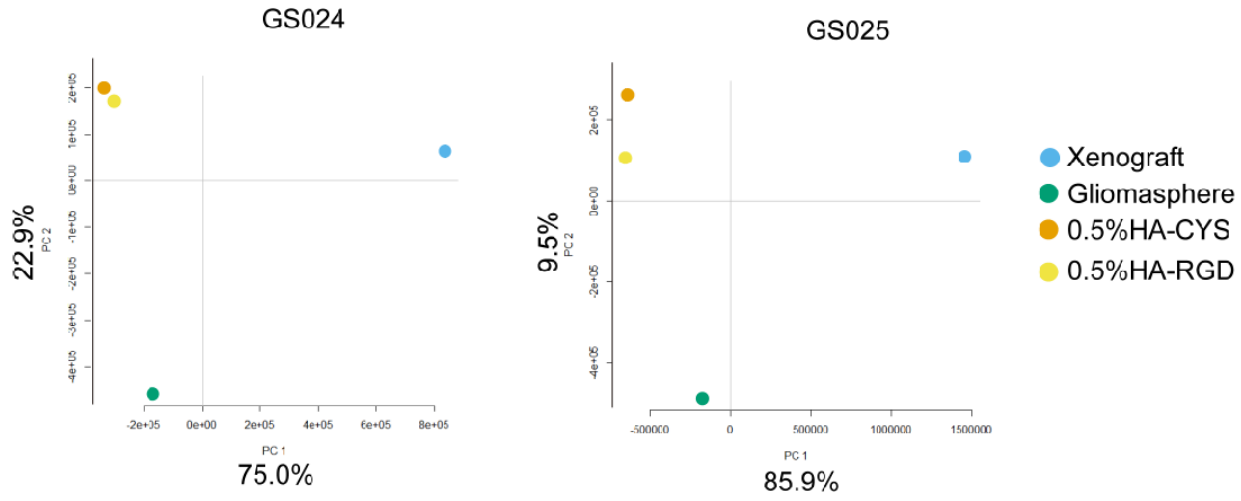

Figure 3.15. Hydrogel culture restores gene expression pattern similar to those in xenograft cultures. PCA analysis of RNA sequencing data. Principal Component Analysis (PCA) plot was constructed based on individual samples gene expression profiles. Numbers in x and y axis show percentage of variation accounted in the graphical representation.

Figure 3.16

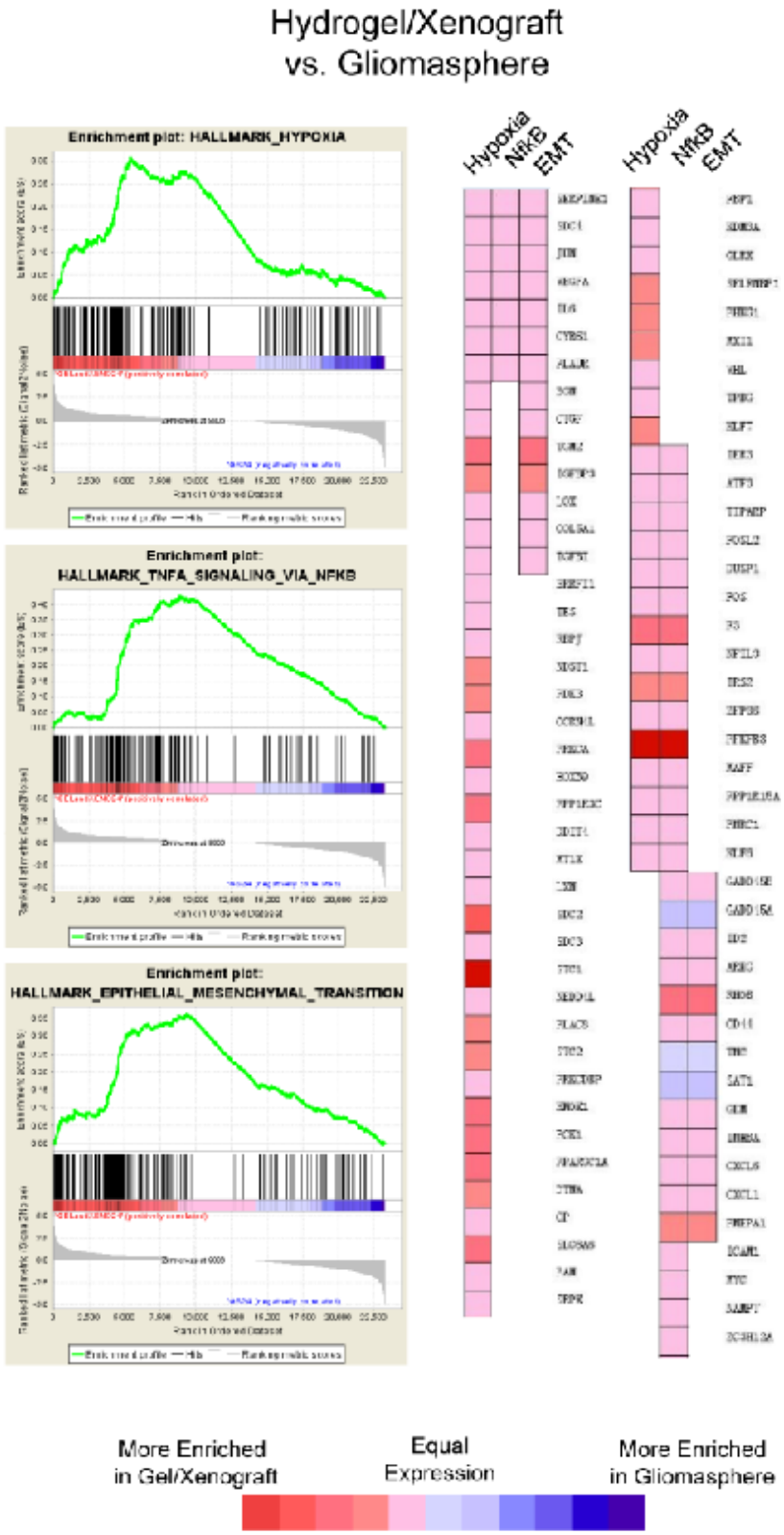
Hydrogel/Xenograft
vs. Gliomasphere
Enrichment plot: HALLMARK_HYPOXIA
Enrichment plot:
HALLMARK_TNFA_SIGNALING_VIA_NFKB
Enrichment plot:
HALLMARK_EPITHELIAL_MESENCHYMAL_TRANSITION
Hypoxia
NfkB
EMT
Hypoxia
NfkB
EMT
More Enriched
in Gel/Xenograft
Equal
Expression
More Enriched
in Gliomasphere

Figure 3.16. GSEA comparison of encapsulated cells and gliomasphere. On the left panels, for selected representative gene sets (Hypoxia, TNF-nfkb and epithelial mesenchymcal transition (EMT)) in GS024 cell line, enrichment plots are shown for the comparison between the conditions (Gel+Xenograft vs. Gliomasphere). The horizontal bar in graded color from red (left) to blue (right) represents the GeneList ranked from high expression in the subset indicated on the left to high expression in the subset indicated on the right. Equivalent expression between subsets is reached at the red to blue border. The vertical black lines represent the projection onto the ranked GeneList of the individual genes of the gene sets. The curve in green corresponds to the calculation of the enrichment score (ES) that reflected correlation of the genes with the phenotype. The bold horizontal line indicates the 0 value for the ES. The more the green ES curve is shifted to the upper left of the graph, the more the GeneSet is enriched in the red subset. On the left panels, representative individual genes from leading edge analysis that are more enriched in Gel+Xenograft compared to gliomaspheres are shown as heat map.

Discussion:

In this chapter, we constructed a novel hydrogel platform with several key features. First, HA was minimally modified (only around 5% of disaccharides contain a thiol substitution) to maintain the native ability of high molecular weight HA to interact with CD44 receptors. In contrast, other methods often modify up to 70% of HA disaccharides as described in previous chapters. Second, while previous methods have relied on HA polysaccharides with molecular weights at or below 200 kDa, we incorporated HAwith a range of high molecular weights from 500–750 kDa. In previous study, this size difference has significant effects on HA bioactivity[184,185] as described in previous chapters. Third, the biomaterial platforms reported here achieved effective decoupling of HA content, stiffness, availability of integrin binding sites and diffusion (**Figure 3.2-3.5**). Previously reported methods for HA hydrogel fabrication typically increased hydrogel stiffness by increasing HA concentration, and thus total polymer content including bioactive components[123,159]. Another common method substitutes gelatin to vary HA concentration without altering total polymer content; however, gelatin is not considered biologically inactive material since it contains RGD sites[194,195]. In our system orthogonal control of these variables enabled systematic investigation of how individual features interact to affect cell morphology.

Encapsulated GBM cells maintained high viability and high proliferation (**Figure 3.6-3.7**). This feature allowed the ex vivo model to carry out culture-based experiments as fast as traditional culture methods. Moreover, stimulated expression of HA receptor through HA content further indicated our engineered matrix microenvironment could help GBM cells retain a native state. Deposition of other ECM proteins is cell line and

matrix content dependent (**Figure 3.11-3.14**). From this point, we suspected matrix environment may affected global gene expression and eventually cell fate. Finally, RNAseq experiment provided comprehensive analysis of how hydrogel environment resembles a correct native microenvironment that is seen in mouse brain (**Figure 3.15-3.16**). In GBM, EMT transition can be seen as “pro-neural to mesenchymal (PMT) transitions. Mesenchymal GBM cells are reported to be more aggressive and resistant to radiations. in experiments[196]. Therefore, xenograft and hydrogel cultures potentially brought GBM cells into a more original state. All these results are exciting and provide basis for further investigations using this model.

In next chapter, we will introduce using of this model in actual drug response and resistance mechanistic investigation.

Chapter 4

Investigation of resistance to EGFR inhibition in GBM mediated by matrix features

Brief introduction:

Glioblastoma (GBM) tumors exhibit potentially actionable genetic alterations against which targeted therapies have been effective in treatment of other cancers. However, these therapies have largely failed in GBM patients[42,197]. A notable example is EGFR kinase inhibitors, which display poor clinical efficacy despite overexpression and/or mutation of EGFR in >50% of GBM[42].

In addressing this issue, preclinical models may be limited by the inability to accurately replicate pathophysiological interactions of GBM cells with unique aspects of the brain extracellular matrix (ECM), which is relatively enriched in hyaluronic acid (HA) and flexible, as described in previous chapters. In the last chapter, we have presented a brain-mimetic biomaterial ECM platform for 3D culturing of patient-derived GBM cells, with improved pathophysiological properties as an experimental model.

We investigated GBM resistance to EGFR inhibition experimentally using the novel experimental model system we have constructed. Compared to orthotopic xenograft assays, the novel biomaterial cultures we developed better preserved the physiology and kinetics of acquired resistance to the EGFR inhibition than gliomasphere cultures. Orthogonal modulation of both HA content and mechanical properties of biomaterial scaffolds was required to achieve this result. Overall, our findings show how specific interactions between GBM cell receptors and scaffold components contribute significantly to resistance to the cytotoxic effects of EGFR inhibition.

Additional information on materials and methods:

Hydrogel fabrication, immunostaining, xenograft modeling and cell culture procedures were described in Chapter 2 and Chapter 3.

Drug treatment for animal experiment: Erlotinib (50 or 75 mg/kg, Cayman Chemicals, Ann Arbor, MI USA) was administered through oral gavage. Tissues from mice used for survival studies were extracted, paraffin-embedded, sectioned (5 µm) and analyzed using immunohistochemistry.

Drug treatment for cell culture experiment: Encapsulated single cells were cultured in hydrogels for 1 week before treatment. Gliomasphere cultures were treated right after dissociation, as previously described[172]. Erlotinib was re-constituted as a 10 mM stock solution in dimethylsulfoxide (DMSO). Erlotinib was then diluted to 1 µM in culture medium. DMSO alone was used as a vehicle (i.e., negative control). Cyclo-RGD (cilengitide, Millipore Sigma) was dissolved in PBS as 10 mM stock then dissolved in media as 50 µM. Culture medium and drug were replenished every third day.

Quantification of apoptosis: Cryopreserved hydrogel blocks were prepared and stained in parallel for each experimental repeat (n=3 individual repeats) using an antibody against cleaved poly ADP polymerase (c-PARP) and Hoechst 33342 as a nuclear counterstain. At least four images from randomly chosen locations per section were taken from least 2 different sections. Data were analyzed using ImageProPlus software. The area fraction of c-PARP$^+$ to Hoescht$^+$ was defined as percentage of apoptotic cells. Only cells with nuclear co-localization of both c-PARP and Hoescht 33342 were considered to be apoptotic.

Western blotting: Hydrogels (80 µL) were incubated for 20 min in 110 µL RIPA buffer and protease/phosphatase inhibitor (Sigma-Aldrich) on ice. Samples were passed through 20G needle 20 times to mechanically dissociate cultures, then incubated on ice for 30 min. during which time they were vortexed to mix every 5 min. For gliomasphere cultures, cells were pelleted down at 500xg for 5 min and resuspended in 100 µL RIPA buffer and protease/phosphatase inhibitor solution, then mixture was incubated on ice for 20 minutes, during which time they were vortexed to mix every 5 min. Lysate was centrifuged at 17,000xg for 20 min at 4 °C, then aliquoted and stored at -80 °C until assayed. Total protein concentration was determined by BCA protein assay. Lysate was denatured in Laemmli loading buffer (BioRad) at 95 °C for 5 mins. After proper dilution with 1x Laemmli loading buffer prepared with complete RIPA buffer, equal mass and volume of sample was loaded to 4-20% Bis-Tris gel, and gel electrophoresis was conducted in SDS-MOPS running buffer at 165 V for 90 min. Transfer was conducted in 1x Nupage transfer buffer at 20 V for 1.5 hours onto a PVDF membrane that was presoaked in 100% methanol for 5 mins. The membrane was blocked in 5% bovine serum albumin (BSA) in 20 mM Tris 0.9% NaCl and 0.1% Tween-20 (TBST) for 1 hour. Primary antibodies were applied to membrane with 1:1000 dilution solution that is enough to cover the whole membrane at 4 °C overnight with gentle shaking. The next day, the membrane was washed 3 times in TBST and incubated with secondary antibodies at dilution of 1:5000 in blocking solution. Finally, the membrane was washed 3 times in TBST, incubated in Clarity ECL substrate (Biorad), and imaged (MyECL imager) without overexposing the target bands. Primary antibodies against phospho-AKT (pThr308, clone D25E6, Cell Signaling Technologies 13038, Danvers, MA USA), phospho-ERK (p42/p44, pThr202/pThr204, Cell Signaling

Technologies, 4370S), phospho-zyxin (pSer142/pSer143, Cell Signaling Technologies 8467S), phospho-FAK (pTyr397, clone D20B1, Cell Signaling Technologies 8556P), total FAK (Cell Signaling Technologies 3285S), GAPDH (GA1R, ThermoFisher MA4-15738) and CD168 (ThermoFisher PA5-32309) (dilution 1:1000) were used. Horse-radish peroxidase (HRP)-conjugated secondary antibodies against mouse and rabbit were used (dilution 1:5000). Images of blots were analyzed using ImageJ (NIH). Integrated intensity of target bands above background threshold were measured and normalized to signal of loading control (GAPDH).

Results:

Brain microenvironment facilitates resistance to EGFR inhibition

To investigate how the unique brain microenvironment influences physiology and treatment response of xenografted tumors, we transplanted patient-derived GBM cells at either intracranial or subcutaneous (dorsal flank) sites in nude mice. Once tumors were established, mice were treated with either erlotinib or vehicle (DMSO). Orthotopic transplants of both primary GBM cell lines (GBM39, HK301) responded poorly to erlotinib (**Figure 4.1, 4.2**) despite its effectiveness in gliomasphere cultures (**Figure 4.3**). Erlotinib treatment suppressed growth of intracranially xenografted GBM39 tumors for only 10 days, after which time the tumors failed to respond (**Figure 4.1)**. In mice with orthotopically implanted HK301 tumors, erlotinib had no detectable effect on tumor growth or survival **(Figure 4.1)**. In contrast, erlotinib treatment inhibited growth of subcutaneously xenografted GBM39 tumors for more than 200 days before tumors exhibited acquired resistance (**Figure 4.1**). Tumors of HK301 cells could be established at orthotopic, but

not subcutaneous, transplantation site, further indicating that the subcutaneous tissue microenvironment may not be amenable to GBM tumor growth.

In order to investigate relationship between implanted cells and microenvironment in the context of matrix HA and EGFR, expression of phosphorylated EGFR (p-EGFR) and CD44 remained high in intracranial xenografts regardless of treatment (**Figure 4.4**). However, minimal expression was observed in subcutaneous xenografts (**Figure 4.5**). Furthermore, after erlotinib treatment, CD44 and p-EGFR expression were nearly undetectable (**Figure 4.5**). Based on these results, we posited that the ubiquitous abundance of HA in the brain ECM, as reported in previous chapters, might contribute to faster acquisition of resistance to EGFR inhibition. This hypothesis was further supported by the observation that CD44 and p-EGFR were often co-expressed by GBM cells (**Figure 4.4-4.6**).

Figure 4.1

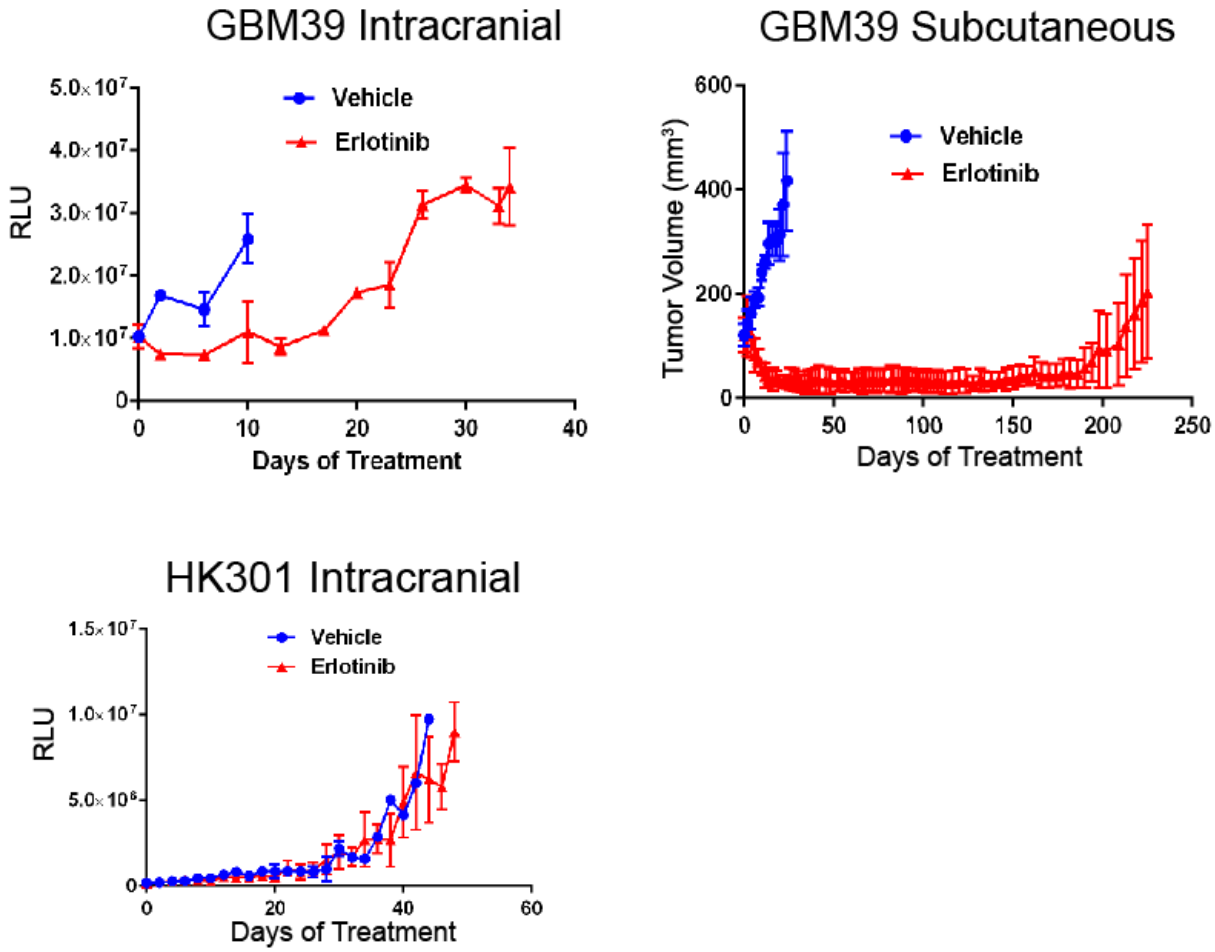

Figure 4.1. Glioblastoma xenografts acquire resistance to erlotinib at intracranial sites with faster kinetics than at subcutaneous sites. Top left, bioluminescence imaging of orthotopic xenografts of GBM39 cells (normalized to day 0 before treatment with 50mg/kg erlotinib). Error bars represent standard deviation (n=3). Top right, volume of subcutaneously xenografted tumors of GBM39 cells (normalized to day 0 before treatment with 50mg/kg erlotinib). Error bars represent standard deviation (n=4). Lower left, bioluminescence imaging of orthotopic xenografts of HK301 cells (normalized to day 0 before treatment with 75mg/kg erlotinib). Error bars represent standard deviation (n=4).

Figure 4.2

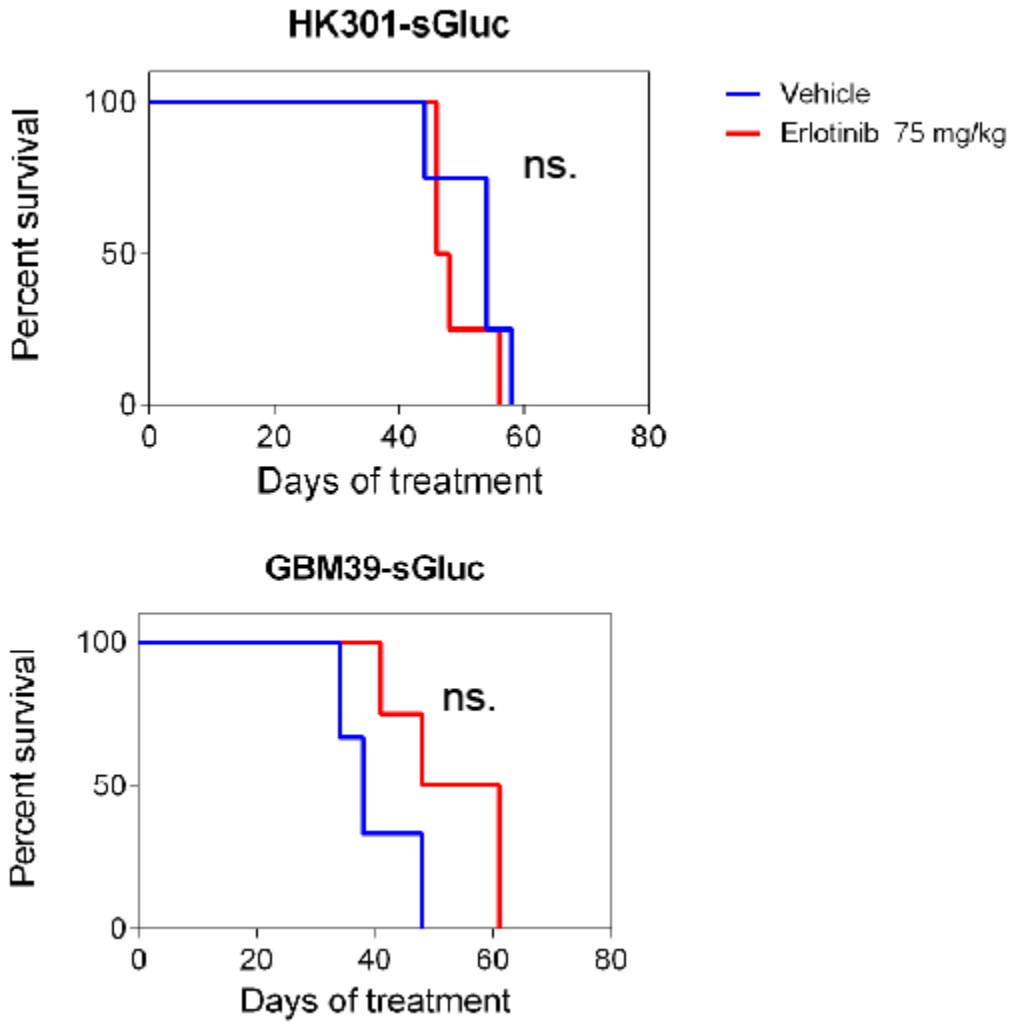

Figure 4.2. Erlotinib treatment does not affect survival of mouse bearing orthotopic xenograft GBM tumor. Kaplan-Meier survival plots of mice with patient-derived xenografts, HK301 xenografts treated with 75mg/kg erlotinib (n=8), and GBM39 xenografts treated with 50mg/kg erlotinib (n=7). Log-Rank (Mantel-Cox) test was used to compare survival curves. “ns.” represents non-significance.

Figure 4.3

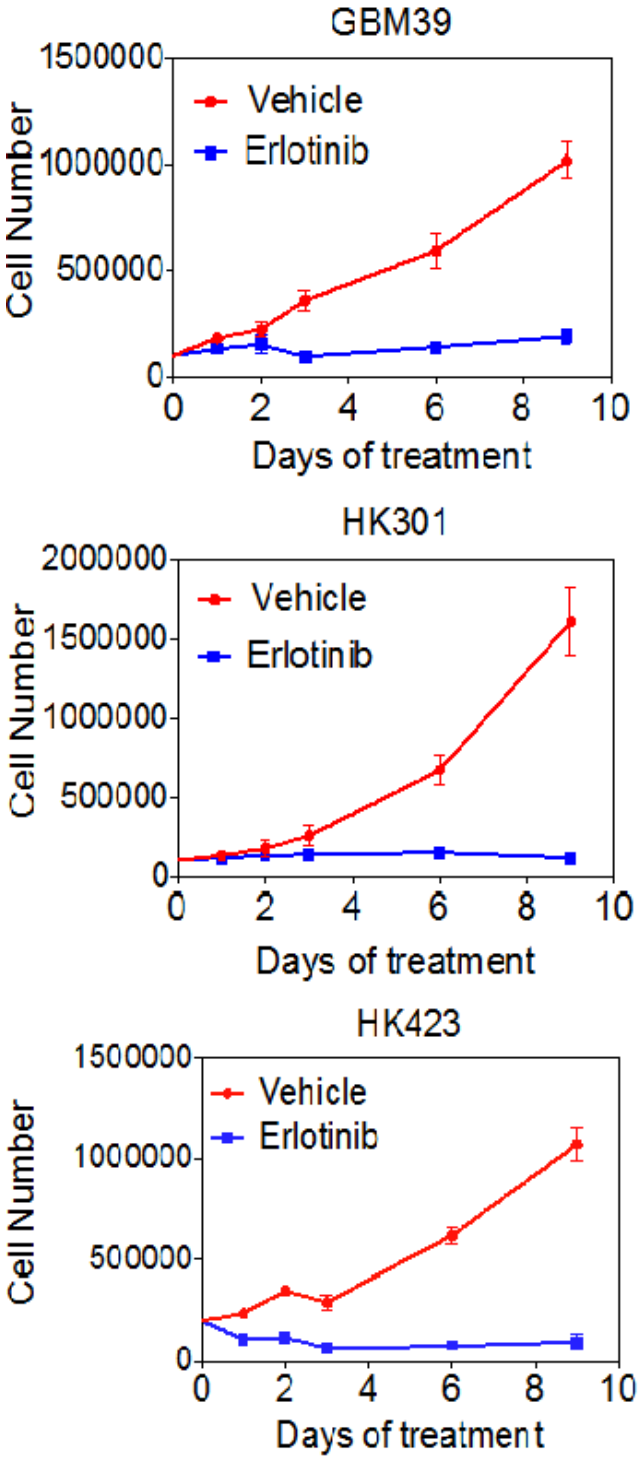

Figure 4.3. GBM cells cultured in gliomasphere samples are highly susceptible to erlotinib treatment. Numbers of cells 3 days after treatment with1μM erlotinib or vehicle (DMSO). Error bars represent standard deviation (n=3).

Figure 4.4

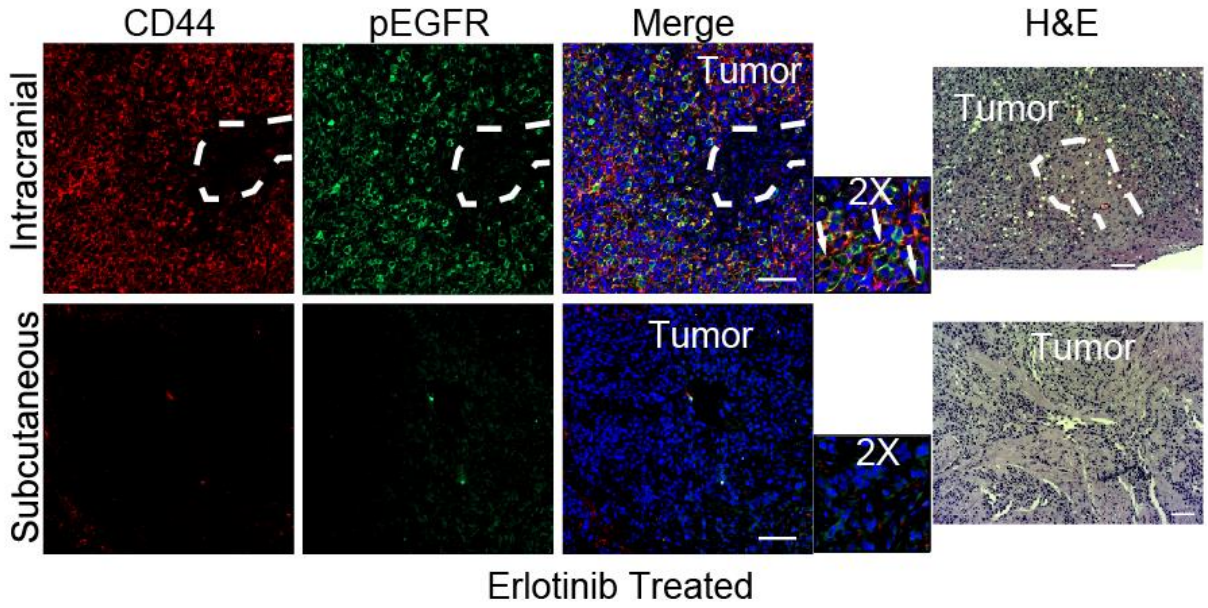

Figure 4.4. CD44 expression colocalizes with activated EGFR in intracranially planted GBM39 treated with erlotinib. On left, representative images of immunofluorescence staining for CD44 (red), p-EGFR (Tyr1068) (green) and Hoechst 33342 (blue) of intracranial and subcutaneous xenografts of GBM39 cells. Arrows indicate cells expressing both p-EGFR and CD44. On right, H&E images of adjacent sections from the same tissues. Scale bars = 200 μm.

Figure 4.5

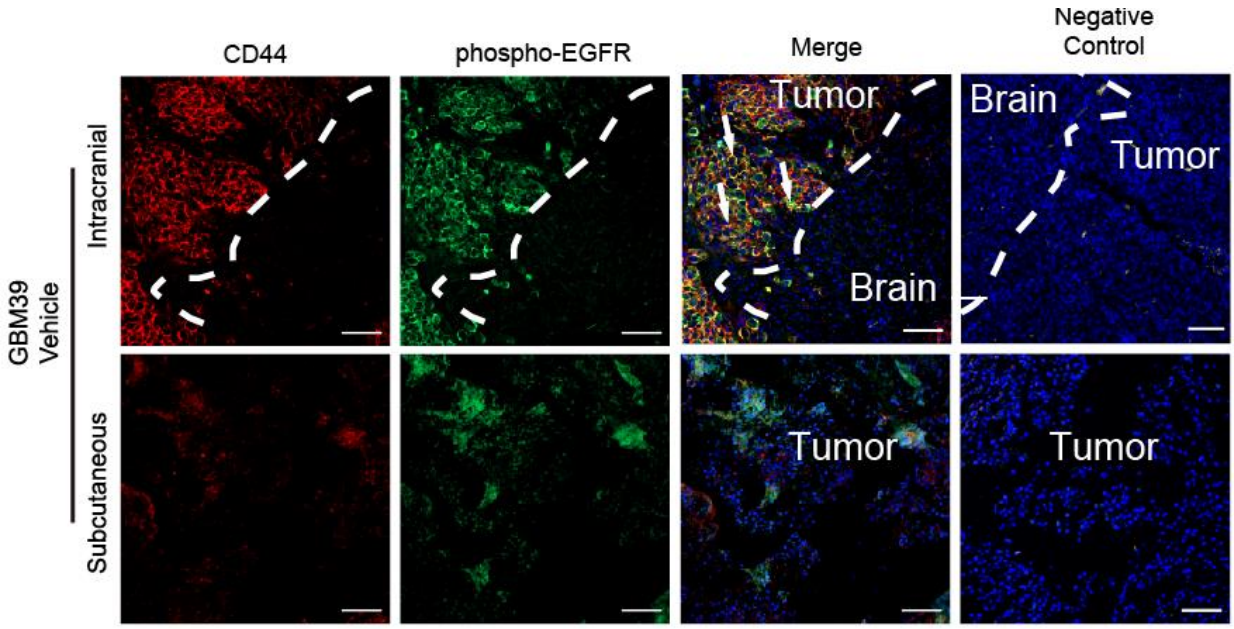

Figure 4.5. CD44 expression colocalizes with activated EGFR in intracranially or subcutaneously planted GBM39 without treatment. Representative images of immunofluorescence staining for CD44 and p-EGFR in murine xenografts of vehicle-treated xenografts of GBM39 cells.

Figure 4.6

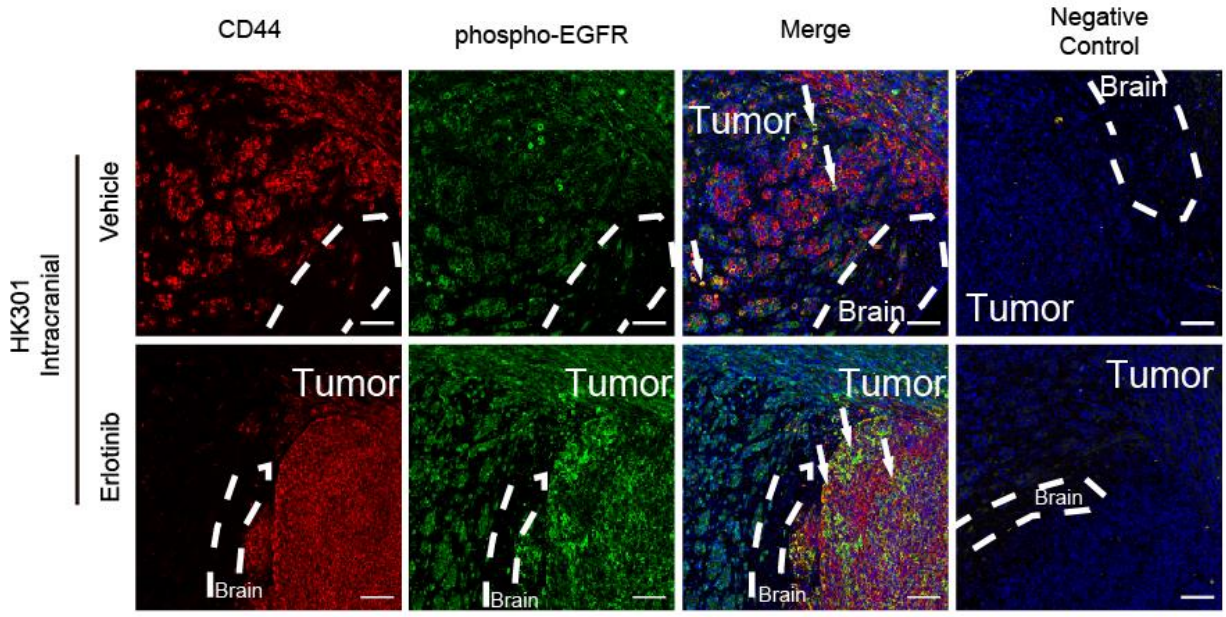

Figure 4.6. CD44 expression colocalizes with activated EGFR in intracranially planted HK301. Representative images of immunofluorescence staining for CD44 and p-EGFR in murine xenografts of intracranial xenografts of HK301 cells. CD44 (red), p-EGFR (green), and Hoechst 33342 (blue). Scale bars = 100 µm.

GBM cells in brain-mimetic hydrogels rapidly acquire drug resistance

Using the *ex vivo*, brain-mimetic culture model developed in the previous chapter, we investigated effects of erlotinib treatment on GBM cells cultured in hydrogels or gliomaspheres. To characterize the cytotoxic effects of erlotinib, numbers of cells positive for nuclear cleaved poly ADP polymerase (c-PARP) were counted (**Figure 4.7**). By the 6^{th} day of treatment, GBM cells cultured within hydrogels displayed levels of apoptosis indistinguishable from non-treated controls (**Figure 4.7**). Gliomasphere cultures had significantly more apoptotic cells when treated with erlotinib **(Figure 4.7)**. In contrast to gliomasphere cultures, after 12 days of treatment GBM cells cultured within hydrogels also had acquired resistance to the cytostatic effects of erlotinib (**Figure 4.8**).

While HK423 cells express only wtEGFR and not the truncated and constitutively activate mutant, EGFRvIII, HK301 cells express both wtEGFR and EGFRvIII and GBM39 cells express only EGFRvIII[198]. Although erlotinib-treated HK301 cells cultured in gliomaspheres or hydrogels upregulated total expression of wtEGFR (**Figure 4.9, 4.10**), only in hydrogel cultures was p-EGFRvIII increased. Likewise for HK423 cells, erlotinib treatment induced higher total wt-EGFR levels in hydrogel and gliomasphere. While erlotinib treatment did attenuate p-wtEGFR in HK423 cells cultured in hydrogels or gliomaspheres, this effect was only partial in hydrogel cultures. As with HK301 cells, GBM39 cells cultured in HA hydrogels increased p-EGFRvIII (**Figure 4.9, 4.10**). While erlotinib treatment reduced p-EGFRvIII, levels remained higher than treated gliomaspheres. In all three cell lines when treated, p-EGFR levels were always significantly higher when cultured in HA hydrogel than gliomasphere cultures (**Figure 4.9, 4.10**).

Downstream pathways of EGFR include PI3K-AKT and MAPK-ERK, both of which many studies have reported maintain survival and growth potential of GBM tumors[197]. Thus, we characterized the effects of erlotinib treatment on phosphorylation of AKT and ERK1/2 (**Figure 4.9, 4.11**). For all three cell lines, culture in HA hydrogels increased p-AKT levels compared to gliomaspheres. While p-AKT levels were not altered significantly in erlotinib-treated gliomaspheres, p-AKT levels significantly increased in hydrogel-cultured HK301 and HK423 cells (**Figure 4.9, 4.11**). In HK301 gliomaspheres, erlotinib treatment significantly decreased p-ERK levels. Although not statistically significant, a similar trend was observed for HK423 and GBM39 gliomaspheres (**Figure 4.9, 4.11**). In all hydrogel cultures, erlotinib treatment had no significant effects on p-ERK and p-ERK levels were significantly higher than in erlotinib-treated gliomaspheres (**Figure 4.9, 4.11**).

Figure 4.7

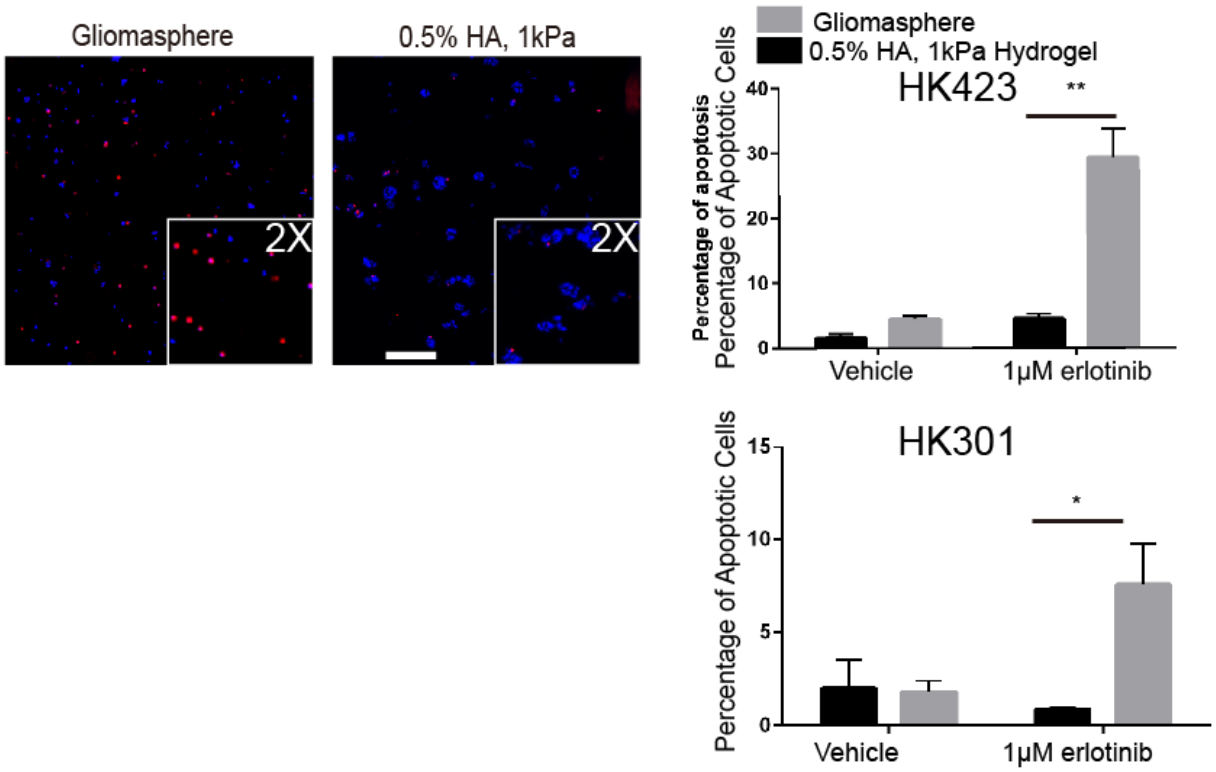

Figure 4.7. GBM cells in 3D, HA hydrogel cultures acquire cytotoxic resistance to erlotinib. Left panel, representative images of immunofluorescence staining of c-PARP in HK301 cells after 6 days of erlotinib treatment. Scale bar = 200 μm. Right panel, quantification of apoptotic cells (c-PARP^{+}) after 6 days of erlotinib treatment. Error bars indicate S.E.M. (n=3). Students' t-tests were performed (*$p < 0.05$, **$p < 0.01$).

Figure 4.8

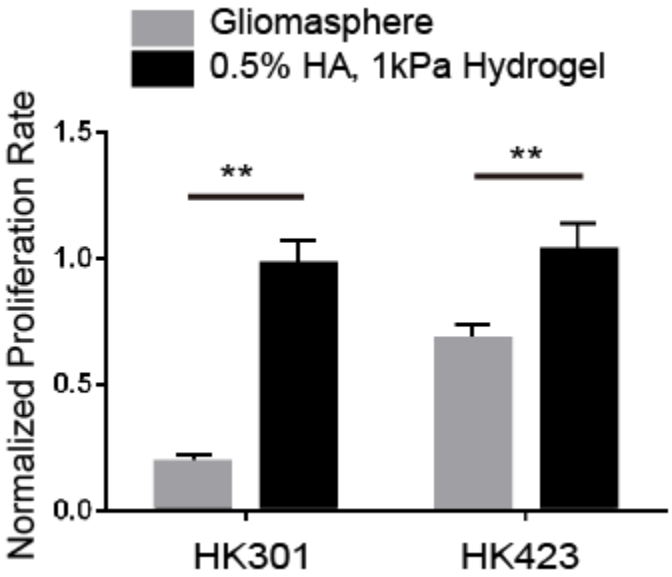

Figure 4.8. GBM cells in 3D, HA hydrogel cultures acquire cytostatic resistance to erlotinib. Proliferation rate of cells (EdU incorporation over 2.5 hours) after 12 days of erlotinib treatment. Erlotinib-treated samples were normalized to non-treated samples for each condition. Students' t-test was performed (**$p < 0.01$). Error bars indicate S.E.M. (n=3).

Figure 4.9

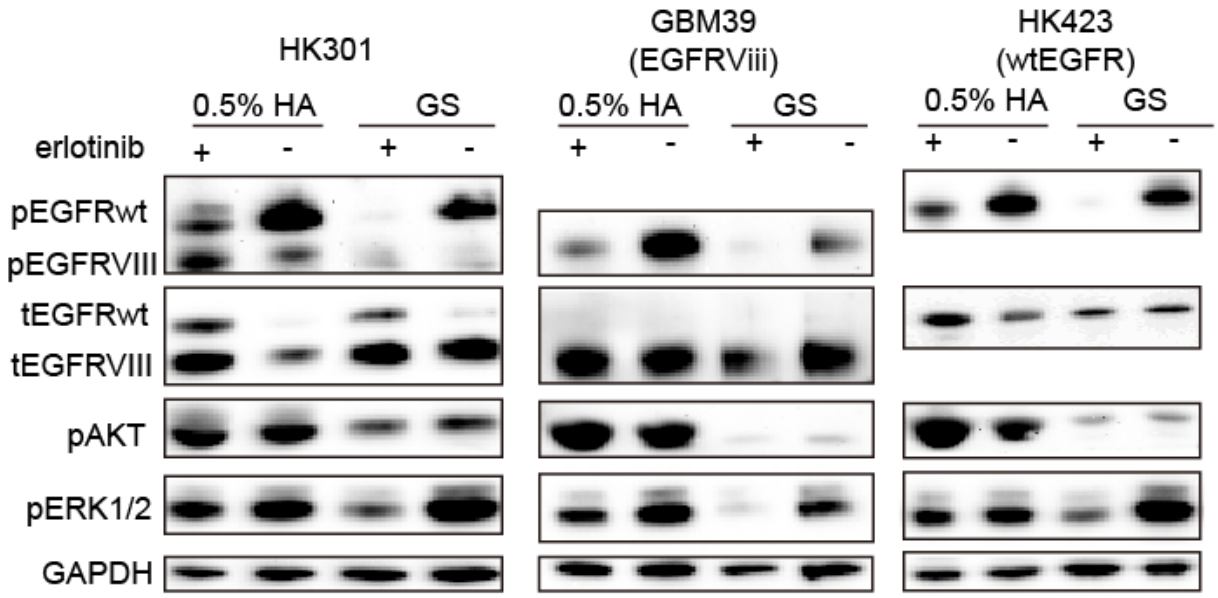

Figure 4.9. 3D HA hydrogel cultured GBM cells maintain oncogenic signaling downstream of EGFR despite of erlotinib treatment. Representative Western blot images of 72 hours after erlotinib treatment. HA percentage indicates volume to weight (% w/v).

Figure 4.10

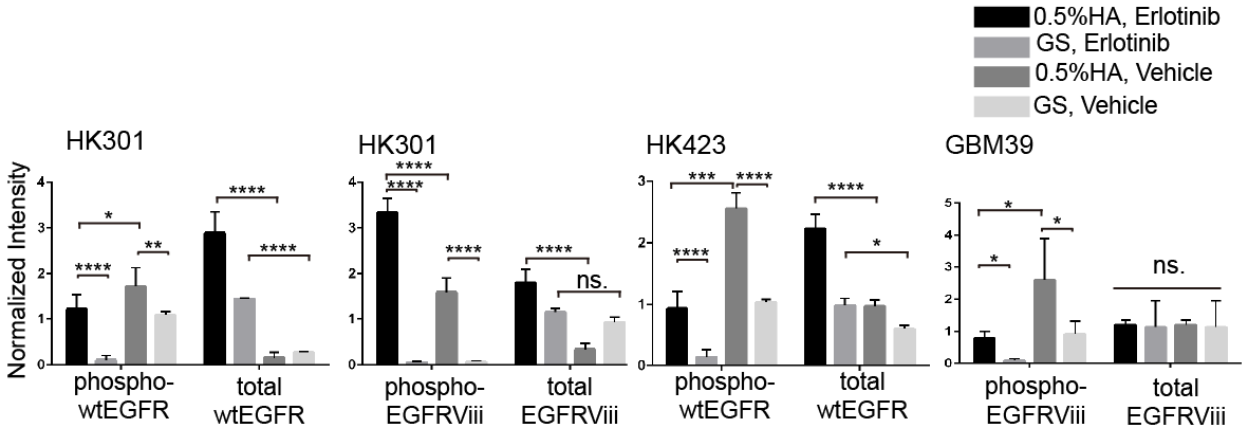

Figure 4.10. 3D HA hydrogel cultured GBM cells maintain oncogenic signaling downstream of EGFR despite of erlotinib treatment. Quantification (integrated intensity signals) of phospho-EGFR for Western blots. Error bars represent standard deviation from independent repeats (HK301 (n=5), HK423 (n=4), and GBM39 (n=3)). One-way ANOVA and Tukeys's multiple comparison test were used (*p<0.05, **p<0.01, ***p<0.001, ****p<0.0001).

Figure 4.11

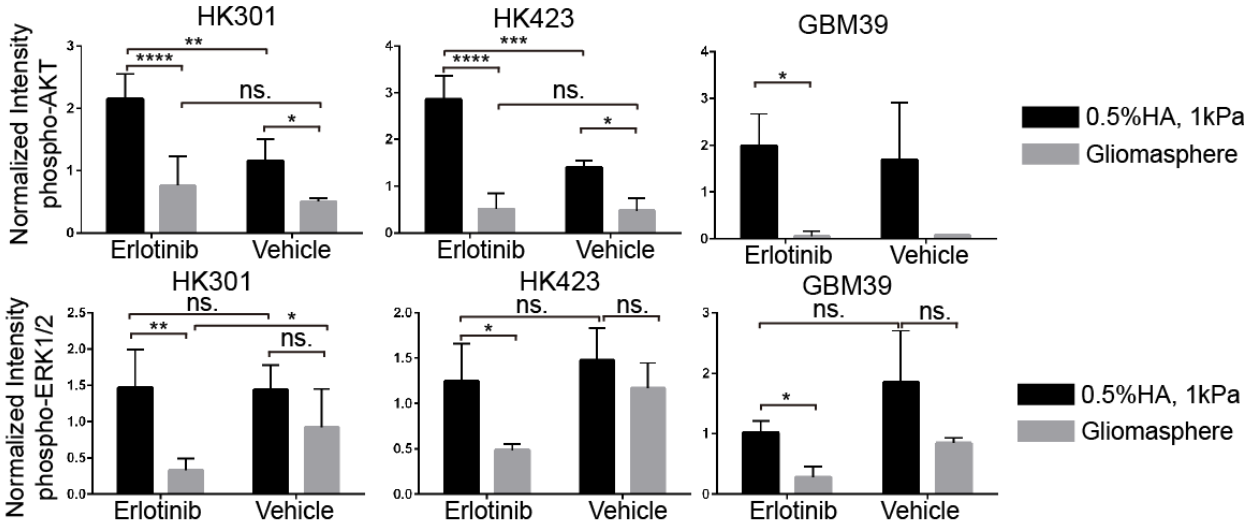

Figure 4.11. 3D HA hydrogel cultured GBM cells maintain oncogenic signaling downstream of EGFR despite of erlotinib treatment. Quantification (integrated intensity signals) of phospho-AKT and phosphor-ERK1/2 for Western blots. Error bars represent standard deviation from independent repeats (HK301 (n=5), HK423 (n=4), and GBM39 (n=3)). One-way ANOVA and Tukeys's multiple comparison test were used (*p<0.05, **p<0.01, ***p<0.001, ****p<0.0001).

Biomaterials to quantify effects of ECM cues on drug resistance

Figures 4.1-4.11 suggest that CD44 expression and HA content support the ability of GBM cells to gain erlotinib resistance. Others have reported that the mechanical microenvironment contributes to GBM tumor progression[30,192]. Unlike gliomaspheres, biomaterial platforms also provide a defined, 3D mechanical environment to cultured cells. Thus, we explored the cooperative influence of hydrogel compressive modulus and HA content on acquisition of resistance to EGFR inhibition via erlotinib. Importantly, mechanical modulus was varied independently of HA concentration, so that the individual and combined contributions of each were experimentally decoupled.

Patient-derived GBM cells (HK301) were cultured in HA hydrogels to characterize the independent effects of HA concentration and compressive modulus on response to erlotinib. Total numbers of cells were tracked using bioluminescence imaging of live cultures transduced to constitutively express firefly luciferase. Results demonstrate that cells cultured in 3D hydrogels with a higher HA concentration (0.5% w/v) and lower compressive modulus (1 kPa) gained resistance to erlotinib by the 9th day of treatment (**Figure 4.12**). By the 15th day of treatment, there were more total cells in erlotinib-treated than untreated cultures, indicating that erlotinib-resistant cells proliferate faster. GBM cells cultured in hydrogels with high HA content (0.5% w/v), but with a stiffer modulus (2 kPa), also acquired some resistance to erlotinib; however, not until the 12th day of treatment. In addition, cell numbers in treated cultures remained only ~50% of those in non-treated cultures after 15 days. Finally, GBM cells cultured in soft hydrogels (1 kPa) with a low HA concentration (0.1% w/v) did not acquire erlotinib resistance within 15 days. Instead their response was comparable to that of gliomasphere cultures, with

bioluminescence signals close to background on the 15th day of treatment. Furthermore, minimal HA was observed in cultured gliomaspheres (**Figure 4.12**). Together, these results indicate that high HA content was required for acquisition of resistance.

Cytotoxic and cytostatic effects of erlotinib treatment on GBM cells cultured in hydrogels were evaluated. Erlotinib-treated cells cultured in soft hydrogels (1 kPa) with high HA content (0.5% w/v) proliferated significantly faster than their untreated controls at the 3- and 6-day time points (**Figure 4.13**). This increase in proliferation correlated to the increased total numbers of viable cells observed by the 12th day of treatment (**Figure 4.12**). Erlotinib treatment also induced a slight increase in cell proliferation on the 3rd day in other hydrogel conditions (**Figure 4.13**). While proliferation had decreased by the 6th day of treatment in all conditions, it remained elevated in 3D hydrogel cultures compared to gliomaspheres. Finally, only GBM cells cultured in soft, high HA hydrogels had escaped the cytotoxic effects of erlotinib on the 6th day of treatment (**Figure 4.14**). Notably, the kinetics of resistance acquisition to erlotinib of GBM cells cultured in soft, high HA hydrogels (**Figure 4.12-4.14**) were comparable to those observed in patient-matched orthotopic xenografts in mice (**Figure 4.1**). For all cell lines evaluated, culture in hydrogels with high HA (0.5% w/v) induced increased CD44 expression compared to culture in hydrogels with low HA (0.1% w/v) or gliomaspheres (**Figure 4.15, 4.16**). These findings agree with our *in vivo* results, where murine xenografts robustly express CD44 when seeded in the HA-rich brain, but not at subcutaneous sites.

To further investigate the role of CD44, we used shRNA lentivirus to knockdown CD44 expression (**Figure 4.17**) and repeated erlotinib-treatment experiments. Lack of CD44 mitigated both cytotoxic and cytostatic resistance to erlotinib (**Figure 4.18-4.20**). Despite

restoration of erlotinib efficacy for the first 6 days of treatment, even cells lacking CD44 expression gained resistance to the cytostatic effects of erlotinib by the 12th day of treatment (**Figure 4.20**). Although CD44 is a major receptor for HA, other HA receptors, such as CD168, may act to compensate for lost CD44 activity and facilitate delayed acquisition of erlotinib resistance. In soft, high HA hydrogel cultures, we observed a unique pattern of CD168 expression around the edges of cell masses resembling that of CD44 (**Figure 4.21**). In low HA hydrogels, CD168 expression was confined to the nucleus, where it participates in formation of mitotic spindles[199].

Figure 4.12

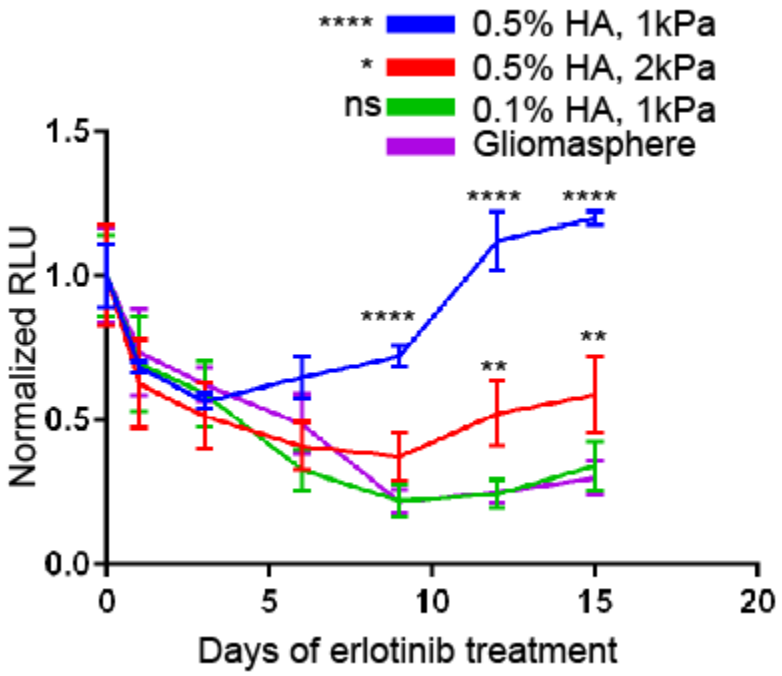

Figure 4.12. HA content and modulus contribute to kinetics of acquisition of erlotinib resistance. Chemiluminescent signal measured 2 hrs after addition of D-luciferin (1 mM). Signals of erlotinib-treated HK301 cells were normalized to non-treated samples and signal before treatment (day 0) for each condition. Two-way ANOVA (culture condition, time) with Šidák's test for multiple comparisons of hydrogel condition against gliomasphere culture were performed. Error bars show standard deviation (n=3). *p < 0.05, **p < 0.01, ****p < 0.0001.

Figure 4.13

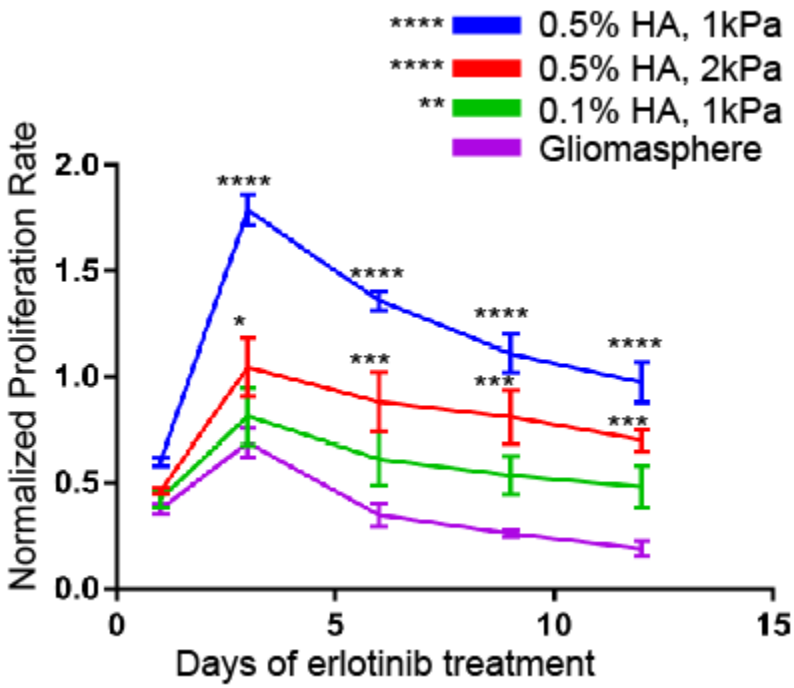

Figure 4.13. HA content and modulus contribute to kinetics of acquisition of erlotinib resistance. Proliferation rate of HK301 cells (EdU incorporation over 2.5 hours) during erlotinib treatment. Erlotinib-treated samples were normalized to non-treated samples for each condition. Error bars indicate S.E.M. (n=3). Two-way ANOVA (culture condition, time) with Šidák's test for multiple comparisons of hydrogel condition against gliomasphere culture were performed. *$p < 0.05$, **$p < 0.01$, ***$p < 0.001$, ****$p < 0.0001$.

Figure 4.14

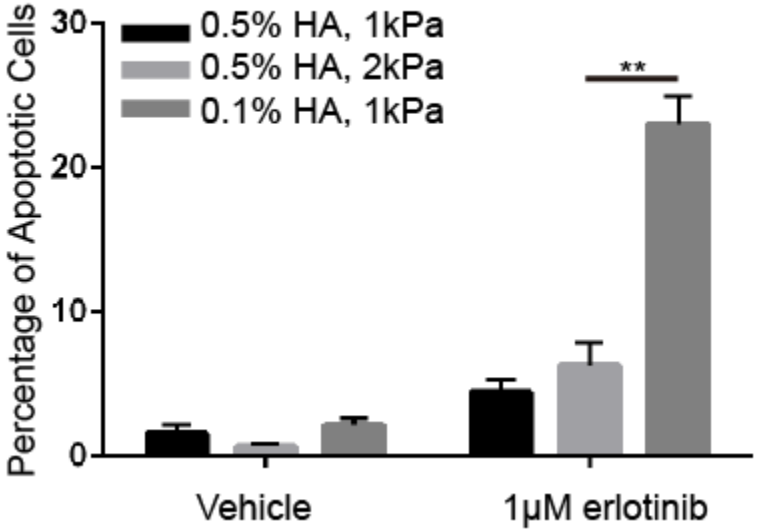

Figure 4.14. HA content and modulus contribute to kinetics of acquisition of erlotinib resistance. Percentage of apoptotic cells (c-PARP^{+} HK301 cells) after 6 days of erlotinib treatment. Error bars indicate S.E.M. (n=3) One-way ANOVA with Tukey's test for multiple comparisons was performed. ***p* < 0.01.

Figure 4.15

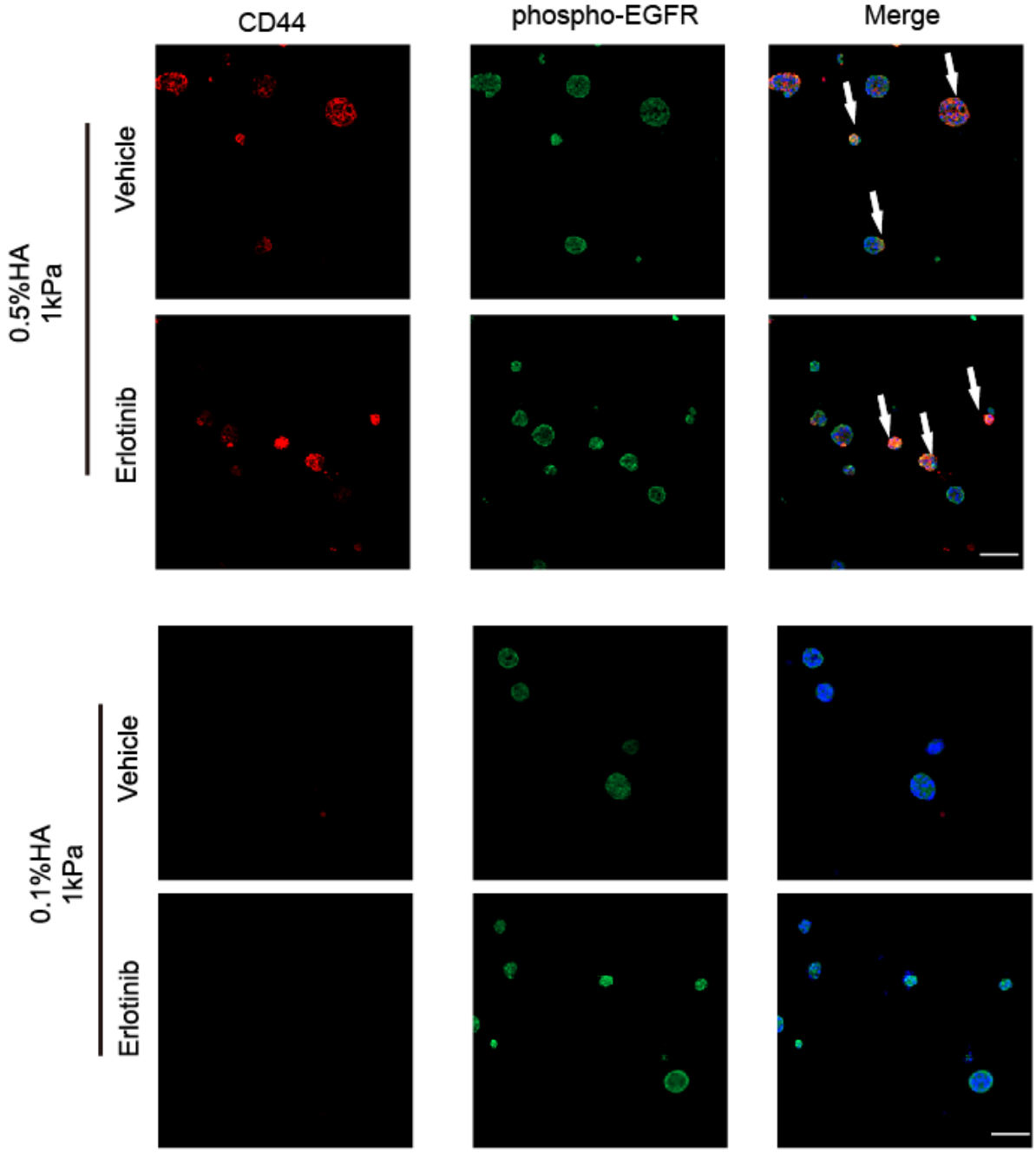

Figure 4.15. CD44 and activated EGFR co-localize in high HA content hydrogel cultured HK301. Representative images of immunofluorescence staining for CD44 (red), p-EGFR (green), and Hoechst 33342 (blue) in hydrogel cultures in which HK301 cells were cultured 0.5% or 0.1% (w/v) HA, 1 kPa hydrogels 6 days after treatment. Arrows indicate overlapping staining for CD44 and p-EGFR.

Figure 4.16

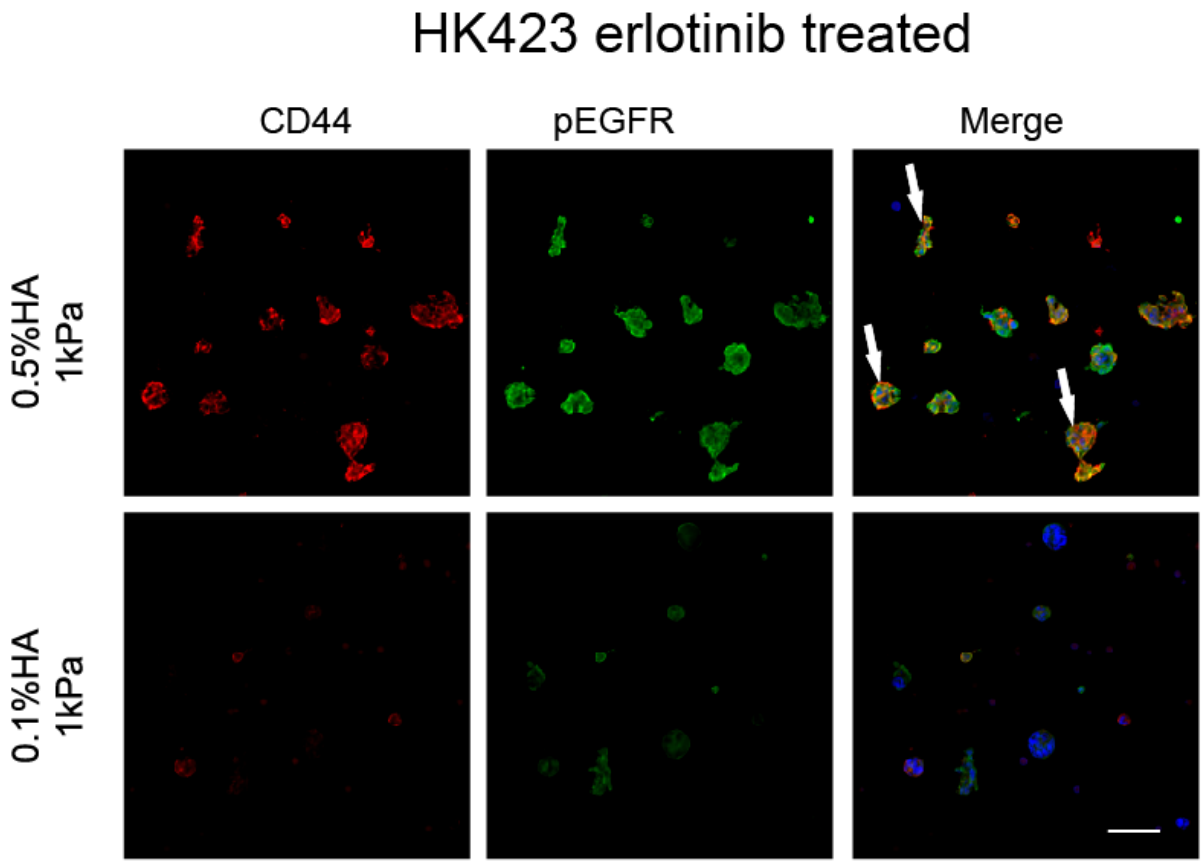

Figure 4.16. CD44 and activated EGFR co-localize in high HA content hydrogel cultured HK423. Representative images of immunofluorescence staining for CD44 (red), p-EGFR (green), and Hoechst 33342 (blue) in hydrogel cultures in which HK423 cells were cultured 0.5% or 0.1% (w/v) HA, 1 kPa hydrogels 6 days after treatment. Arrows indicate overlapping staining for CD44 and p-EGFR.

Figure 4.17

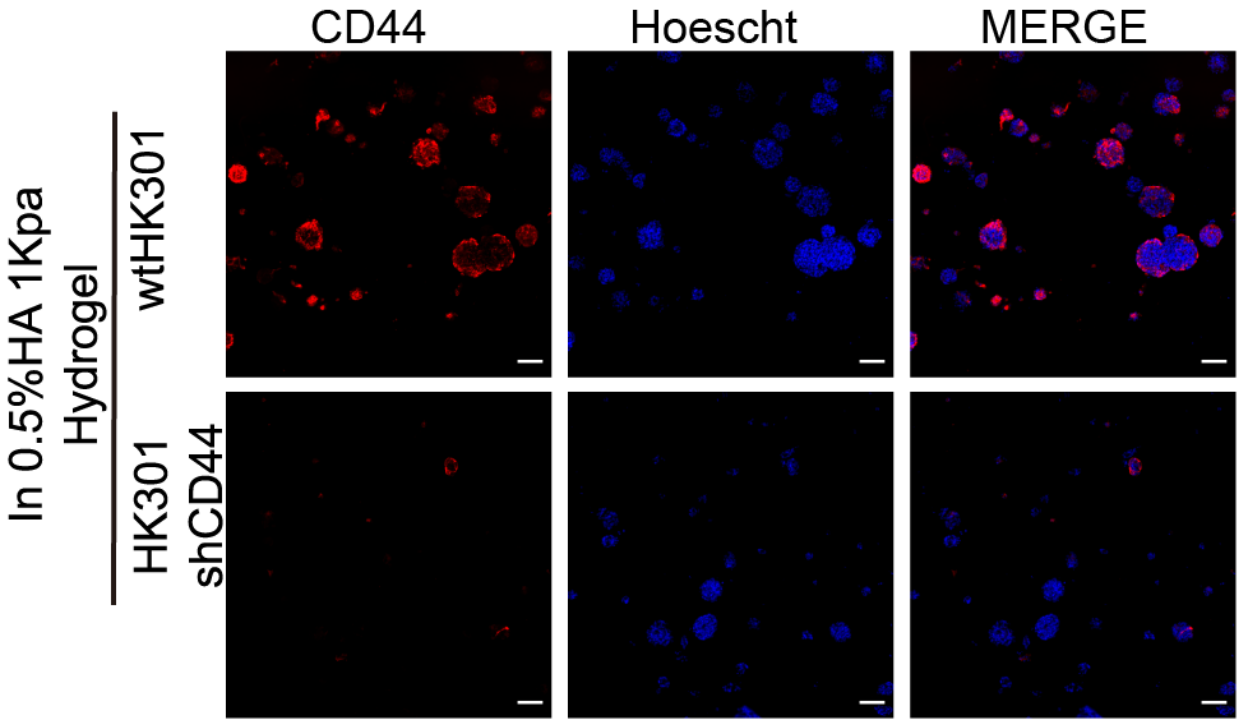

Figure 4.17. Successful knockdown of CD44 in HK301 cells. Representative images of immunofluorescence staining for CD44 (red) and Hoechst 33342 (blue) in hydrogel cultured HK301.

Figure 4.18

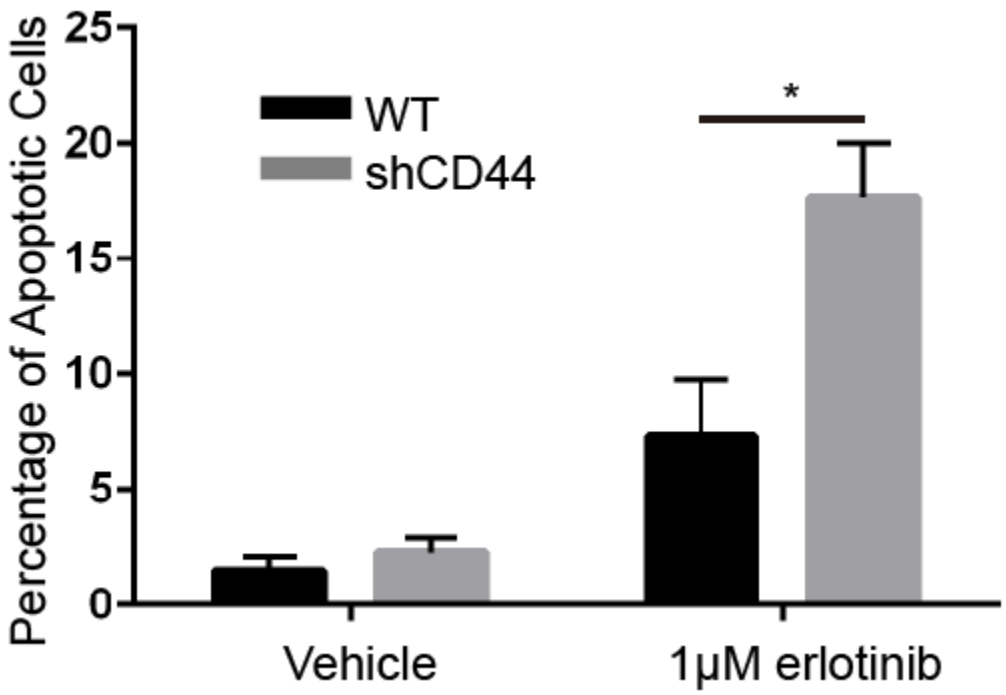

Figure 4.18. CD44 mediates cytotoxic resistance through HA content in hydrogel microenvironment. Percentage of apoptotic cells (c-PARP^{+} HK301 cells) after 6 days of erlotinib treatment. Error bars indicate S.E.M. (n=3) One-way ANOVA with Tukey's test for multiple comparisons was performed. *$p < 0.05$.

Figure 4.19

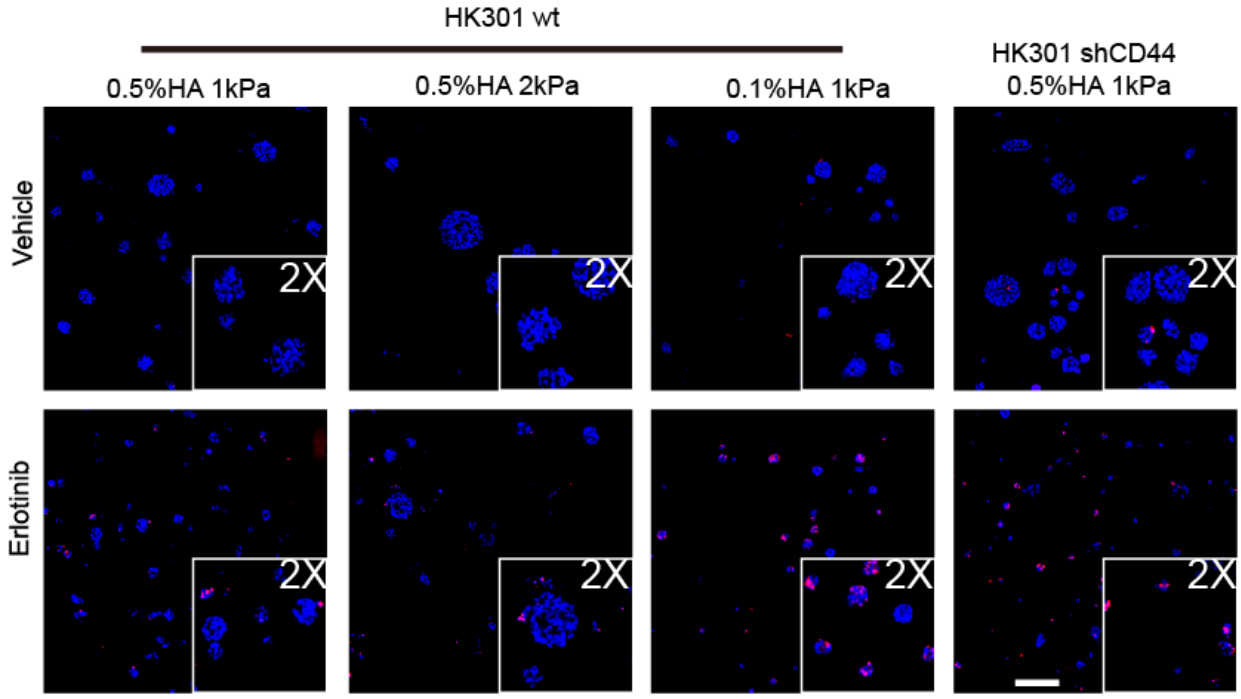

Figure 4.19. Hydrogel conditions and receptor knockdown affect apoptotic efficacy of erlotinib on HK301 cells. Representative images of immunofluorescence staining for c-PARP (red) and Hoechst 33342 (blue) after 6 days of erlotinib treatment. Scale bars = 200 μm.

Figure 4.20

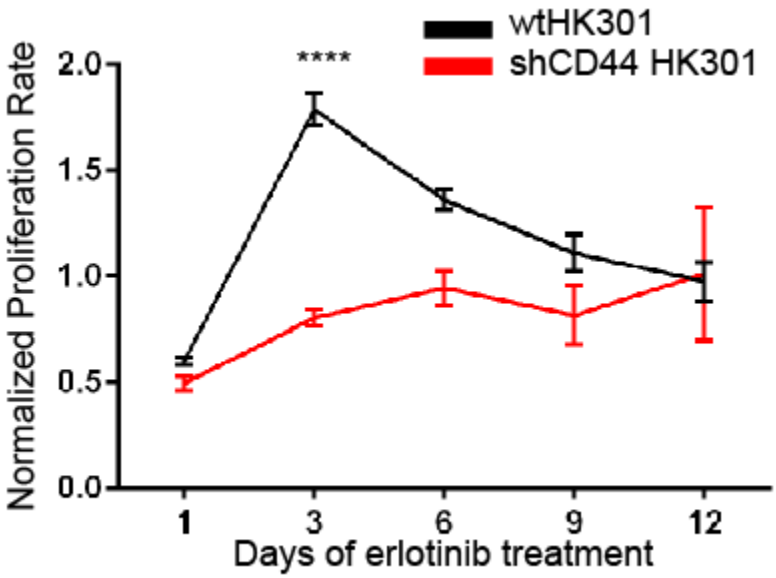

Figure 4.20. CD44 mediates cytostatic resistance through HA content in hydrogel microenvironment. Proliferation rate of HK301 cells (EdU incorporation over 2.5 hours) during erlotinib treatment. Erlotinib-treated samples were normalized to non-treated samples for each condition. Error bars indicate S.E.M. (n=3). Two-way ANOVA (cell type, time) with Šidák's test for multiple comparisons were performed. HA percentage indicates volume to weight percentage (% w/v). ****$p < 0.0001$.

Figure 4.21

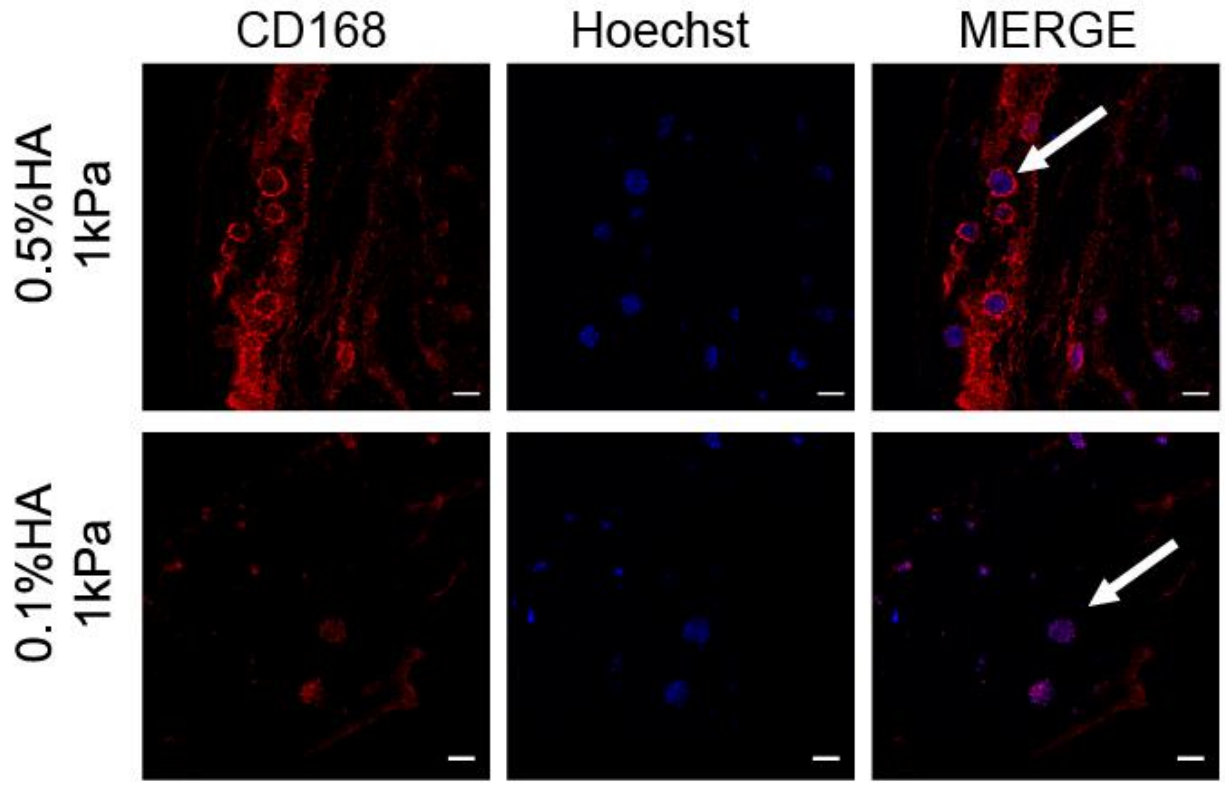

Figure 4.21. CD168 is upregulated by HA content in hydrogel. Representative images of immunofluorescence staining for CD168 (red) on HK301 cells cultured in either 0.5% (w/v) or 0.1% (w/v) HA hydrogels. Samples were collected from vehicle group at day 6 after initiation of drug treatment. Scale bars = 100 μm. Arrows indicate localization of staining (surrounding the sphere or in nuclei).

RGD and HA cooperate to evade erlotinib-induced apoptosis

Like CD44, integrins can relay both biochemical and mechanical cues through activation of FAK-PI3K-AKT and MAPK-ERK pathways – all previously implicated as mediators of resistance to treatment in GBM[30,192,200]. To investigate cooperative interactions with HA-bound CD44, the ubiquitous integrin-binding sequence RGD was incorporated into hydrogel platforms as described in previous chapters. First, incorporation of RGD peptides into in soft hydrogels (1 kPa) with high HA content (0.5% w/v) facilitated GBM cell spreading out of spheroidal masses into the surrounding hydrogel as described in previous chapter. Next, we investigated how RGD incorporation into hydrogels affected cytotoxic effects of erlotinib treatment. On the 3rd day of treatment, GBM cells cultured in high HA (0.5% w/v) hydrogels with RGD provided significant protection against erlotinib-induced apoptosis compared to those in high HA hydrogels without RGD or low HA (0.1% w/v) hydrogels with RGD (**Figure 4.22**). These results imply that engagement of integrin and HA receptors cooperate to amplify resistance to EGFR inhibition.

To investigate downstream effects of integrin engagement, we investigated phosphorylation of zyxin and FAK – prominent signaling proteins associated with integrin activation. When cultured in high HA hydrogels containing RGD, GBM cells upregulated p-zyxin (**Figure 4.23**). This result is not unexpected given the role of zyxin in integrin-mediated cell spreading and migration in 3D culture[201] and the invasive morphology of cells cultured in 3D hydrogels. However, erlotinib treatment did not affect p-zyxin levels in HK301 or HK423 cells (**Figure 4.23, 4.24**).

Integrin activation of FAK is thought to facilitate cancer cell resistance to drug-induced apoptosis[31]. Levels of p-FAK were similar in untreated cultures in HA hydrogels with or without RGD. However, when cultured in hydrogels containing RGD, erlotinib treatment increased p-FAK activity (**Figure 4.23**). To further confirm that apoptotic resistance was mediated by cell-RGD interactions, cyclo-RGD was used as an inhibitor[202]. Addition of cyclo-RGD effectively reversed cell spreading, as reported in previous chapter, and reduced p-zyxin (**Figure 4.24**). When treated with erlotinib and cyclo-RGD, p-FAK levels were comparable to non-treated cells (**Figure 4.24**). Moreover, this combined treatment reversed the ability of RGD to rescue cells from erlotinib-induced apoptosis (**Figure 4.25**).

Figure 4.22

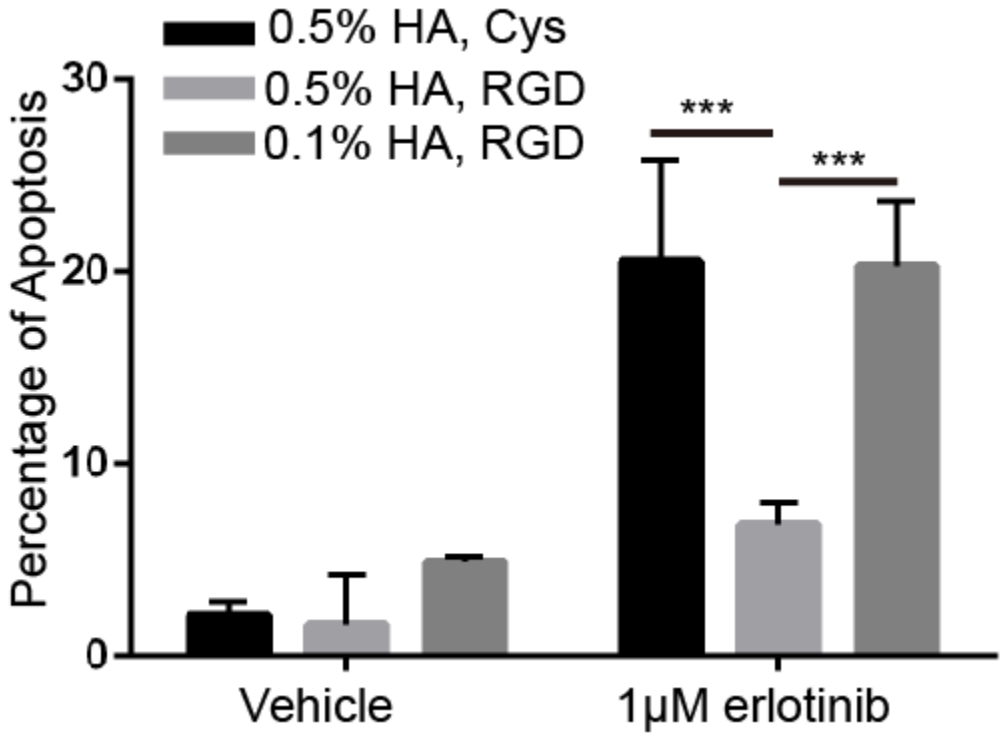

Figure 4.22. Interactions of integrins and CD44 with the scaffold protect glioblastoma cells from erlotinib-induced apoptosis (HK301 cells). Percentage of apoptotic cells (c-PARP^{+}) after 3 days of erlotinib treatment. Error bars indicate S.E.M. (n=3). Two-way ANOVA (hydrogel condition, treatment) with Šidák's test for multiple comparisons were performed (***$p < 0.001$).

Figure 4.23

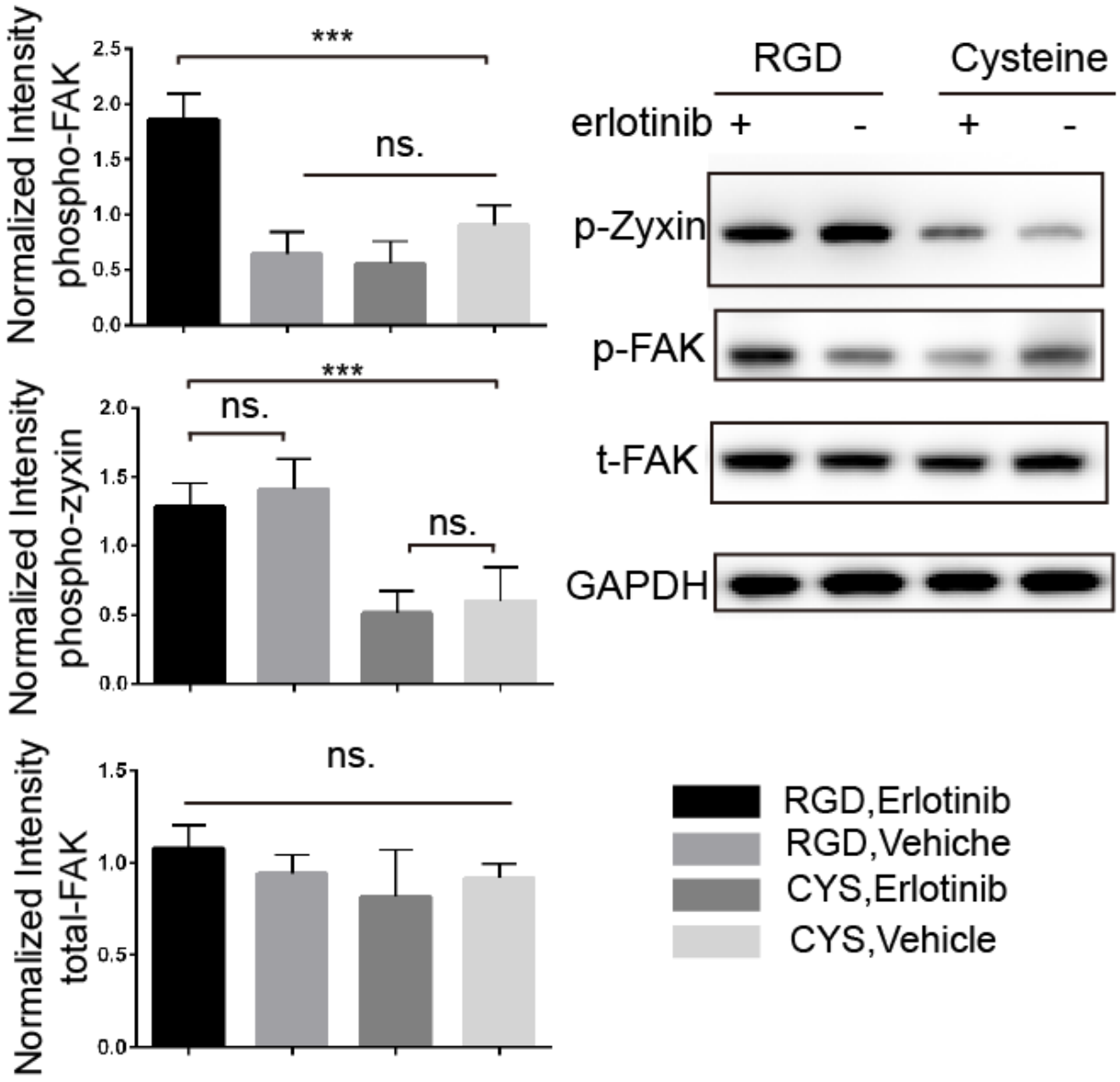

Figure 4.23. Integrin-matrix RGD interaction protects erlotinib induced apoptosis through FAK and Zyxin signaling. Right panel, representative Western blot images 6 days after erlotinib treatment. HK301 was encapsulated in different gel types. Left panels, normalized integrated intensity signals of phospho-FAK, total-FAK and phospho-zyxin. Error bars represent standard deviation across individual experimental repeats (n=4).

Figure 4.24

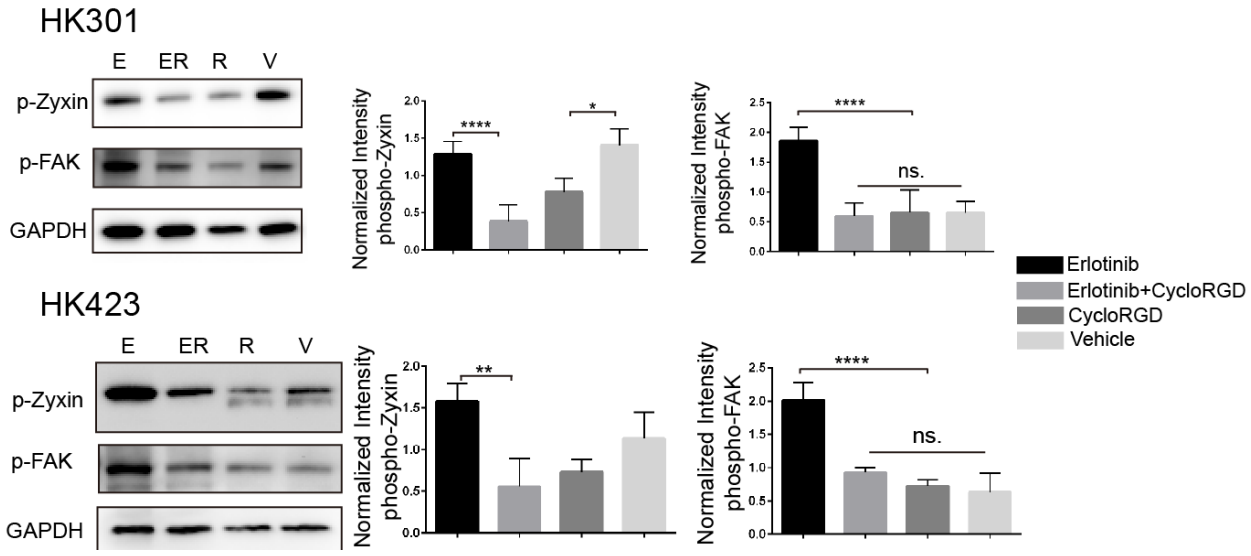

Figure 4.24. Integrin-matrix RGD interaction protects erlotinib induced apoptosis through FAK and Zyxin signaling. Left panels, representative Western blot image (HK301 and HK423 cells after 6 days of treatment). Right bar graphs, normalized integrated intensity signals of phospho-FAK and phospho-zyxin. Error bar represents standard deviation across individual experimental repeats (n=4 for HK301 n=3 for HK423). Error bars represent standard deviation from individual experimental repeats. One-way ANOVA and Tukeys's multiple comparison test were used. *p<0.05, **p<0.01, ***p<0.001, ****p<0.0001.

Figure 4.25

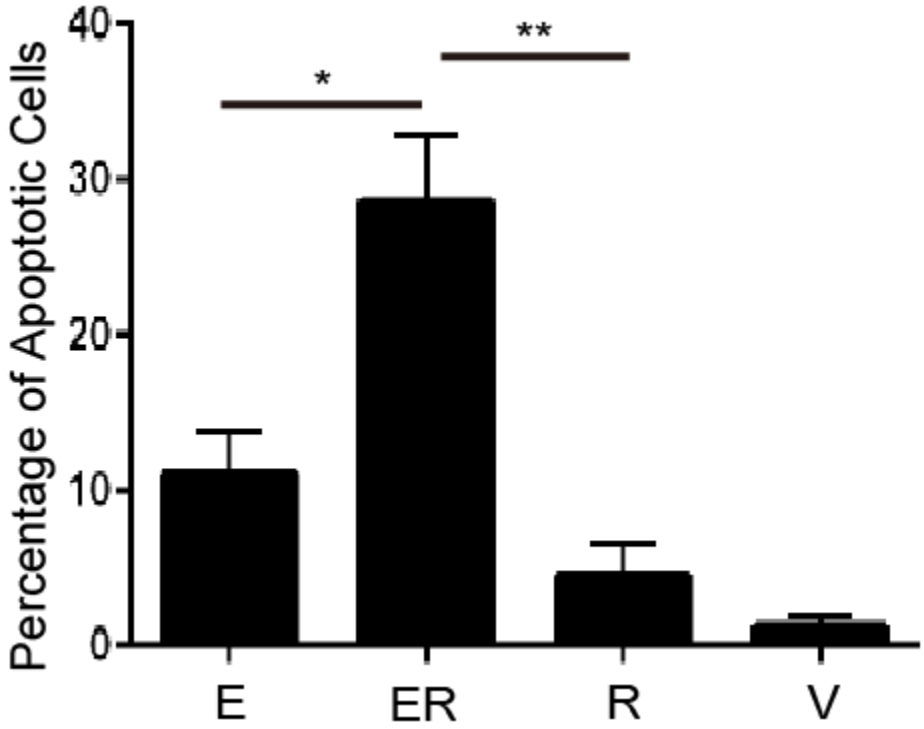

Figure 4.25. Cyclo-RGD treatment reverted integrin-matrix RGD interaction mediated cytotoxic resistance to erlotinib. Percentage of apoptotic cells (c-PARP^{+}) 3 days after cyclo-RGD treatment. Error bars indicate S.E.M. (n=3). One-way Anova with Tukey's test for multiple comparisons were performed (*$p < 0.05$, **$p < 0.01$). HA percentage indicates volume to weight (% w/v). "E" - 1μM erlotinib, "ER" - 1μM erlotinib and 50 μM cyclo-RGD, "R" - 50 μM cyclo-RGD, "V" - vehicle (DMSO or PBS).

Figure 4.26

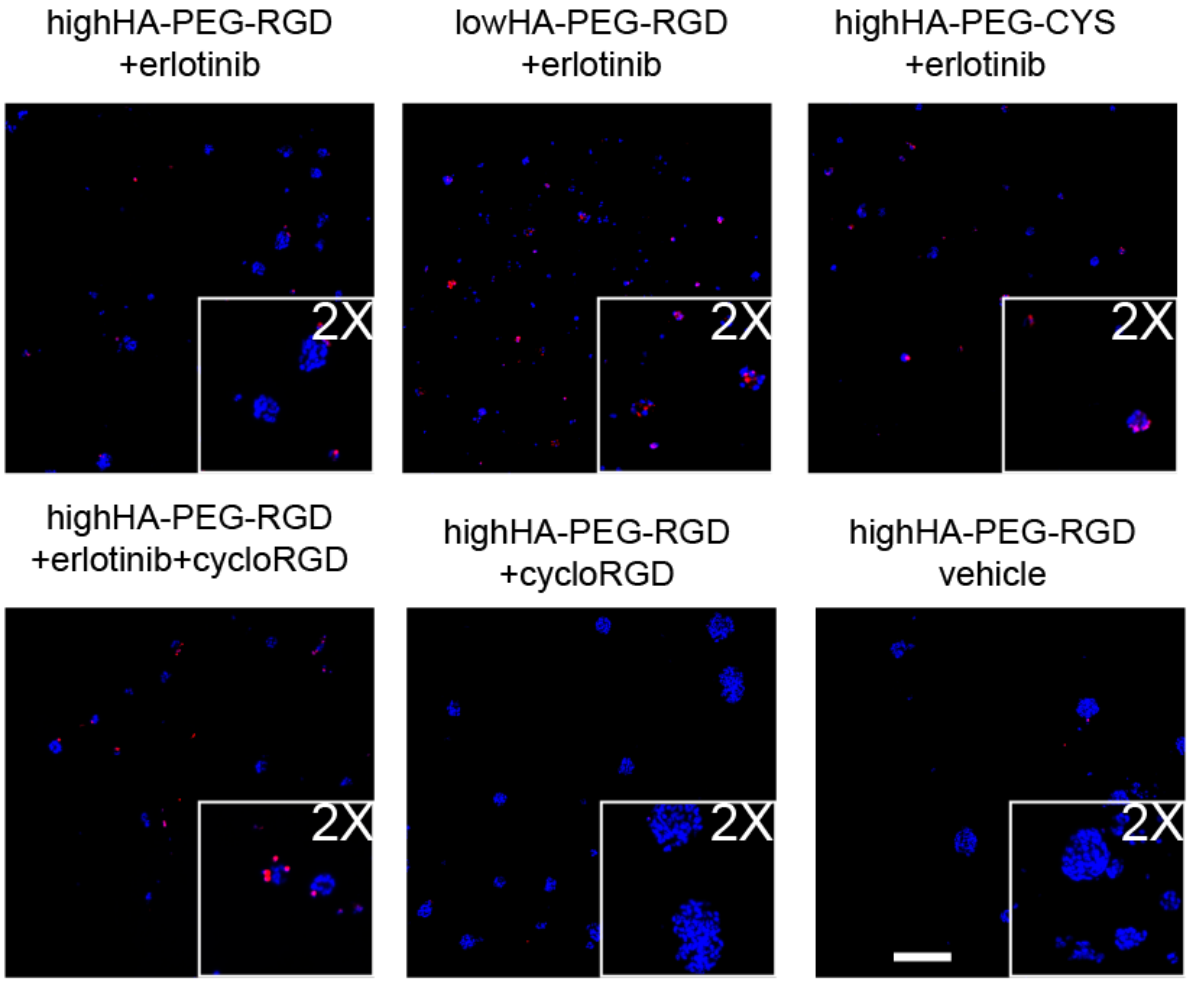

Figure 4.26. Integrin-matrix RGD interaction protects erlotinib induced apoptosis. Representative images of immunofluorescence staining for c-PARP (red) after 3 days of treatment with erlotinib and/or cyclo-RGD (or vehicle). HA percentage indicates volume to weight percentage (% w/v). Nuclear counterstain (Hoechst 33342) in blue.

Discussion

Therapeutic resistance plays a critical role in GBM lethality. However, preclinical studies have inadequately accounted for the influence of the unique properties of brain tissue. Our data demonstrate that GBM tumors xenografted at non-CNS anatomical sites, which contain less HA in their ECM, acquire resistance to RTK inhibition on a significantly longer time scale (**Fig. 4.1**). Orthogonal tuning of biomaterial features revealed that an HA-rich, mechanically soft culture environment is required for GBM cells to acquire resistance to RTK inhibition (**Fig. 4.12-4.14**). Furthermore, 3D cultures of patient-derived GBM cells in biomaterials with defined HA content and mechanical properties rapidly developed resistance to erlotinib in a manner consistent with patient-matched mouse xenografts (**Figure 4.1, 4.12**) and clinical reports[203]. Specifically, in both orthotopic animal and high HA hydrogel experimental settings, GBM cells acquired erlotinib resistance between 9 and 12 days of treatment. Taken together, results demonstrate the utility of these biomaterial cultures as *ex vivo* models of GBM that better recapitulate the brain microenvironment than standard culture methods yet are easier, more affordable, less time consuming (days versus weeks to establish tumors) and provide a more controlled experimental context than animal models.

For all primary GBM cell lines evaluated, changes in cytotoxic and cytostatic effects of erlotinib over time were consistent with acquisition of resistance – where despite an initial inhibition of p-EGFR, treatment reduced apoptosis while increasing proliferation (**Figure 4.12-4.14**). 3D culture in HA-rich hydrogels alone increased p-AKT, while erlotinib treatment further upregulated p-AKT levels (**Figure 4.9-4.11**). This finding indicates that

GBM cells resistant to EGFR inhibition may be more aggressive – a possible explanation of increased proliferation in HK301 after treatment in high HA hydrogel (**Figure 4.12, 4.13**).

As described in previous chapters, we implemented several key improvements over previously reported HA-based biomaterials for 3D cell culture[30,123,128,141,194,195] that enabled development of culture platforms representing a compelling new preclinical model for studying mechanisms of drug resistance in brain cancers. The majority of previous studies of GBM in 3D biomaterial models have explored only immortalized cells lines, such as U87 cells, which likely have significant phenotypic deviations from primary, patient-isolated GBM cells[103]. Although logistically more challenging, primary GBM cells – as used here – are more likely to yield clinically translatable findings. Moreover, compatibility of an *ex vivo* experimental platform with primary GBM cells isolated from multiple patients will facilitate future application to personalized medicine.

The lack of CD44 expression in hydrogel cultures with lower HA content (**Figure 4.15, 4.16**) indicates HA may induce upregulation of CD44 receptors that can then respond to mechanical cues. Previous studies have shown that mechanical cues are transduced through the PI3K-AKT pathway, despite EGFR inhibition[27]. This may explain why EGFR resistance is more pronounced in GBM cultures with comparable HA levels and CD44 expression, but different mechanical moduli. As knockdown of CD44 restored the cytostatic and cytotoxic effects of erlotinib, we are confident that HA-CD44 interactions contributed to acquisition of erlotinib resistance (**Figure 4.18, 4.20**). However, cytostatic effects were lost over time – implying that GBM cells eventually acquired resistance through a CD44-independent mechanism. The observation that the CD168 receptor was highly expressed at the cell membrane in these cultures (**Figure 4.17**) suggests that

CD168-HA interactions may compensate for the loss of CD44 to permit acquisition of erlotinib resistance.

Our results are in agreement with previous reports that HA-bound CD44 facilitates activation of wtEGFR, and thus resistance to EGFR inhibition[27,43,185] **(Figure 4.12-4.14**). The observations that areas of CD44 and p-EGFR expression overlap in GBM cells cultured in HA-rich hydrogels (**Figure 4.15, 4.16**) and tumors xenografted in HA-rich brain (**Figure 4.4, 4.5**) indicate that HA-bound CD44 may increase activation of EGFR through physical interactions at the cell membrane and facilitate resistance to EGFR inhibition. This has been previously reported to occur in orthotopic xenografts and clinical samples[27,43]. CD44 may also effect activation of EGFRvIII, a common variant in clinical tumors associated with resistance to EGFR inhibition and worse patient outcomes[42,172,204]. Notably, RGD peptides acted synergistically with HA in hydrogels to induce cell spreading and protect GBM cells from erlotinib-induced apoptosis (**Figure 4.22**). These results imply that a combination therapy of integrin, CD44 and EGFR inhibition may have clinical potential.

Given the complexity of GBM tumors *in vivo* – including powerful cooperative mechanisms and the presence of confounding variables such as the blood-brain barrier – it has been challenging to isolate the contributions of individual ECM features using animal models. On the other hand, standard *in vitro* culture methods do not account for key features of the brain ECM that are crucial to preserving tumor physiology and obtaining experimental results with clinical relevance. Here, we describe biomaterial platforms that recapitulate the brain microenvironment to produce *ex vivo* cultures of primary GBM cell lines with unique genetic and phenotypic profiles that are physiologically

representative of clinical tumors. Specifically, mechanisms and kinetics of acquisition of resistance to EGFR inhibition were preserved in biomaterial, but not in standard gliomasphere cultures. Compared to animal models, these biomaterial scaffolds provide researchers with a platform in which to perform highly controlled experiments faster, cheaper and more reproducibly. In addition, scaffolds are optically transparent – permitting imaging of 3D cultures – and compatible with standard techniques for tissue processing – including sectioning and histological staining. The ability to independently vary individual parameters within the ECM enables characterization of how multiple ECM cues act together to facilitate acquisition of treatment resistance and amplify aggressive characteristics. Here, this function was used to demonstrate how mechanical modulus, HA content and RGD peptides mediate acquisition of resistance to RTK inhibition through cooperative interactions among HA, CD44, integrins and EGFR. In conclusion, these biomimetic scaffolds with orthogonal control over ECM parameters provide a unique tool for researchers to better understand how the complex microenvironment in GBM tumors fuels treatment resistance and cancer progression.

Chapter 5

Investigation of resistance to chemotherapies in GBM mediated by matrix features

Brief introduction:

The alkylating chemotherapy temozolomide (TMZ) is routinely used as an adjuvant chemotherapy following surgical resection of tumors and post-surgery radiotherapy. TMZ is administered systemically in cycles for 6 or more cycles; for example, a typical patient is given the drug for 5 continuous days followed by no treatment for the remaining days of a 28-day cycle [205]. Although less common than TMZ treatment, biodegradable wafers, which continuously deliver the alkylating chemotherapy agent carmustine (also known as BCNU), have been used widely for treatment as well. These Gliadel™ wafers are implanted locally at the tumor site at the same time as surgical resection[206]. Unfortunately, even with treatment the median survival of GBM patients is only 12-15 months[207].

Alkylating chemotherapies, including TMZ and carmustine, work by adding methyl groups to the O-6 position of guanine[207,208], creating DNA lesions to induce apoptosis[209]. A known mechanism of resistance in GBM involves expression of O^6-methylguanine-DNA methyltransferase (MGMT), which can actively repair drug-induced DNA lesions[210]. As such, methylation of the MGMT promoter is recognized as an important molecular indicator of chemo-sensitivity[208,211]. However, more recent analyses of clinical data found that the MGMT methylation status prolonged median survival of patients treated with TMZ by only 2 months and had no effect on clinical outcome for

patients treated with carmustine [205,212,213]. Thus, it is likely that mechanisms other than MGMT promoter activity contribute substantially to treatment resistance.

ECM engagement with either integrin or CD44 receptors has been reported to activate Src protein-tyrosine kinase (Src) in [214–216]. In sarcoma and ovarian cancer, Src has been observed as a modulator of treatment sensitivity, where its inhibition promoted chemotherapy-induced apoptosis[217,218]. In GBM, a number of studies have found correlations between Src hyper-activation and tumorigenesis, invasion and progression [214,215,218,219]. However, these previous studies were largely focused on elucidating the role of Src in GBM invasion and how Src activation may influence treatment response in GBM remains largely unknown.

Here, we employed hydrogel biomaterials that surround 3D cultured, patient-derived GBM cells with a bioengineered matrix composed of HA and integrin-binding sites based on the “RGD” adhesive tripeptide. As the mechanical microenvironment can also have profound effects on tumor cells[220,221], hydrogel matrices were designed to approximate the mechanical properties of native brain. Previously, we demonstrated that patient-derived GBM cells cultured in these tunable, 3D culture matrices better approximated responses to therapeutic inhibition of epidermal growth factor receptor (EGFR) observed in patient-matched, orthotopic xenografts than did patient-matched GS cultures [198]. Here, we used these hydrogel cultures to demonstrate that CD44-HA and integrin-RGD interactions act together to drive chemotherapy resistance. Furthermore, we have identified Src activation as a key signaling event mediating both chemotherapy resistance and invasive morphology. Finally, we demonstrate that ECM

components act to protect GBM cells from chemotherapy-induced apoptosis through downstream, Src-mediated inhibition of BCL-2 family pro-apoptotic factors.

Results:

High HA scaffolds facilitate chemotherapy resistance

We employed a 12-day treatment protocol where cells were exposed to two treatment cycles — 3 days with drug followed by 3 days without — to approximate treatment cycles used for TMZ chemotherapy in clinical practice[205] (**Figure 5.1**). Drug response was observed in patient-derived GBM cells cultured in 3D hydrogels fabricated with either high (0.5% w/v) or low (0.1% w/v) HA content, as previously described[198]. After 12 days in culture HK301 cells formed spheroid aggregates with similar morphologies in both scaffold conditions without treatment (vehicle control) and high HA scaffolds wither treatment (TMZ or carmustine) (**Figure 5.2**). In contrast, cell aggregates were clearly smaller in low HA scaffolds with treatment. Growth kinetics of scaffold cultures tracked over time through bioluminescence imaging of a constitutively overexpressing luciferase reporter confirmed that HK301 cells in high HA hydrogels had grown significantly more than those in other conditions, starting at day 6 of the treatment scheme (**Figure 5.3**). No obvious differences in cell morphology or aggregation were observed with scaffold type or treatment for GBM6 cells (*data not shown*). Growth kinetics of GBM6 cultures were also highly variable over the first 9 days of treatment (**Figure 5.4**). However, quantification of the bioluminescence signal from treated cultures, normalized to that from untreated, at the end of the treatment on day 12 confirmed that both HK301 and

GBM6 cells cultured in high HA hydrogels were less responsive to alkylating chemotherapies than those cultured in low HA content hydrogels or as GS (**Figure 5.5**).

In clinical cases, a cycle of TMZ chemotherapy is typically defined as 5 days of treatment followed 23 days of not treatment, or "rest"[207]. During this "rest" period, tumors have the opportunity to recover, adapt and/or grow. Here, we applied 3 days of treatment followed by 3 days of "rest". During the first "rest" period (days 3-6), tumor cell cultures appeared to switch to a state that was less responsive to treatment with either TMZ or carmustine and average growth rates were more similar to untreated controls (**Figure 5.3**).

Figure 5.1

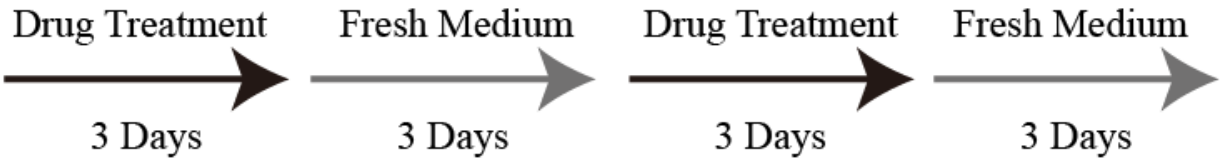

Figure 5.1. Schematic of 12-day chemotherapy treatment regimen consisting of 2 cycles of 3 days of treatment followed by 3 days of “rest”. Drug treatments included carmustine, temozolomide (TMZ), or vehicle (ethanol for carmustine, DMSO for TMZ).

Figure 5.2

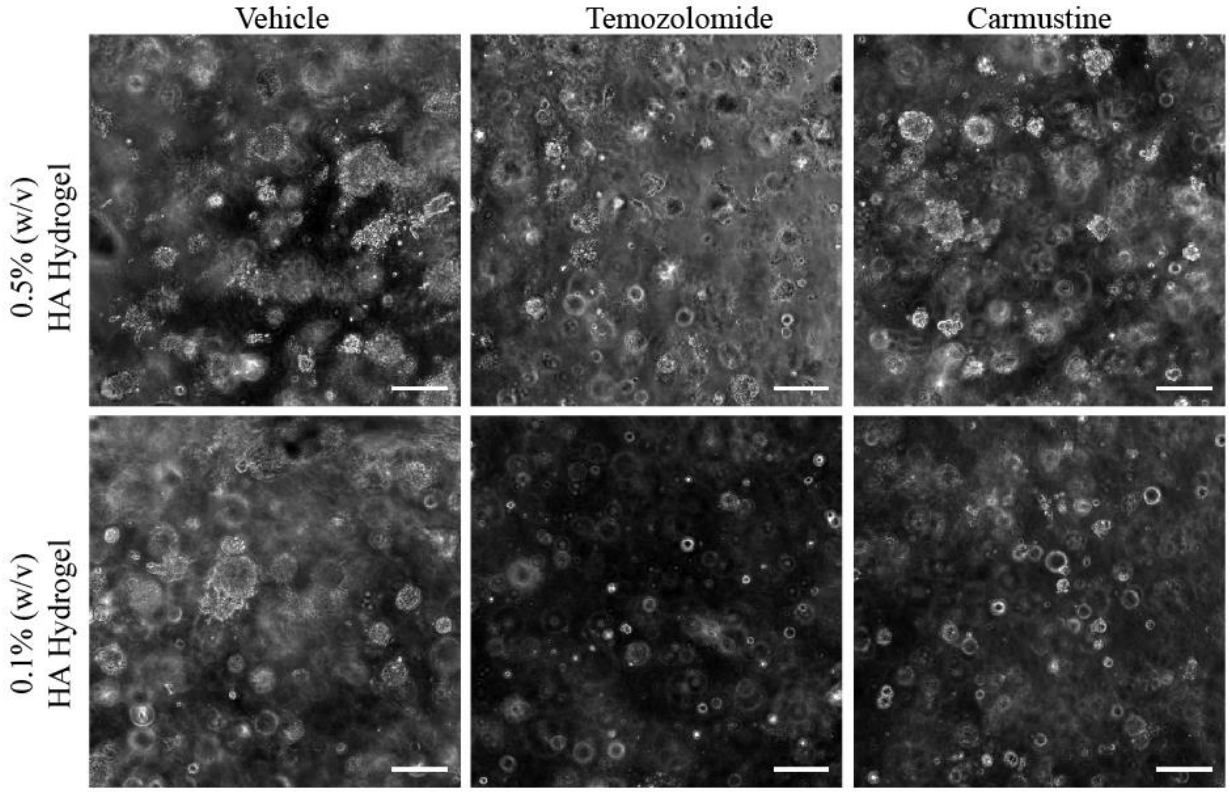

Figure 5.2. Representative phase contrast image of HK301 cells cultured in 3D scaffolds with low (0.1% w/v) or high (0.5% w/v) hyaluronic acid (HA) after the 12-day drug treatment. Scale bars = 200 μm.

Figure 5.3

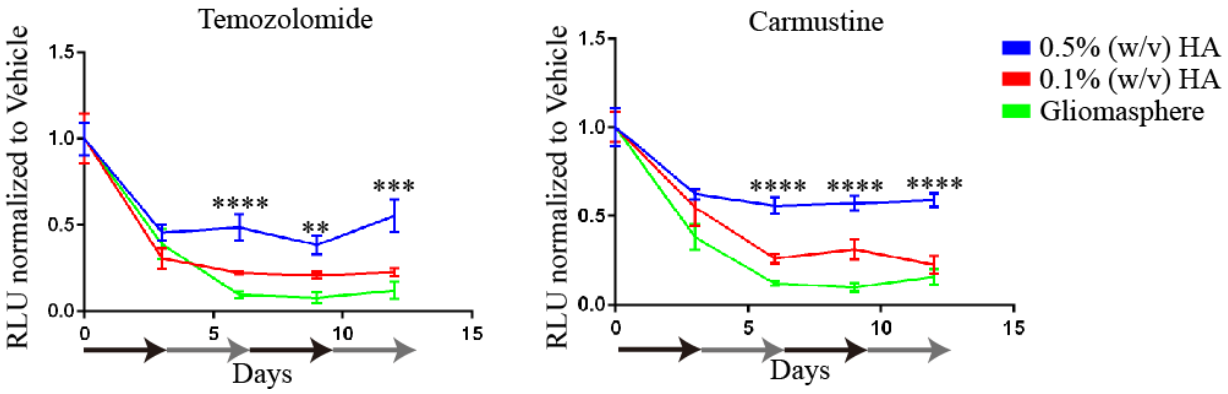

Figure 5.3. Bioluminescence measurements of HK301 cells over 12 days of treatment. Within each condition, treated samples were normalized to vehicle controls at each time point, then to signal before treatment (day 0). Two-way ANOVA (culture condition, time) was performed. Error bars show standard deviations (n=3).

Figure 5.4

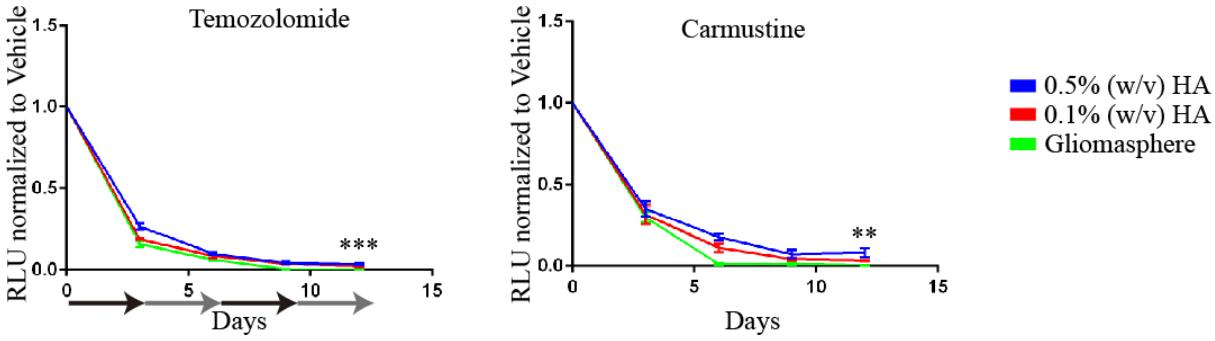

Figure 5.4. Representative luciferase bio-luminescence signals of treated GBM6 cells were normalized to non-treated samples and then the signal before treatment (day 0) for each condition. Two-way ANOVA (culture condition, time) was performed. Error bars show standard deviations (n=3). ** $p<0.01$, *** $p<0.001$.

Figure 5.5

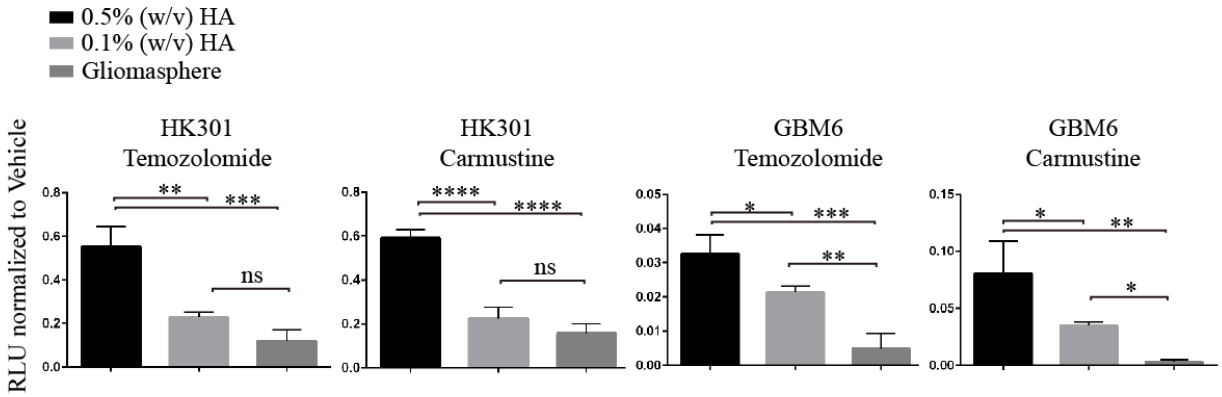

Figure 5.5. Bioluminescence signal in treated cultures of HK301 and GBM6 cells normalized to vehicle controls at the end of the 12-day chemotherapy regimen (n=3). One-way ANOVA followed by Tukey's multiple comparison tests were performed. Error bars show standard deviations. *p<0.5, **p<0.01, ***p<0.001, ****p<0.0001, "ns" represents non-significance.

Matrix HA interacts with CD44 to protect against chemotherapy-induced apoptosis

To investigate the mechanism by which the HA-rich hydrogel scaffolds create a microenvironment that facilitates drug resistance, we first tested whether culture in hydrogels prevented DNA damage from exposure to chemotherapy agents. Using an EdU-based assay, we found that carmustine treatment reduced DNA incorporation (i.e., proliferation rate) in both high HA hydrogel and GS cultures as measured on the 3rd day of carmustine treatment (**Figure 5.6, Figure 5.7**). TMZ treatment had a similar cytostatic effect on cultures in high HA (**Figure 5.8**). When GS were treatment with either drug, too few cells remained to perform reliable measurements of EdU incorporation via flow cytometry (*data not shown*). Although carmustine treatment attenuated cell proliferation in both hydrogel scaffold and GS cultures, proliferation in GS was essentially halted while some proliferation persisted in hydrogel cultures, prompting further investigation.

Alkylating agents induce cell cycle arrest, eventually leading programmed cell death, or apoptosis[222]. Thus, we suspected hydrogel-cultured cells may have gained resistance to the cytostatic effects of carmustine via reduced cytotoxicity. As predicted, when treated with carmustine, relative expression of cleaved poly ADP ribose polymerase (cl-PARP), a marker for late-stage apoptosis, in HK301 cells was higher in GS than in high HA hydrogel cultures (**Figure 5.9**). This exact comparison could not be make with GBM6 cells, as too many cells died with treatment to make it possible to collect lysate for Western blotting. By comparing cl-PARP expression in high and low HA hydrogel cultures of HK301 cells, we further confirmed that increased HA content led to a reduction in apoptosis (i.e., cl-PARP expression) in response to treatment (**Figure 5.10**). To evaluate the contribution of the CD44 receptor to anti-apoptotic protection

provided by the HA matrix, we repeated experiments with GBM cells transduced with shRNA to knockdown CD44 expression. Treatment-induced apoptosis increased significantly with the CD44 knockdown (**Figure 5.11**). No treatment (vehicle) controls confirmed that the CD44 knockdown alone was not sufficient to induce cl-PARP expression.

Figure 5.6

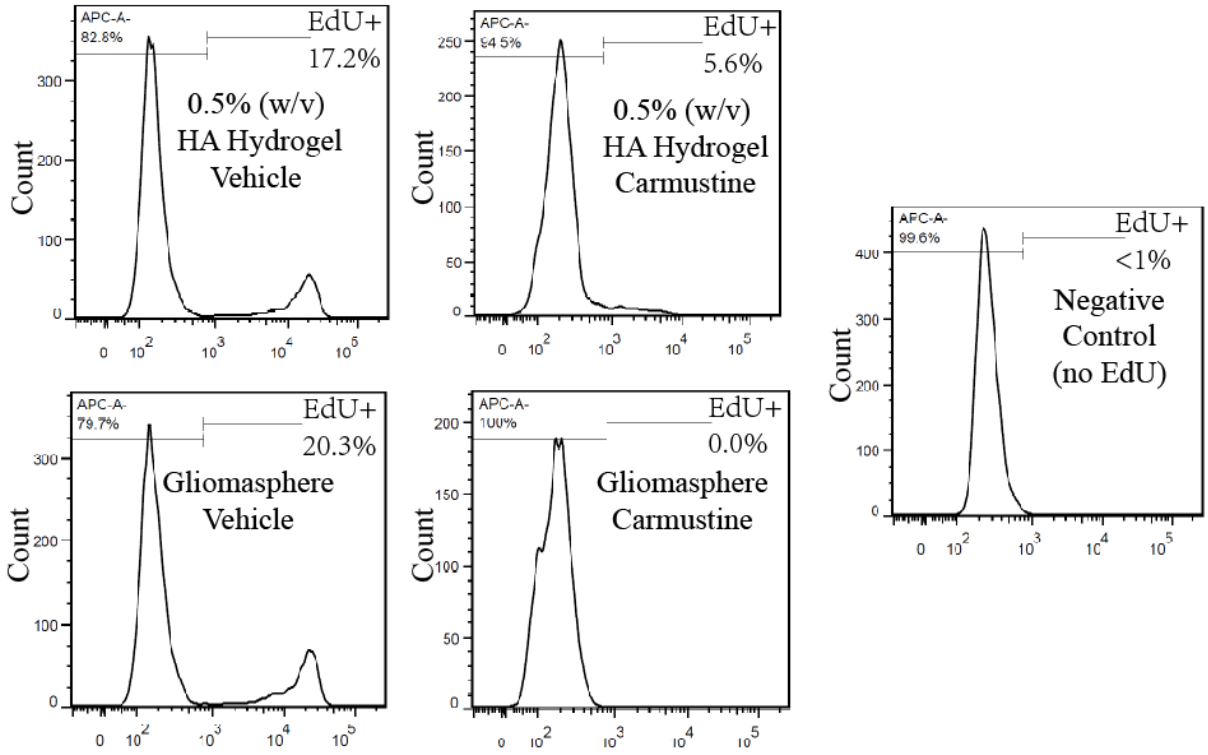

Figure 5.6. Representative plots of flow cytometry analysis showing EdU+ GBM6 cells (EdU incorporation by cells undergoing division during a 2.5 hr incubation) after 3 days of carmustine treatment (100 µM).

Figure 5.7

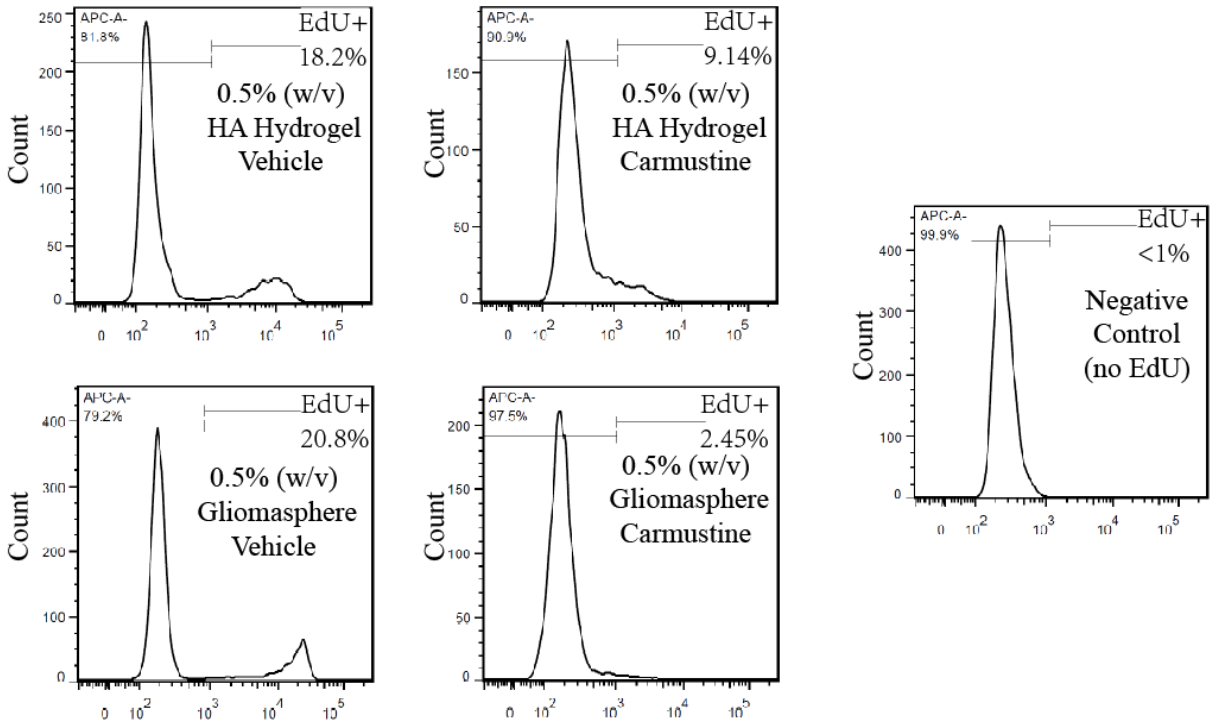

Figure 5.7. Representative flow cytometry graph showing proliferation rate of HK301 cells (EdU incorporation over 2.5 hrs) 3 days after 50µM carmustine or vehicle treatment.

Figure 5.8

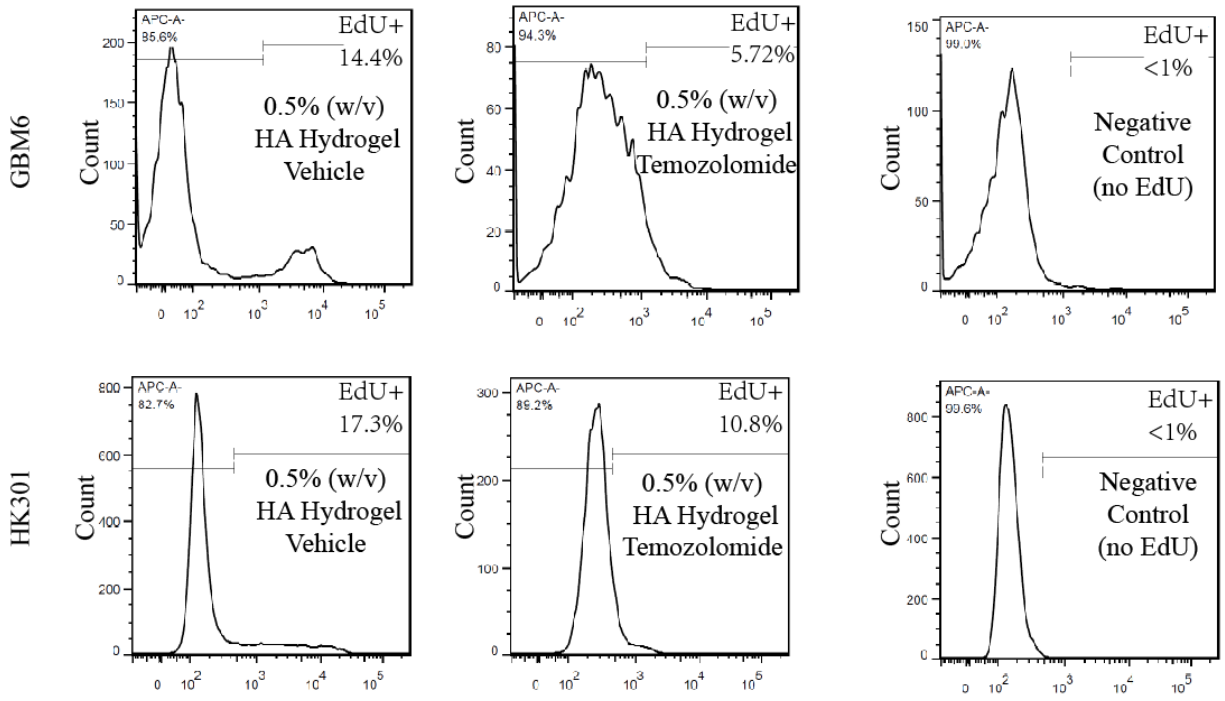

Figure 5.8. Representative flow cytometry graphs showing proliferation rate of HK301 and GBM6 cells (EdU incorporation over 2.5 hrs) 3 days after 500µM temozolomide or vehicle treatment.

Figure 5.9

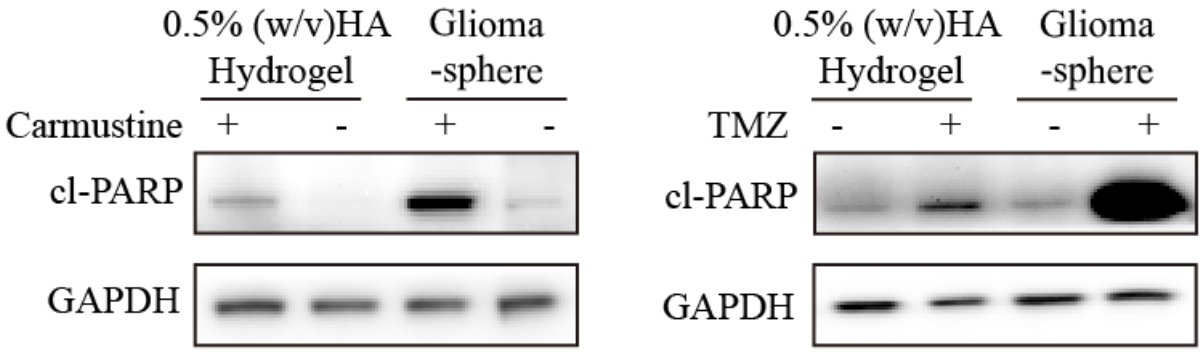

Figure 5.9. Representative Western blots showing cl-PARP expression in HK301 cells cultured in high HA (0.5% w/v) matrices or as gliomaspheres (GS) after 3 days of carmustine (50μM) or TMZ (500μM) treatment.

Figure 5.10

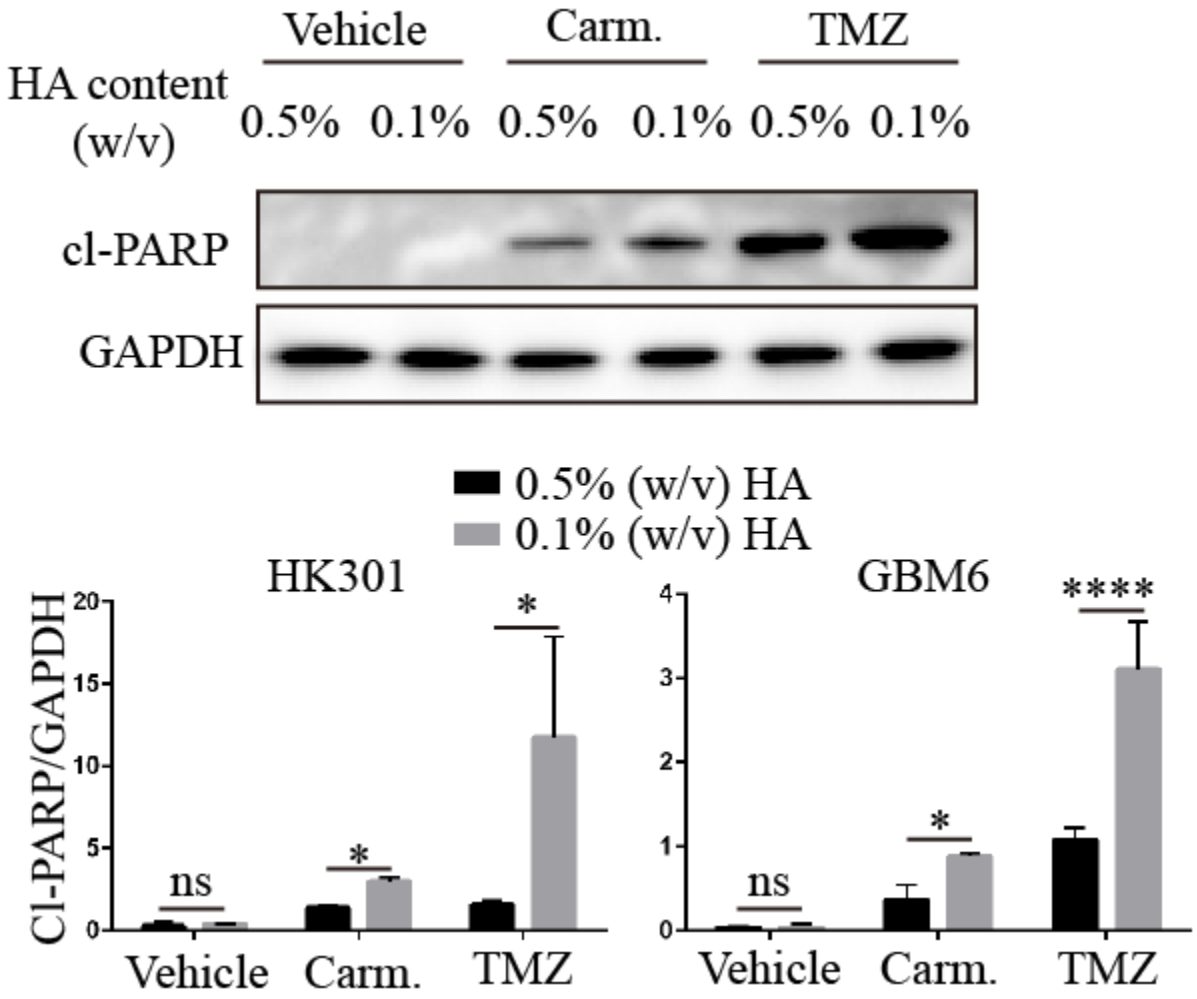

Figure 5.10. Top panel: Representative Western blots showing cl-PARP expression in GBM6 cells cultured in matrices with low (0.1 w/v) or high (0.5% w/v) HA after 3 days of treatment with carmustine (Carm., 100 µM), temozolomide (TMZ, 500 µM), or vehicle. Bottom panel: Densitometry analysis of Western blots, cl-PARP normalized to GAPDH, across independent repeats (n=3). Error bars show standard deviations. A student's t test was used to compare cl-PARP expression within each treatment arm. *p<0.5, **p<0.01, ***p<0.001, ****p<0.0001, "ns" represents non-significance.

Figure 5.11

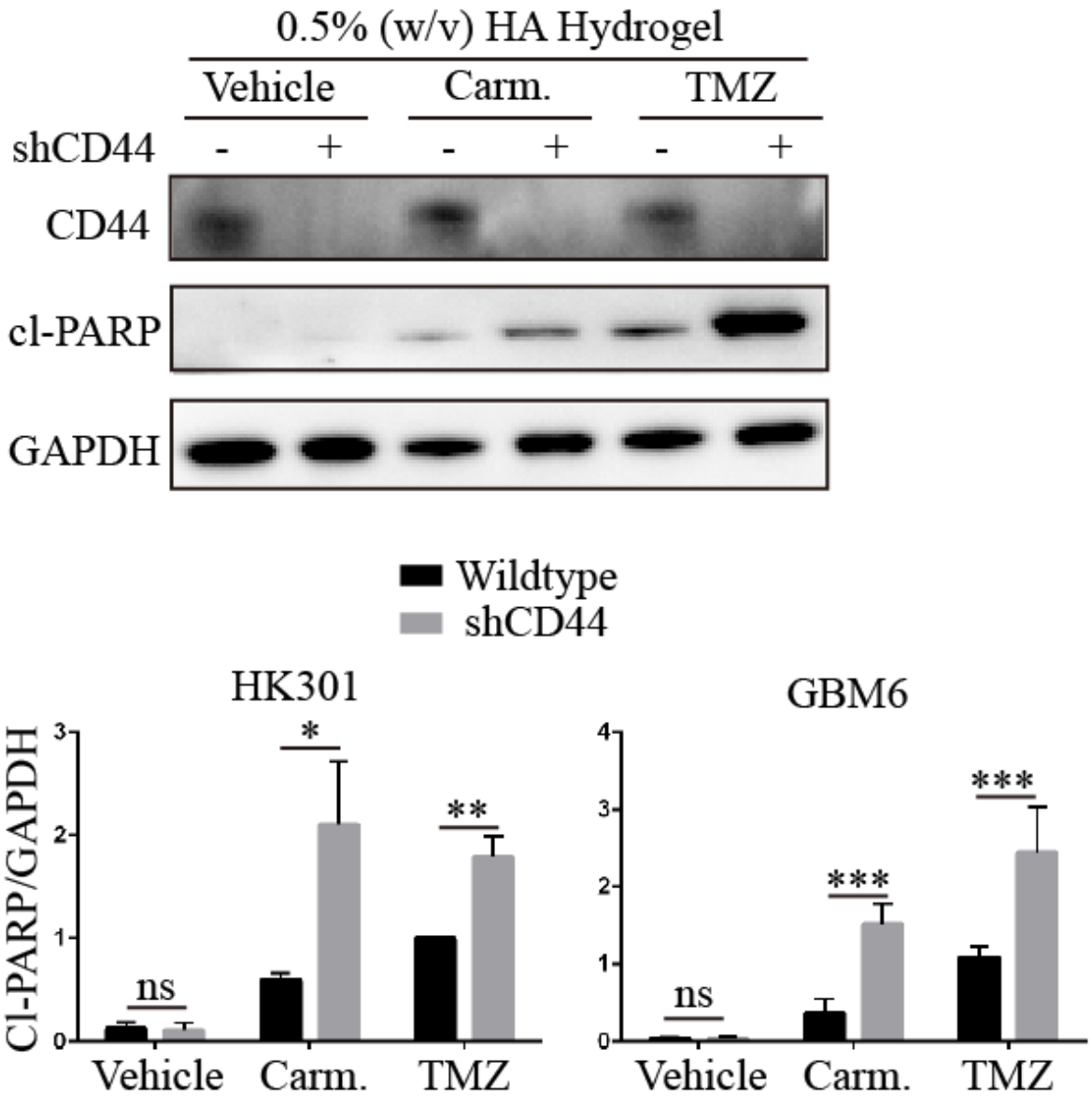

Figure 5.11. Upper panel: Representative Western blots showing cl-PARP expression in GBM6 cells (wildtype and shRNA knockdown of CD44) cultured in high HA matrices after 3 days of treatment with carmustine (Carm., 100 μM), temozolomide (TMZ, 500 μM), or vehicle. Lower panel: Densitometry analysis of Western blots, cl-PARP normalized to GAPDH, across independent repeats (n=3). Error bars show standard deviations. A student's t test was used to compare cl-PARP expression within each treatment arm. *p<0.5, **p<0.01, ***p<0.001, ****p<0.0001, "ns" represents non-significance.

The RGD motif and HA synergistically protect against treatment-induced apoptosis

The integrin-binding RGD motif is found in many ECM proteins, and cell adhesion through RGD has been reported to promote survival and invasion in multiple cancers[179]. Our hydrogel system enables incorporation of ECM-mimetic peptides containing RGD to recapitulate cell-ECM interactions through which biochemical and biomechanical cues may be transduced [198,223]. After GBM cell encapsulation into RGD-incorporated hydrogels, the majority of cells displayed an invasive morphology resembling a multicellular, or collective, migration mode (**Figure 5.12**). In contrast, cells remained as spheroid aggregates when cultured in hydrogels lacking the RGD motif. When treated with TMZ or carmustine, incorporation of RGD provided additional protection against apoptosis, significantly reducing cl-PARP expression over that in high HA scaffolds without RGD (**Figure 5.13**). To further evaluate the role of immobilized RGD in hydrogel matrices, we treated cells with both an alkylating chemotherapy and cilengitide, or cyclo-RGD. Cilengitide was developed as a targeted therapy for GBM which acts through selective disruption of integrin αV interaction with RGD-containing ECM proteins[202]. In HA-rich hydrogels with immobilized RGD peptides, addition of cilengitide competitively abolished the any invasive morphology (**Figure 5.14**). While cilengitide alone did not significantly affect apoptosis, it had a synergistic action when combined with chemotherapy agents, where cl-PARP expression increased by at least 2 times (**Figure 5.15**). These results demonstrate how both HA and RGD motifs in the microenvironment can protect GBM cells from chemotherapy-induced apoptosis.

Figure 5.12

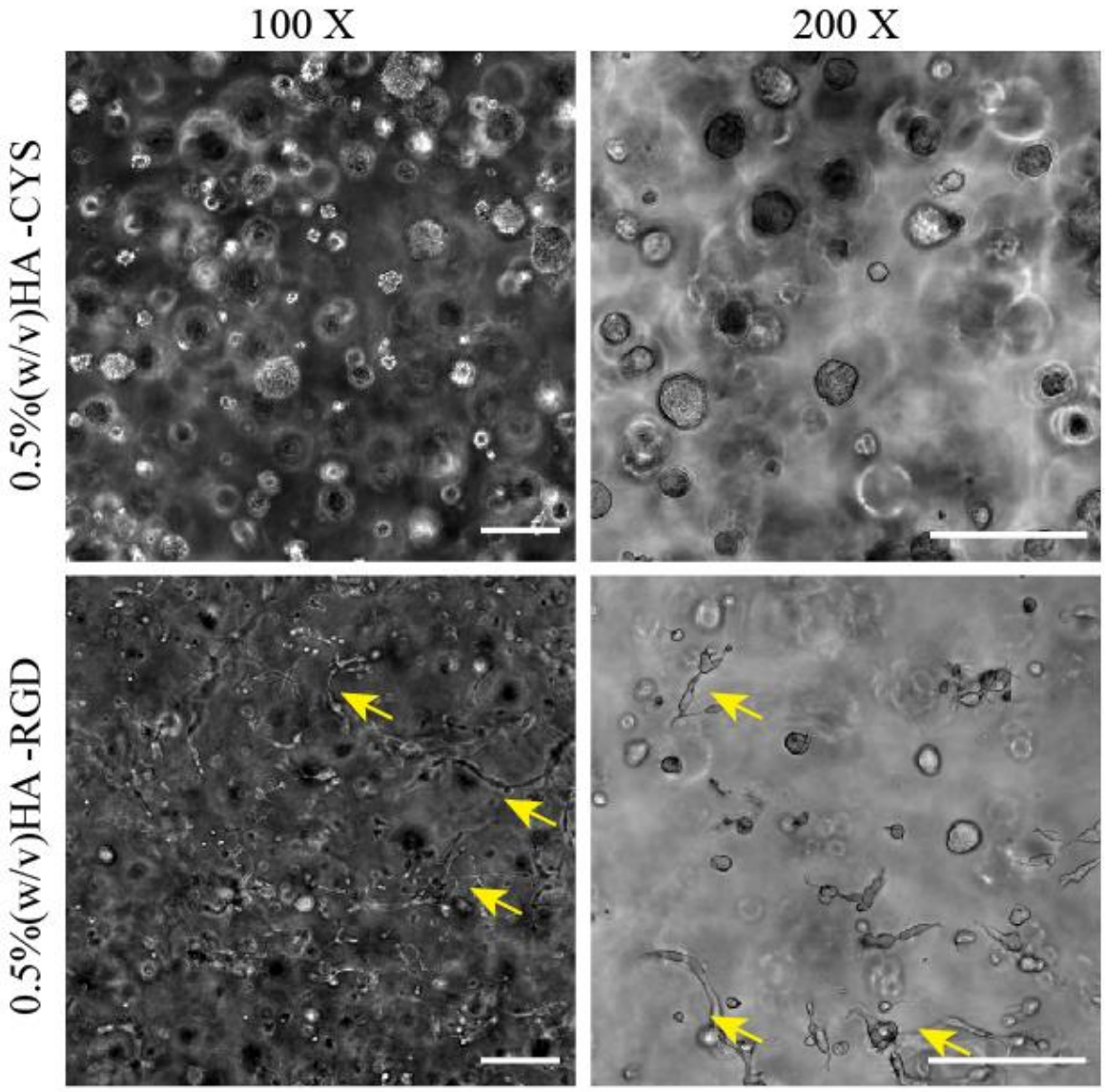

Figure 5.12. Representative phase contrast images of HK301 cells cultured for 8 days in hydrogels with high HA (0.5% w/v) and either adhesive peptides bearing the RGD motif or non-adhesive cysteines (“CYS”) as a negative control. Arrows indicate cells displaying invasive morphologies. Scale bars = 200 μm.

Figure 5.13

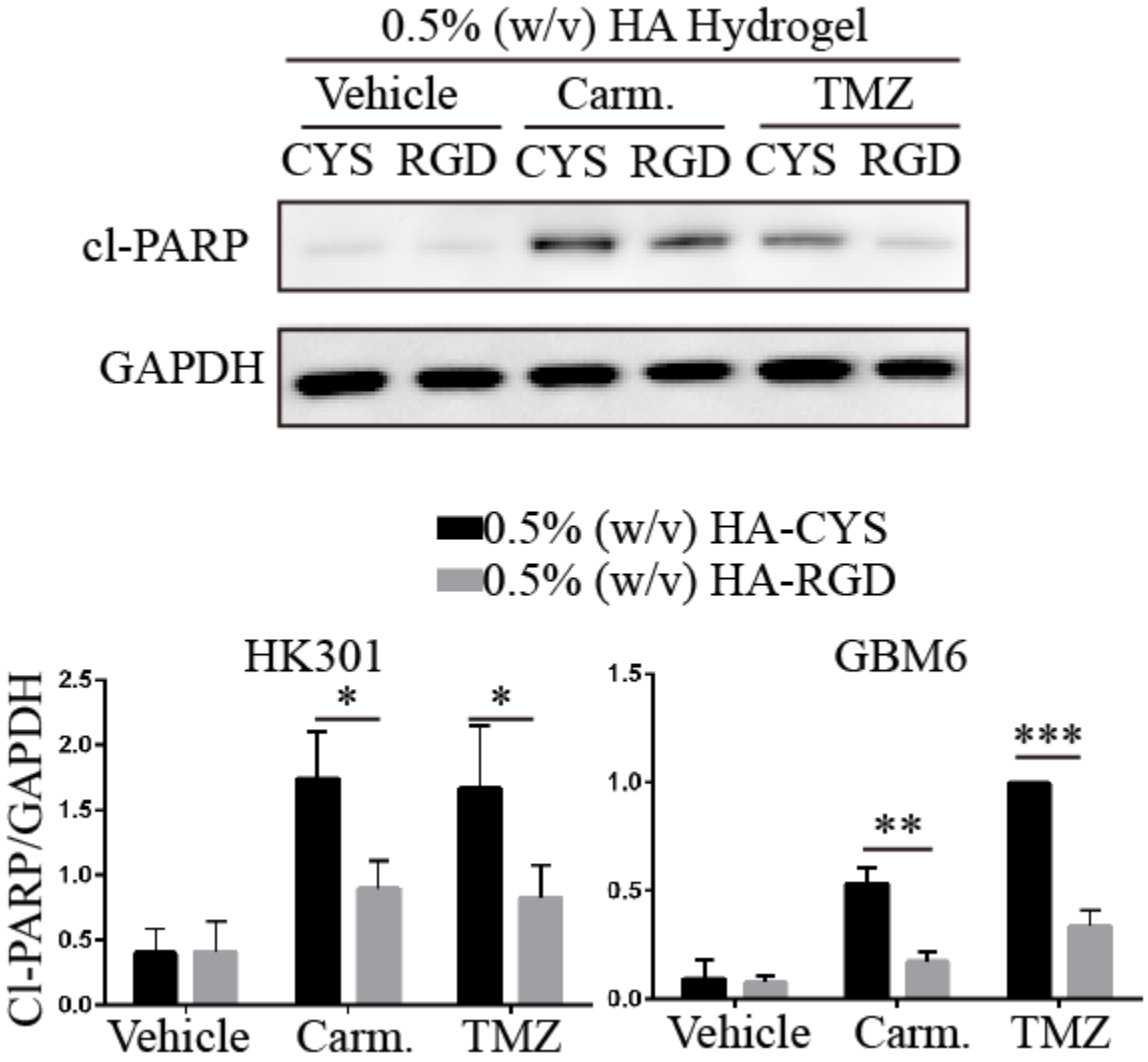

Figure 5.13. Upper panel: Representative Western blots showing cl-PARP expression in HK301 cells, cultured in high HA matrices containing RGD (or CYS control) peptides, after 3 days of treatment with carmustine (Carm., 50 μM), temozolomide (TMZ, 500 μM), or vehicle. Lower panel: Densitometry analysis of Western blots, cl-PARP normalized to GAPDH, across independent repeats (n=3). Error bars show standard deviations. A student's t-test was used to compare cl-PARP expression within each treatment arm. *p<0.5, **p<0.01, ***p<0.001, ****p<0.0001, "ns" represents non-significance.

Figure 5.14

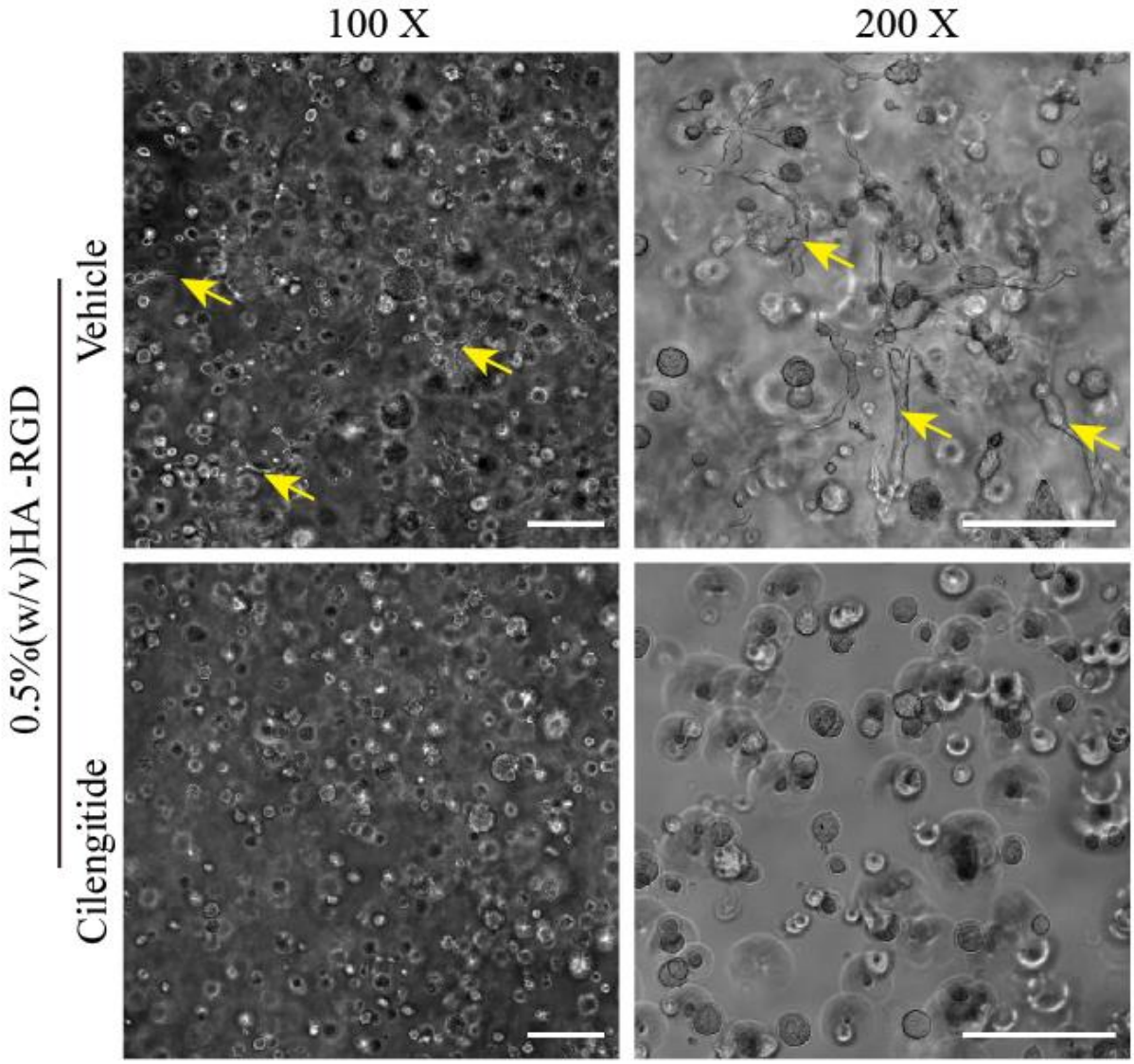

Figure 5.14. Representative phase contrast images of HK301 cells cultured in 3D hydrogel matrices with high HA and RGD after 4 days after cilengitide treatment (50 µM). Cells were cultured for 8 days in hydrogels before starting cilengitide treatment. Arrows indicate cells displaying invasive morphologies. Scale bars = 200 µm.

Figure 5.15

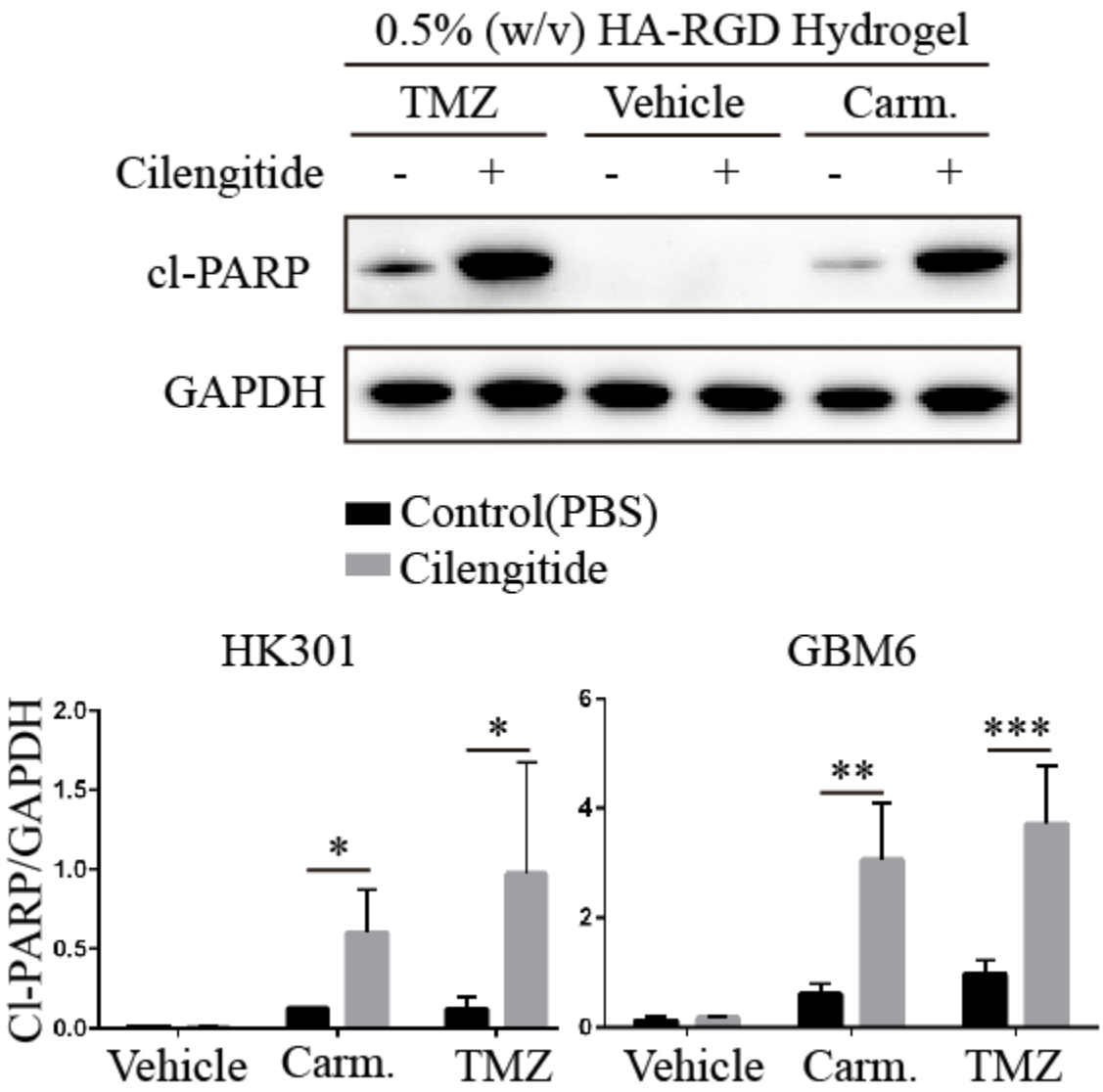

Figure 5.15. Upper panel: Representative Western blots showing cl-PARP expression in GBM6 cells cultured in 3D hydrogel matrices with high HA and RGD after 3 days of treatment with carmustine (Carm., 100 µM), temozolomide (TMZ, 500 µM), or vehicle. Cilengitide treatment (50 µM) was started 4 days before beginning chemotherapy treatment. Lower panel: Densitometry analysis of Western blots, cl-PARP normalized to GAPDH, across independent repeats (n=3). Two-way ANOVA (cilengitide, chemotherapy) was performed. p_{int}= 0.03 for HK301 and p_{int}=0.005 for GBM6. Error bars show standard deviations. A student's t-test was used to compare cl-PARP expression within each treatment arm. *p<0.5, **p<0.01, ***p<0.001, ****p<0.0001, "ns" represents non-significance.

Presence of HA and RGD in hydrogel matrices induce co-expression of CD44 and integrin αV expression in 3D-cultured GBM cells

The RGD motif is reported to be a ligand for integrin αV, which undergoes hetero-dimerization with β integrin subunits upon binding[33,202]. Given that incorporation of RGD peptides into high HA hydrogels significantly enhanced chemotherapy resistance and that this effect was abolished by cilengitide treatment, we posited that integrin αV, whose binding to RGD is selectively disrupted by cilengitide[202], and CD44 may act together to facilitate drug resistance. Immunostaining results indicated that GBM cells cultured within HA hydrogels bearing RGD co-expressed CD44 and Integrin αV within close proximity (within 0.42 μm, the effective resolution of images captured) in cell membranes — indicating possible clustering of receptors through binding to the available ECM (**Figure 5.16**). Moreover, omission of HA from hydrogels or treatment of cultures with cilengitide abolished co-expression of CD44 and Integrin αV (**Figure 5.16**). Together, these results indicate that direct interactions between CD44 and integrin αV may mediate chemotherapy resistance observed in HA-RGD hydrogel cultures.

Figure 5.16

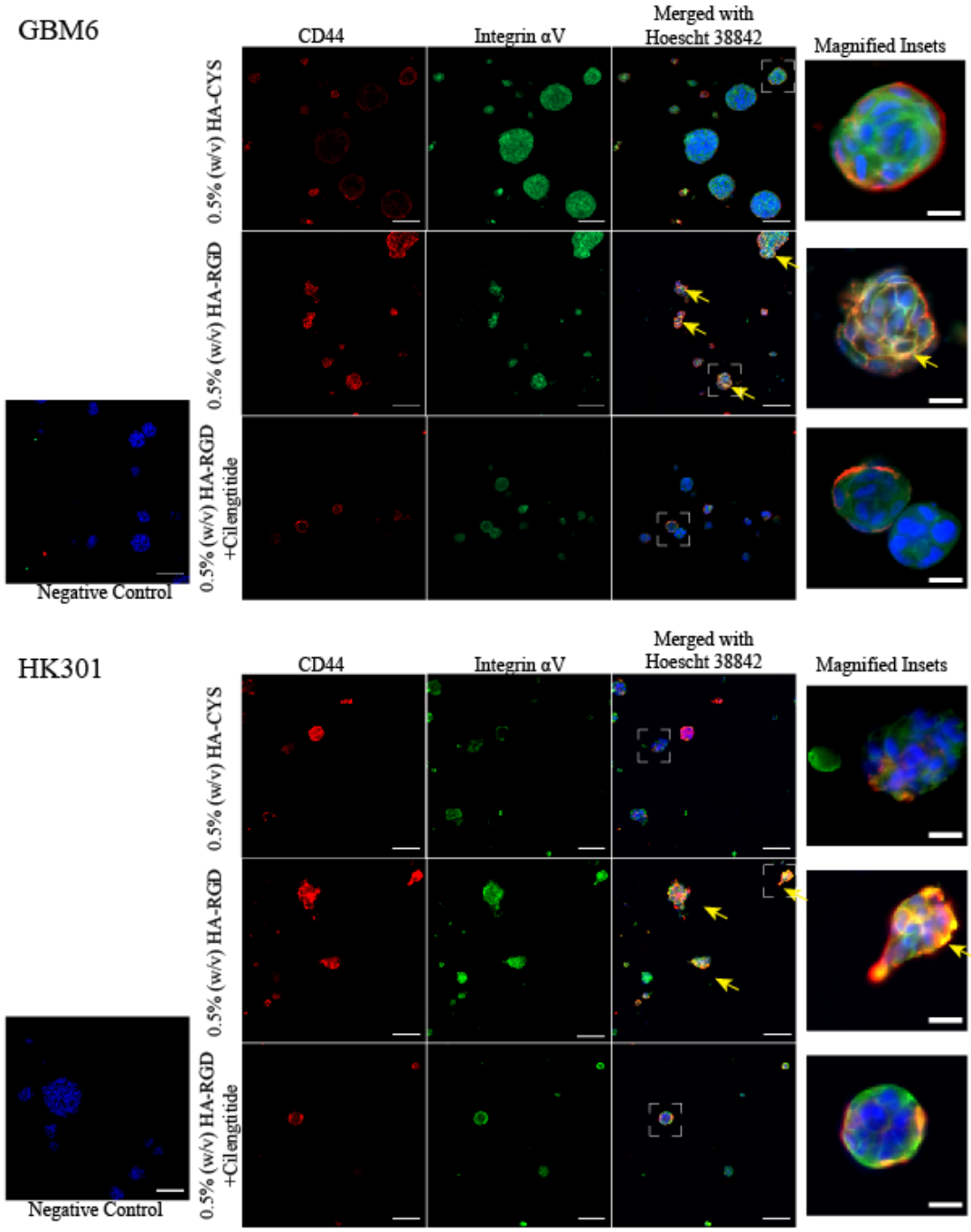

Figure 5.16. Representative fluorescence images of immunostaining for CD44 (red) and integrin αV (green) of GBM6 and HK301 cells cultured in high HA matrices containing RGD (or CYS control) peptide for 8 days. Nuclei were counterstained with Hoescht 33342 (blue). Primary antibody was omitted for negative control images. Arrows indicate areas of CD44 and integrin αV co-expression (yellow). Cells were cultured 8 days

before cilengitide treatment (50 μM), which continued for 3 days. Scale bars = 200 μm (20 μm for magnified insets of areas shown by white boxes).

Integrin αV and CD44 mediate chemotherapy resistance and invasive morphology in 3D matrices

Next, we used lentiviral vectors encoding shRNA against CD44 or integrin αV to further investigate effects of their engagement on GBM cells. Interestingly, knockdown of either CD44 or integrin αV eliminated all invasive characteristics of HK301 cells (**Figure 5.17**). To investigate how integrin αV affects chemotherapy-induced apoptosis, we compared cl-PARP expression between wildtype and integrin αV knockdown cells cultured in hydrogels with identical formulations. We found increased cl-PARP expression with integrin αV knockdown with carmustine treatment (**Figure 5.18**). While not statistically significant, a similar trend was observed with TMZ treatment. Through bioluminescence tracking of GBM cell growth in live cultures, the critical role of integrin αV in ECM-mediated chemotherapy resistance was confirmed (**Figure 5.19**).

Figure 5.17

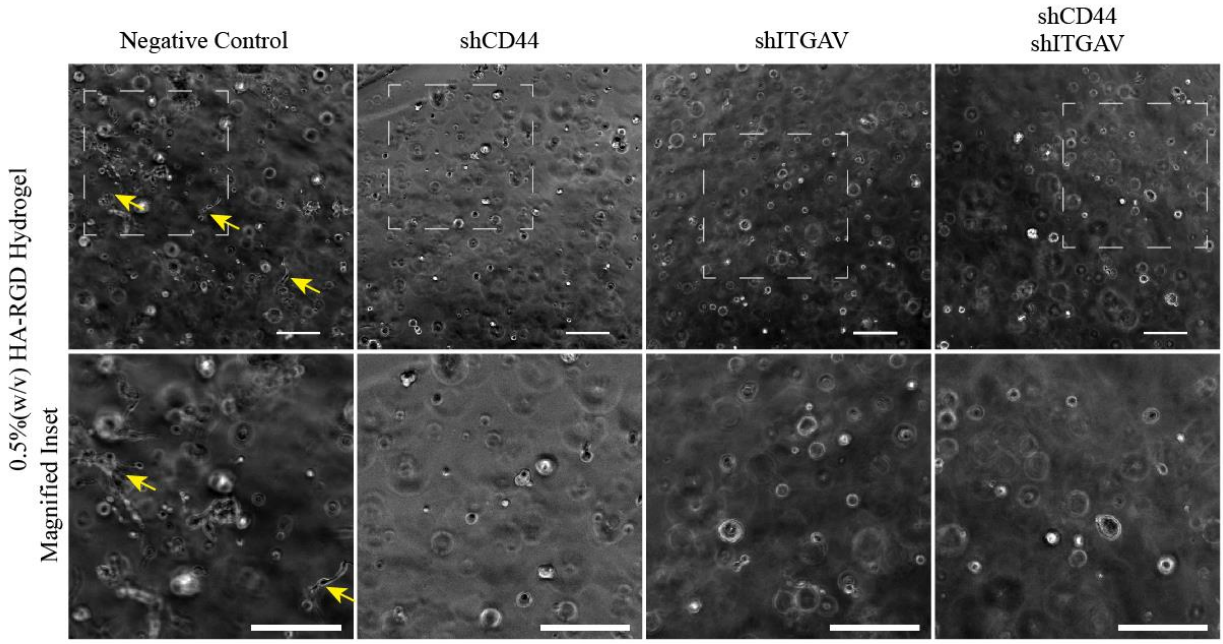

Figure 5.17. Representative phase contrast images of HK301 cells (wildtype and shRNA knockdowns of CD44 and/or integrin αV (ITGAV)) cultured for 8 days in hydrogels with high HA and RGD. Arrows indicate cells displaying invasive morphologies. Areas indicated by white boxes in the top row of images are shown at higher magnification in the bottom row. Scale bars = 200 μm.

Figure 5.18

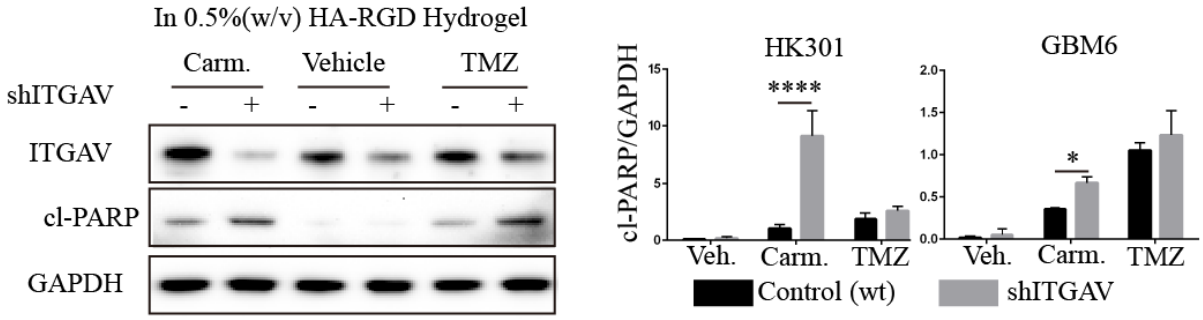

Figure 5.18. Left panel: Representative Western blots showing cl-PARP expression in HK301 cells (wildtype and shRNA knockdown of ITGAV) cultured in hydrogels with high HA and RGD after 3 days of treatment with with carmustine (Carm., 50 μM), temozolomide (TMZ, 500 μM), or vehicle. Right panel: Densitometry analysis of Western blots, cl-PARP normalized to GAPDH, across independent repeats (n=3). A student's t test was performed to compare cl-PARP expression within each treatment arm. Error bars show standard deviations.

Figure 5.19

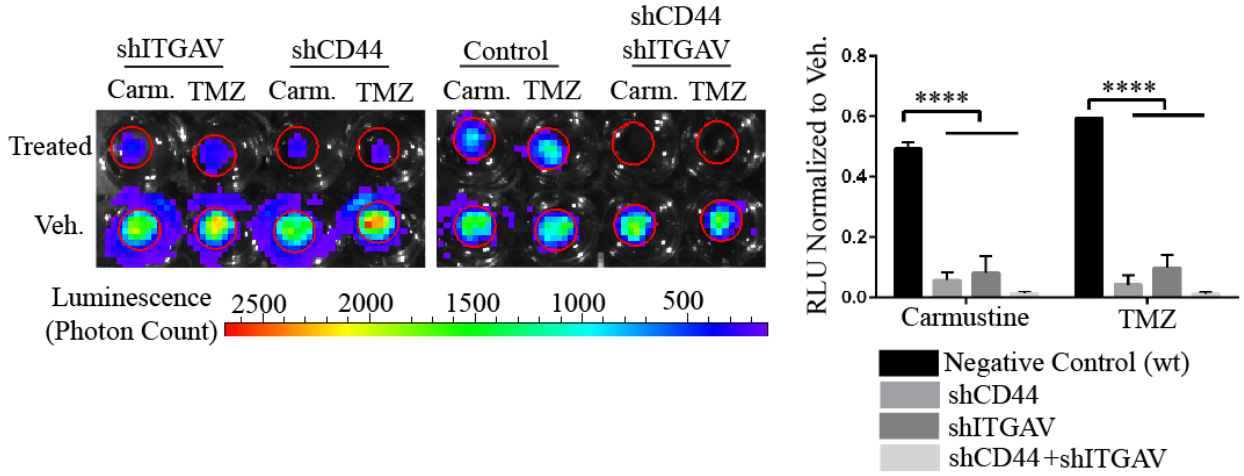

Figure 5.19. Left panel: Representative bioluminescence signal overlaid with a photograph of HK301 cultures on the 12th day 12 of chemotherapy treatment regimen. Red circles indicate locations of hydrogel cultures with the well plate. Right panel: Bioluminescence signal in treated cultures of HK301 cells normalized to vehicle controls at the end of the 12-day chemotherapy regimen (n=3). One-way ANOVA with Tukey's multiple comparison tests was performed. Error bars show standard deviations. ****p<0.0001.

HA-CD44 and RGD-integrin αV interactions act together to promote chemotherapy resistance through Src signaling

In many cancers, including GBM, Src activation is mediated by integrin binding to ECM ligands and can facilitate tumor cell invasion[218,224,225]. In addition, CD44-mediated activation of Src has been reported in colon and ovarian cancers [216,226]. Moreover, in GBM patients, Src has been identified as a downstream effector of EGFR signaling pathways, whose activation directly contributes to chemotherapy resistance[225,227]. Thus, we investigated whether CD44 and integrin αV downstream Src activation in GBM cells cultured in high HA hydrogels with RGD. With shRNA knockdown of either CD44 or integrin αV, Src phosphorylation was significantly reduced (**Figure 5.20A**). Next, we confirmed that disruption of integrin-RGD binding via cilengitide treatment reduced Src activation (**Figure 5.20B**). Finally, we verified that RGD and HA were both required to maximize Src phosphorylation within GBM cells in 3D culture in our engineered matrices (**Figure 5.20C, D**).

Based on these results, we postulated that suppression of Src inhibition via dasatinib[219] could sensitize GBM cells to treatment, even in the presence of resistance-promoting matrix cues. First, we observed that dasatinib treatment abolished the invasive morphology of GBM cells (**Figure 5.21**). Next, we found that while dasatinib alone does not induce apoptosis, dual treatment with an alkylating chemotherapy had a synergistic effect induced significantly more apoptosis (assessed by expression of cl-PARP) than treatment with either TMZ or carmustine alone (**Figure 5.22**). Consistent with these findings, dasatinib alone had no effects on culture growth (measured by

bioluminescence imaging) while combination therapies resulted in a synergistic reduction in cell growth of ≥ 50% (**Figure 5.23**).

Figure 5.20

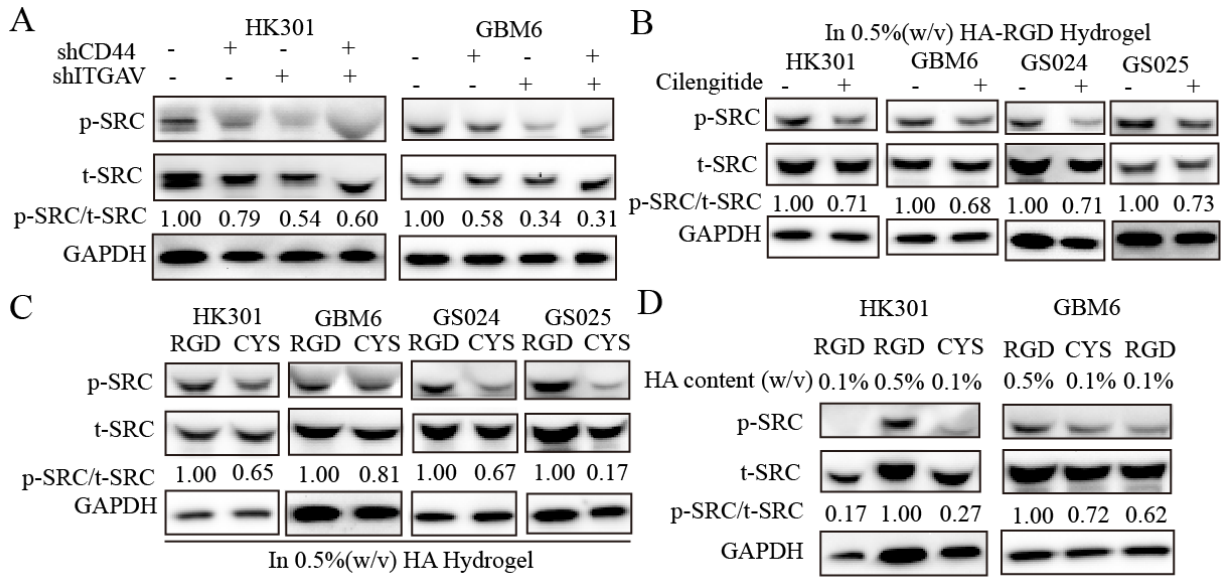

Figure 5.20. Representative Western blots showing Src phosphorylation in GBM cells (HK301, GBM6, GS024, GS025 lines). For A, C and D, cell lysates were collected after 8 days in 3D culture. For B, cilengitide (50 µM) treatment was started on day 8 of culture and cell lysates were collected after 3 days of treatment. Densitometry analysis showing the ratio of p-SRC to t-SRC is indicated within each panel.

Figure 5.21

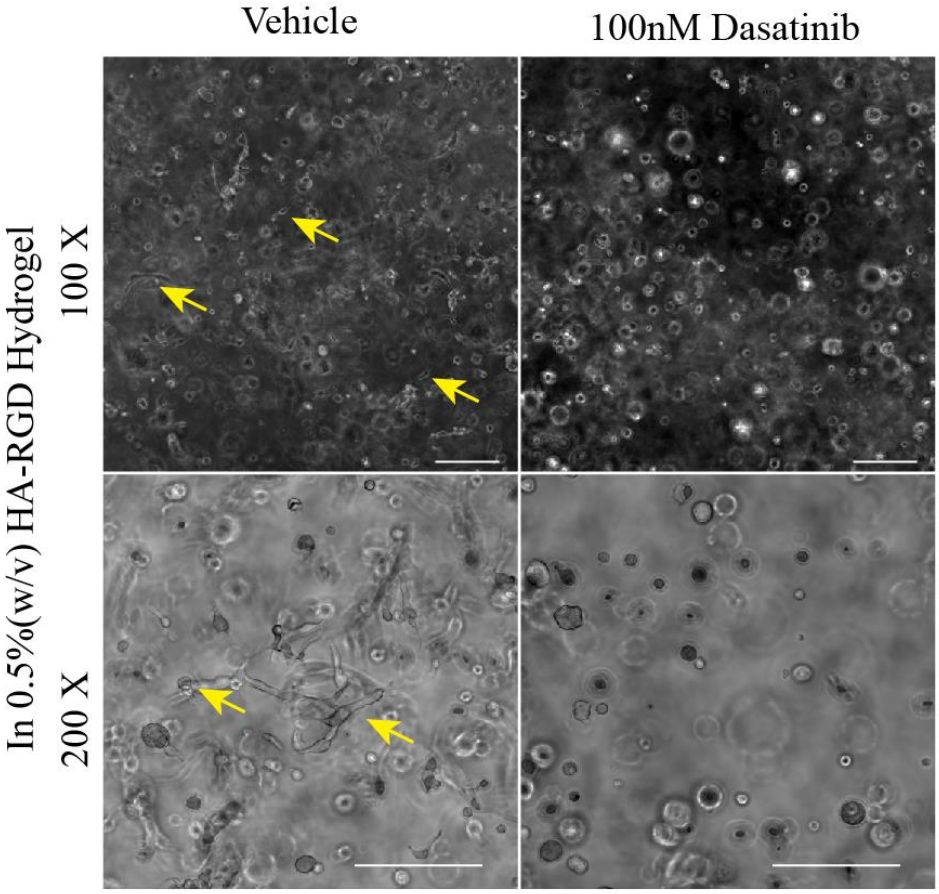

Figure 5.21. Representative phase contrast images of HK301 cells cultured in hydrogel matrices with high HA (0.5% v/w) and RGD for 4 days, then treated for 4 days with dasatinib (100 nM) or vehicle (DMSO). Arrows show cells displaying invasive morphologies. Scale bars = 200 µm.

Figure 5.22

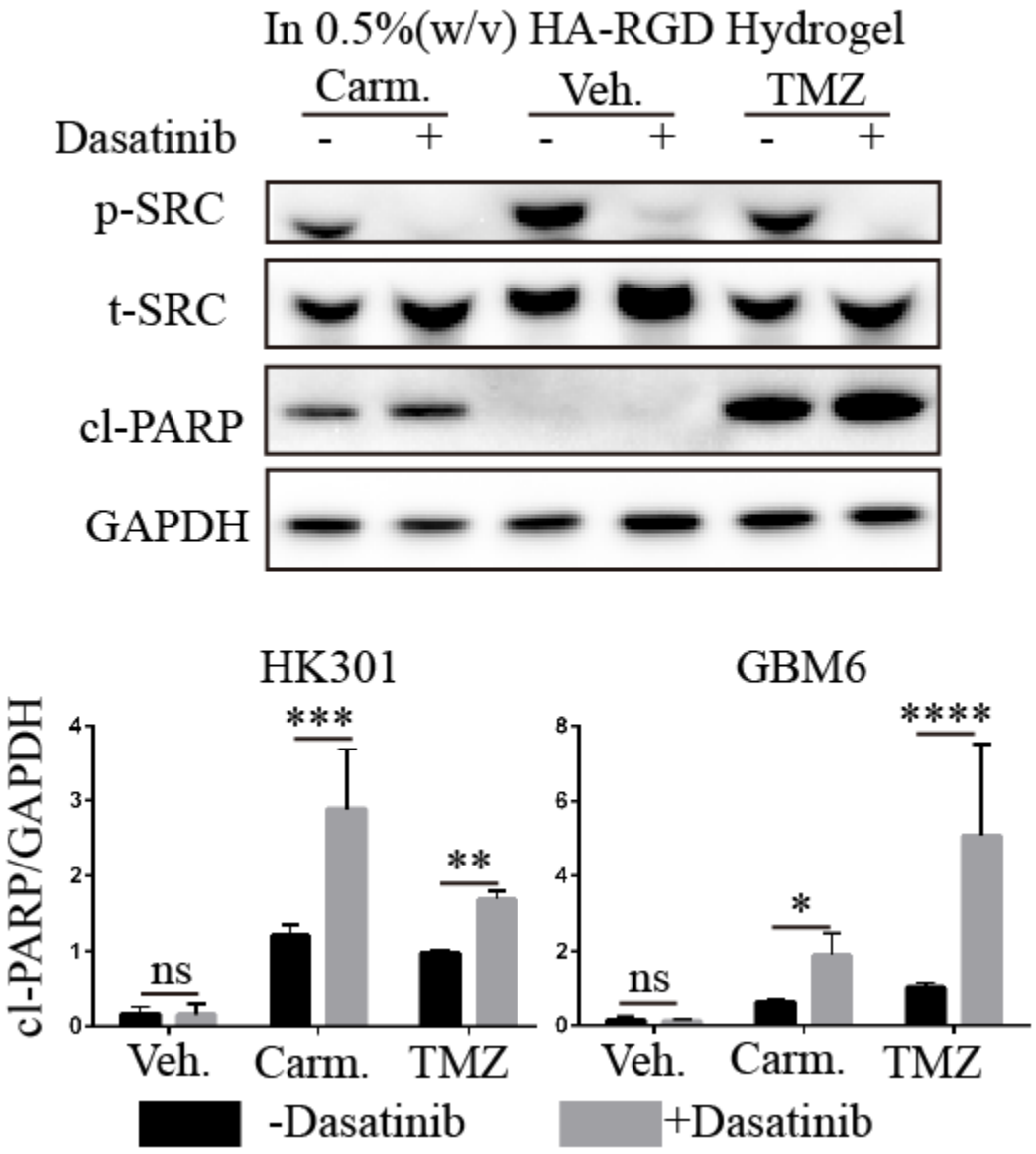

Figure 5.22. Upper panel: Representative Western blots showing Src phosphorylation and cl-PARP expression in GBM6 after 3 days of treatment with carmustine (Carm., 100 μM), temozolomide (TMZ, 500 μM), or vehicle. Dasatinib (100 nM) or vehicle (DMSO) was added 4 days before the start chemotherapy treatment. Lower panel: Densitometry analysis of Western blots, cl-PARP normalized to GAPDH, across independent repeats (n=3). Student's t test was performed to compare cl-PARP expression within each treatment arm. Error bars show standard deviations. Two-way ANOVA (dasatinib, chemotherapy) was performed. p_{int}= 0.003 for HK301 and p_{int}=0.0002 for GBM6.

Figure 5.23

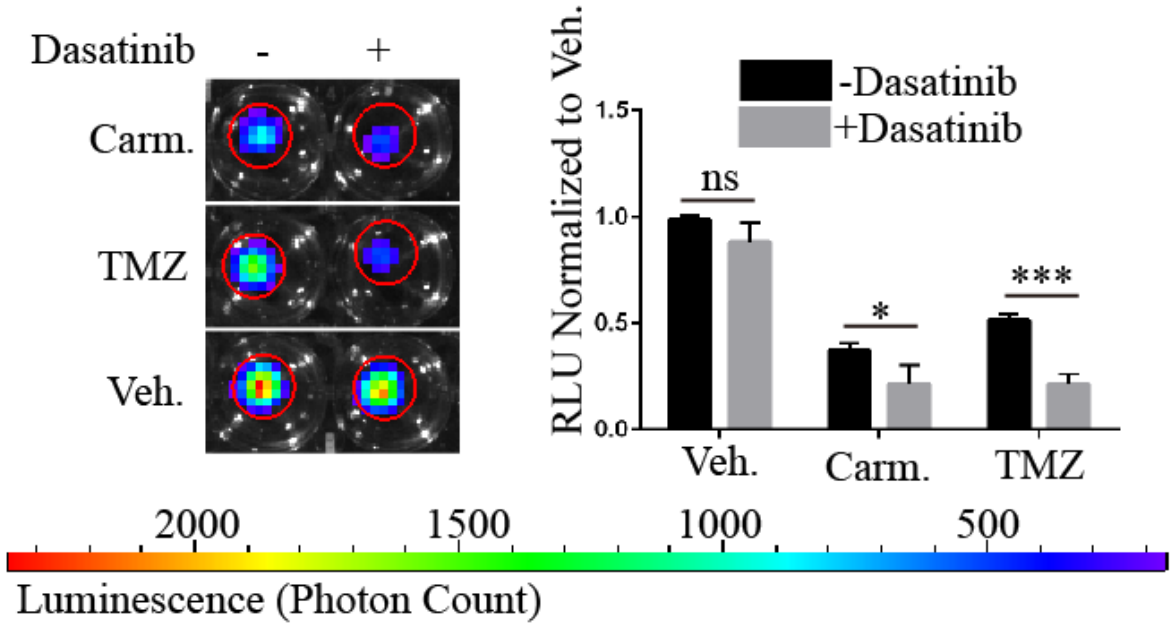

Figure 5.23. Left panel: Representative bioluminescence signal overlaid with a photograph of HK301 cultures on the 12th day 12 of chemotherapy treatment regimen. Red circles indicate locations of hydrogel cultures with the well plate. Right panel: Bioluminescence signal in treated cultures of HK301 cells normalized to vehicle controls at the end of the 12-day chemotherapy regimen (n=3). Two-way ANOVA (dasatinib, chemotherapy) was performed. p_{int}= 0.03. Error bars show standard deviations. *p<0.5, **p<0.01, ***p<0.001, ****p<0.0001, “ns” represents non-significance.

HA and RGD interactions protect GBM cells from treatment-induced apoptosis through suppression of pro-apoptotic members of the BCL-2 family

Src activation has been reported to regulate activities of BCL-2 family proteins, which direct caspase-mediated cleavage of PARP and eventually cause apoptosis[228–230]. To investigate the role of Src activation in GBM chemotherapy resistance, we examined expression of BCL-2 family pro-apoptotic factors, including P53-upregulated modulator of apoptosis (PUMA), BCL-2-associated X protein (BAX) and BCL-2 homologous antagonist killer (BAK), in all conditions. When treated with either alkylating chemotherapy, HK301 cells increased expression of PUMA, BAX, and BAK over vehicle controls (**Figure 5.24A, B**). Dual treatment with either dasatinib or cilengitide further increased this effect, while treatment with dasatinib or cilengitide alone did not alter the expression of any pro-apoptotic factors assayed (**Figure 5.24A, B**). In the case of GBM6 cells, treatment with either dasatinib or cilengitide alone elevated PUMA expression, while treatment with either alkylating chemotherapy decreased expression of all three pro-apoptotic factors (**Figure 5.25**). Notably, co-treatment with cilengitide or dasatinib rescued the expression of these pro-apoptotic factors.

Next, we evaluated the connection between upstream engagement of CD44 and integrin αV receptors by the hydrogel matrix and downstream expression of BCL-2 family pro-apoptotic factors in the presence of treatment. Chemotherapy treatment in cells with CD44 or integrin αV knockdown induced increased expression of pro-apoptotic factors (**Figure 5.26 A-D**). Even without treatment (i.e., vehicle), knockdown of either CD44 or integrin αV elevated expression of the pro-apoptotic factors in GBM6 cells; however, only a slight increase in expression of BAX and BAK occurred in HK301

cells (**Figure 5.26 A,B**). Last, we evaluated whether high HA content and RGD peptide were both required to suppress elevation of PUMA, BAX, and BAK expression with TMZ or carmustine treatment. In HK301 and GBM6 cells, the relative expressions of the pro-apoptotic factors when treated with either chemotherapy were consistent with CD44 and integrin αV knockdown results, where low HA or a lack of RGD binding sites in the matrix resulted in increased expression of pro-apoptotic factors (**Figure 5.26B**, **Figure 5.27 A-C**). Together, results demonstrate that cell-matrix interactions co-activated downstream Src to suppress of expression BCL-2 family pro-apoptotic factors and augment chemotherapy resistance.

Figure 5.24

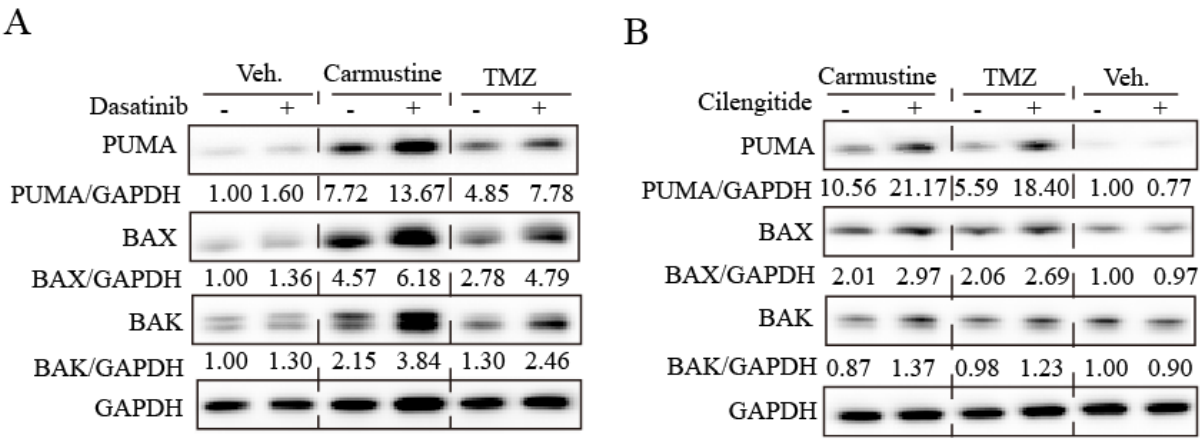

Figure 5.24. Representative Western blots showing expression of BCL-2 family factors, PUMA, BAK and BAX in co-treatment conditions in HK301.

Figure 5.25

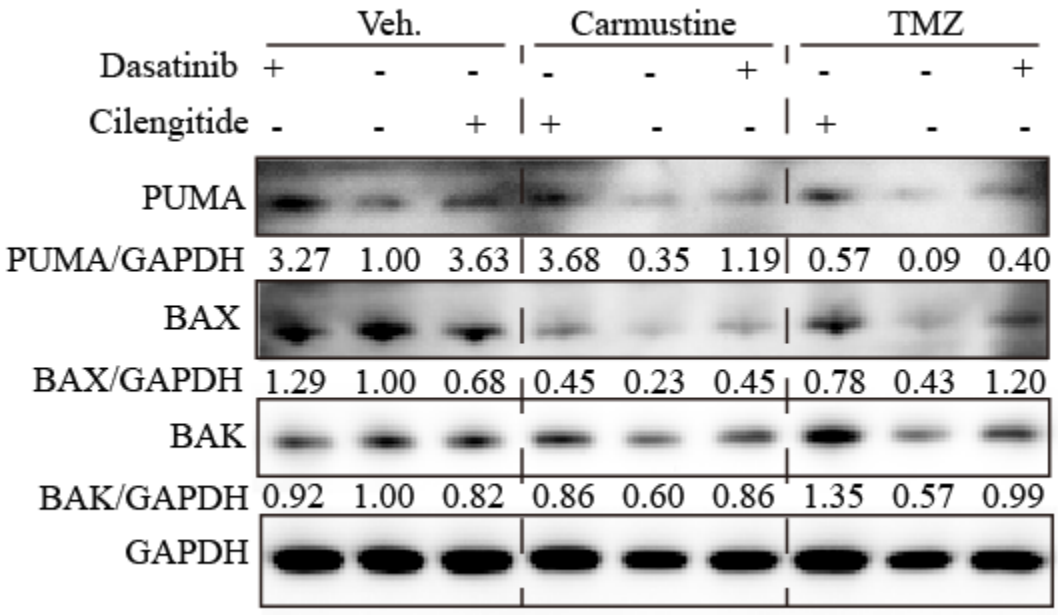

Figure 5.25. Representative Western blots showing expression of BCL-2 family factors, PUMA, BAK and BAX in co-treatment conditions in GBM6.

Figure 5.26

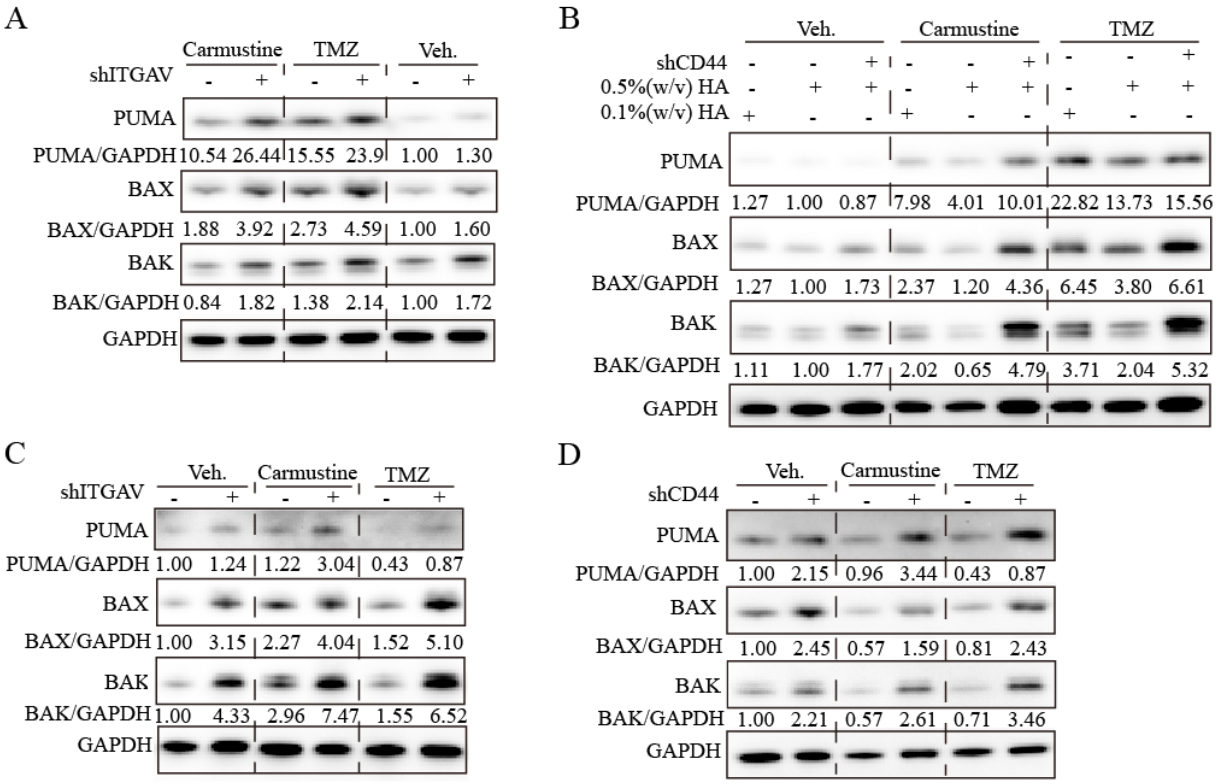

Figure 5.26. Representative Western blots showing expression of BCL-2 family factors, PUMA, BAK and BAX in different knockdown conditions in A, B) HK301 and C, D) GBM6.

Figure 5.27

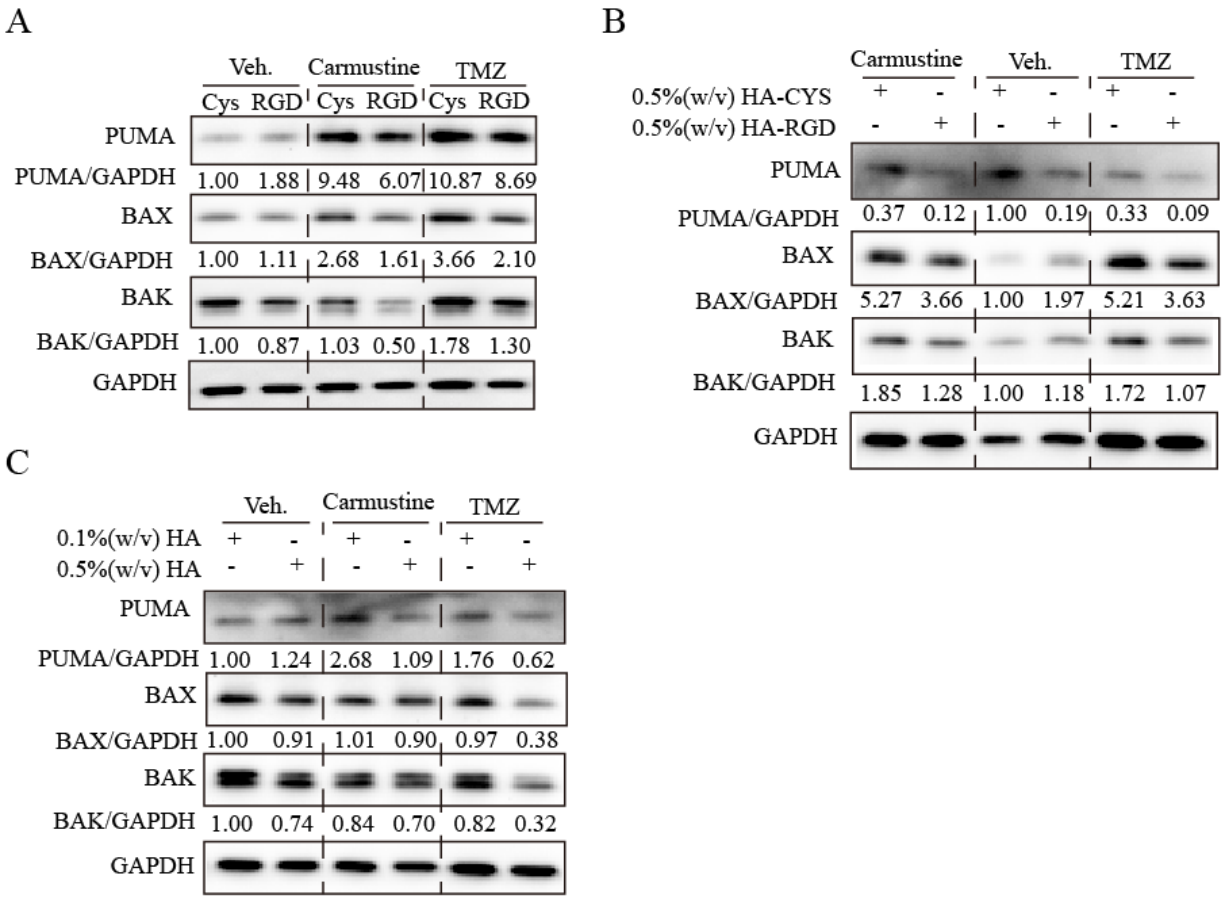

Figure 5.27. Representative Western blots showing expression of BCL-2 family factors, PUMA, BAK and BAX in different hydrogel conditions in A) HK301 and B,C) GBM6.

Discussion:

The extreme propensity of GBM to develop therapeutic resistance, where nearly 100% of tumor stop responding and recur, is a critical area of study[1,211]. While molecular mechanisms leading to treatment insensitivity and resistance, such as MGMT methylation, have been widely investigated and despite a growing body of evidence suggesting a major role for ECM in resistance[180,231,232], few studies have directly evaluated the effects of ECM in the microenvironment on tumor cells. Of studies that have explored this area, the majority have relied on adsorbing purified ECM biomolecules onto hard, 2D surfaces, such as glass or tissue-culture plastic[231], or have added ECM components that do not readily adsorb, such as HA, directly to culture medium in a non-physiological, soluble form[216]. However, these methods fail to recapitulate key aspects of the tumor ECM, which is a soft, HA-rich, microporous scaffold in which cells are embedded in three dimensions. Recent studies have demonstrated that bioengineered, 3D culture systems, designed to mimic the native brain tumor ECM, can be used to study the therapeutic response of GBM cells *ex vivo* in a context that yields resistant phenotypes more similar to those observed *in vivo* than can be achieved using traditional, 2D cultures[132,133,147,233–235]. While the focus of the majority of previous studies has been to demonstrate feasibility and potential utility of such 3D culture platforms, here we have applied a bioengineered culture platform to elucidate detailed mechanisms of ECM-mediated treatment resistance in patient-derived GBM cells.

Here, we used a tunable, bioengineered culture platform 1) to demonstrate that the 3D microenvironment provided by the ECM facilitates acquisition of drug resistance in GBM

and 2) to elucidate mechanisms underlying this phenomenon. Through parallel experiments where either HA was removed from the extracellular milieu or CD44 expression was knocked down, results demonstrate that HA-CD44 interactions promote cytostatic and cytotoxic resistance to treatment with carmustine or TMZ. In particular, resistance was robust compared to patient-matched gliomasphere cultures, which we have previously shown do not express high levels of HA[198], underscoring the critical contributions of the local ECM microenvironment to GBM cell biology. Moreover, our results indicate that HA may promote GBM cell survival during treatment, allowing cells to recover during periods of "rest" from treatment, similar to a typical chemotherapy cycle in a clinical setting. Specifically, scaffolds with high HA content protected GBM cells from chemotherapy-induced apoptosis. HA may have a similar protective effect in clinical GBM, where increased HA expression positively correlates with tumor aggression [16,22],

Furthermore, we incorporated the integrin-binding, RGD tripeptide into HA hydrogel scaffolds to mimic interactions between cells and ECM proteins, many of which have been implicated in GBM aggression (e.g., collagen[236], fibronectin[237], and vitronectin[180]) and contain the RGD motif through which they can interact with integrin receptors[179]. An important design feature of the hydrogel scaffolds used here is that HA and RGD content can be varied independently of culture dimensionality, mechanical properties, and diffusivity[235]. Given that both integrin and CD44 receptors are mechano-responsive[220,221] and that mechanical properties of the 3D microenvironment have strong effects on treatment resistance in GBM[198,238], hydrogel mechanical properties were kept constant around 150 Pa (shear elastic modulus). Previously, we

demonstrated that HA-rich hydrogels with this modulus maximized the ability of GBM cells to acquire resistance to targeted EGFR inhibition[198]. The differential effects of RGD when immobilized to insoluble hydrogel scaffolds, compared to when added as soluble cyclo-RGD (i.e., cilengitide), also provided evidence of force transduction from the matrix. Specifically, while immobilized RGD promoted resistance and an invasive morphology, these effects were reversed by addition of soluble RGD.

Consistent with our previous findings[198], increasing HA content in bioengineered matrices correlated with GBM cell upregulation in expression of the HA receptor CD44. Here, we demonstrate that engagement of CD44 and/or integrin αV induces downstream Src phosphorylation. In turn, activated Src suppressed expression of the BCL-2 family of pro-apoptotic factors in response to chemotherapies. When treated with alkylating chemotherapies — which function by damaging the DNA of rapidly dividing cells, such as cancer cells, to activate downstream apoptosis — this effect was more pronounced. Previous studies have reported that depressed apoptotic signaling in cancer cells may allow the cell to stay alive during an “intermediate” period over which they acquire resistance to treatment through other mechanisms, including repair of alkylated DNA through DNA mismatch repair (MMR) complexes and upregulation of drug efflux pumps such as p-glycoprotein[211]. Notably, we report the novel finding that ECM engagement protects GBM cells from chemotherapy-induced apoptosis through inhibition of PUMA, a critical pro-apoptotic signaling factor downstream of the P53 signaling pathway. This result suggests that treatment with a p53 activator, such as nutlin[189], in combination with alkylating chemotherapies may counteract the pro-survival actions of the tumor ECM.

Here, we found that addition of RGD to HA matrices reduced chemotherapy-induced apoptosis by around 50% — consistent with previous findings in glioma and lung cancer models[180,232]. Furthermore, dual treatment of either chemotherapy with cilengitide, to disrupt integrin-RGD binding, resulted in around three-fold increase in cl-PARP expression over chemotherapy alone. We posit two potential explanations for these findings. First, it is likely that GBM cells deposited additional integrin-binding ECM proteins during the culture period and that cilengitide treatment inhibited these interactions as well as those with hydrogel-immobilized RGD, resulting in higher level of apoptosis. Second, disruption of integrin-RGD interactions may have interfered with chemo-protection provided by CD44-HA interactions, indicating the possibility of cooperative effects of CD44 and integrin αV signaling.

Observations of co-expression and systematic knockdowns of CD44 and integrin αV provided additional evidence that engagement of these two receptors within a 3D matrix acts coorperatively to protect GBM cells from drug-induced apoptosis. These results are in agreement with previous reports indicating that CD44 and integrins can physically interact at the cell membrane[226,239]. Furthermore, our results demonstrate that engagement of CD44 and integrin αV receptors amplified downstream activation of Src to suppress treatment-induced apoptosis. Previously, Src activation has been linked to integrin activation and invasive morphology[216,218,224], as well as survival and chemotherapy resistance[217,240], in various cancer types . However, to the best of our knowledge, this is the first report demonstrating a direct connection between interactions of CD44 and integrins with the 3D ECM leading to Src activation and downstream phenotypic changes in GBM cells. Our previous study demonstrated that

HA and RGD present in 3D culture matrices could promote development of resistance to inhibition of using targeted treatments[198]. In this study, we revealed how the same matrix microenvironment intensifies Src activation, which others have reported to mediate resistance to EGFR inhibition via lapatinib in breast cancer[241]. Thus, we suspect that GBM may also be escape EGFR inhibition through matrix-mediated activation of Src.

While a previous phase II clinical trial (NCT00813943) found that addition of the integrin inhibitor cilengitide to radio- and chemotherapy improved median overall survival improved to 16.3 months from 13.4 months, the phase III trial did not find any improved outcomes (NCT00689221) [167,242]. Given our results showing the contribution of the non-integrin CD44 receptor to chemotherapy resistance, addition of therapies targeting the downstream signaling molecules of matrix-mediated resistance, such as Src, may be more beneficial. Although previous work has identified Src inhibition via dasatinib as a possibly effective monotherapy for treatment of GBM using standard, 2D cell culture experimental set-up[219], phase I/II clinical trials evaluating dasatinib for treatment of recurrent GBM found that dasatinib monotherapy produced worse outcomes than standard therapy (NCT00423735)[243]. This result is consistent with our finding in 3D hydrogel cultures, where the response of GBM cells to dasatinib treatment alone was equivalent to vehicle controls, indicating that our novel hydrogel platform may be a better tool for *in vitro*, pre-clinical screening evaluation of therapeutic strategies than 2D culture methods. While dasatinib was not effective as a monotherapy, our results do indicate that dual treatment with dasatinib and chemotherapy may be effective. There has been one phase II clinical study that investigated the use of dasatinib treatment

after the conclusion of more routine radiation and chemotherapy (TMZ) treatment in newly diagnosed GBM patients (NCT00869401). However, this study did not find any benefits of adding dasatinib over routine therapy alone. Our results indicate that dasatinib may only be effective if given in conjunction with, or even prior to, TMZ to inhibit Src activation and promote apoptosis. Alternatively, it is also possible that inefficient penetration of dasatinib into patient tumors caused the trial failure[244].

In conclusion, we report the use of a bioengineered, 3D culture platform to elucidate mechanisms underlying ECM-mediated chemotherapy resistance in patient-derived GBM cells. Results demonstrate how matrix engagement of CD44 and integrin αV augments downstream Src activation, causing depression of BCL-2 family pro-apoptotic factors. This finding provides a strong rationale for investigating the efficacy of simultaneous treatment with dasatinib and TMZ in future studies.

Chapter 6

Conclusions and future development

As a summary of my dissertation research, we have successfully constructed hyaluronic acid-based brain mimetic hydrogel system to study GBM drug response and mechanisms of drug resistance in the matrix microenvironmental aspect. At the same time, we successfully adapted and deployed multiple molecular biology techniques to our novel culture system. However, our system faces certain limitations, and further improvements are expected, which leads to two primary directions for future development of our culture system.

Currently, our platforms require culture of hydrogel in 12-well plate, and our hydrogel size is set at 80μL to ensure enough sample for subsequent experiments. As a result, we cannot make more than 50 gels per round of experiment, which limits the number of conditions that can be tested at once. Therefore, automated and smaller gel formation procedures are desired for real high-throughput drug screening system.

In addition, when hydrogel cultures are initiated, single cells are distributed evenly in the hydrogel, which resembles the scenario when GBM cells are present everywhere in the brain. However, this is not realistic as the tumor should be in fact developing from one area and infiltratively invade other “brain” regions. Therefore, we are currently developing a new “fusion” gel system that allows GBM cells grow/develop from a defined area and invade into “native brain”. The fusion gel formation consists of multi-step radical-initiated polymerization. Basically, a mixture of thiolated hyaluronic acid, 4-arm-20kDa PEG-norbornene, 4-arm-20kDa PEG-thiol and lithium phenyl-2,4,6-

trimethylbenzoylphosphinate (LAP) (w/v) 0.025% was mixed with GBM cells in HEPES buffer. The gel precursor was exposed to ultra violet (UV, 365nm) for 15 seconds to form the first gel. Later, the formed gel was placed inside a larger customized PDMS mold, and the vacant area was filled with gel precursor solution that contains no cells. At last, the whole sample was exposed to another round of 15 seconds UV to form a fusion gel, in which the “cell side” and empty gel side can be distinguished very clearly **(Figure 6.1)**. The fusion gel has many potential applications such as precise measurement of invasion in 3D culture. Researchers would be able to separate invading cells and non-invading cells under certain conditions such as drug treatment. For example, therapeutic induced tumor invasion can be seen through fusion gel system after temozolomide or erlotinib treatment **(Figure 6.2)**. Moreover, influences of mechanobiology on GBM invasion can be studied by making one side of the gel stiff and another side of the gel soft, and a preference of a soft microenvironment can be visualized **(Figure 6.3)**.

In general, our hydrogel-based 3D culture platform has immense potential to expand the applications into many more areas in biomedical research. We believe 3D culture platforms are necessary to advance the discovery through *in vitro* methods and hopefully these novel platforms can one day replace the currently commonly used culture platforms.

Figure 6.1

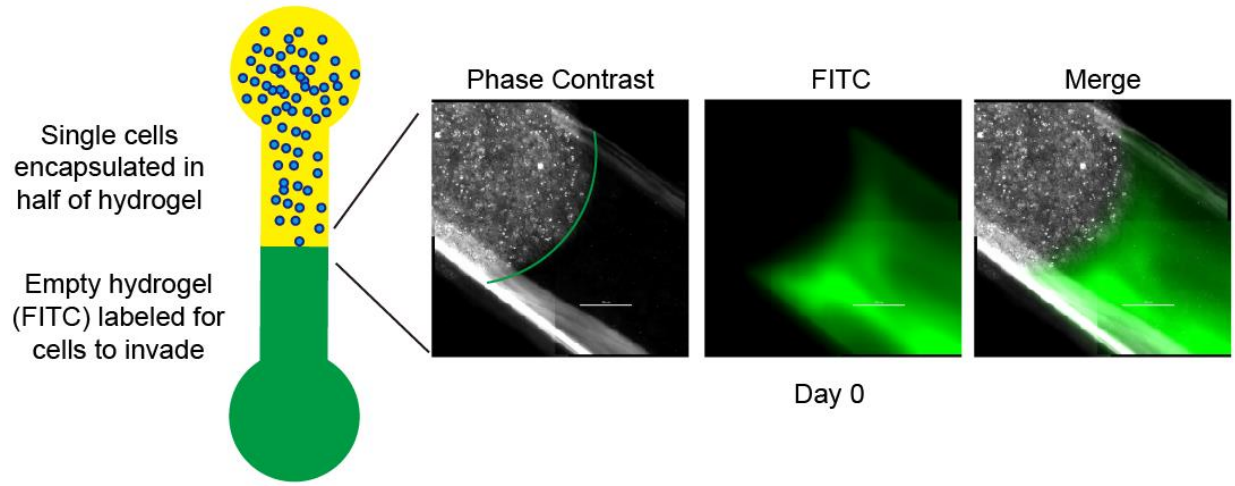

Figure 6.1. Schematic representation of the fusion gel system after gel formation. The hydrogel solution consisted of HEPES buffered 0.5%(w/v) HA, 250µM cysteine, 0.09%(w/v) thiolated PEG and 0.36%(w/v) PEG-norbornene plus 0.025%(w/v) LAP in HEPES buffer. The seeding concentration was 1million HK301 cells/mL of gel solution. The empty gel side was labeled with FITC. Therefore, the border can be distinguished throughout the experiment.

Figure 6.2

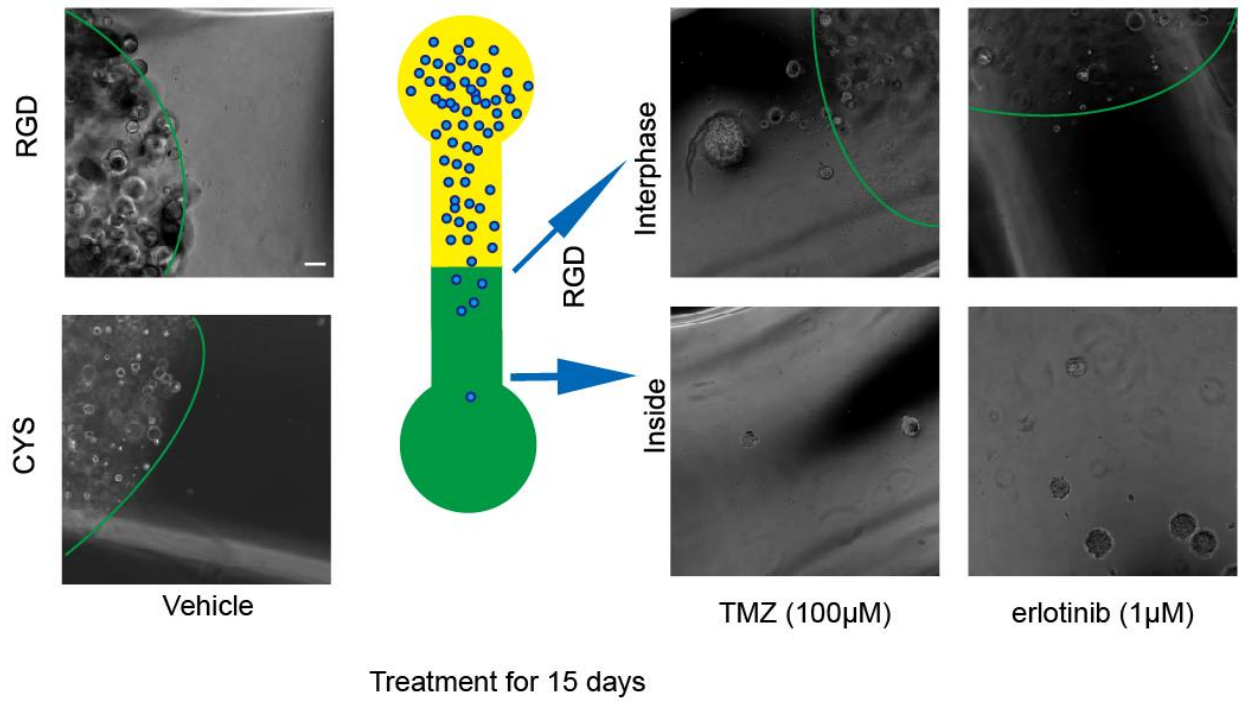

Figure 6.2 Schematic representation of the fusion gel system after drug treatment for 15 days. The hydrogel solution consisted of HEPES buffered 0.5%(w/v) HA, 250μM cysteine, 0.09%(w/v) thiolated PEG and 0.36%(w/v) PEG-norbornene plus 0.025%(w/v) LAP in HEPES buffer. The seeding concentration was 1million HK301 cells/mL of gel solution. The borderline of cell-non cell side was labeled with solid green line.

Figure 6.3

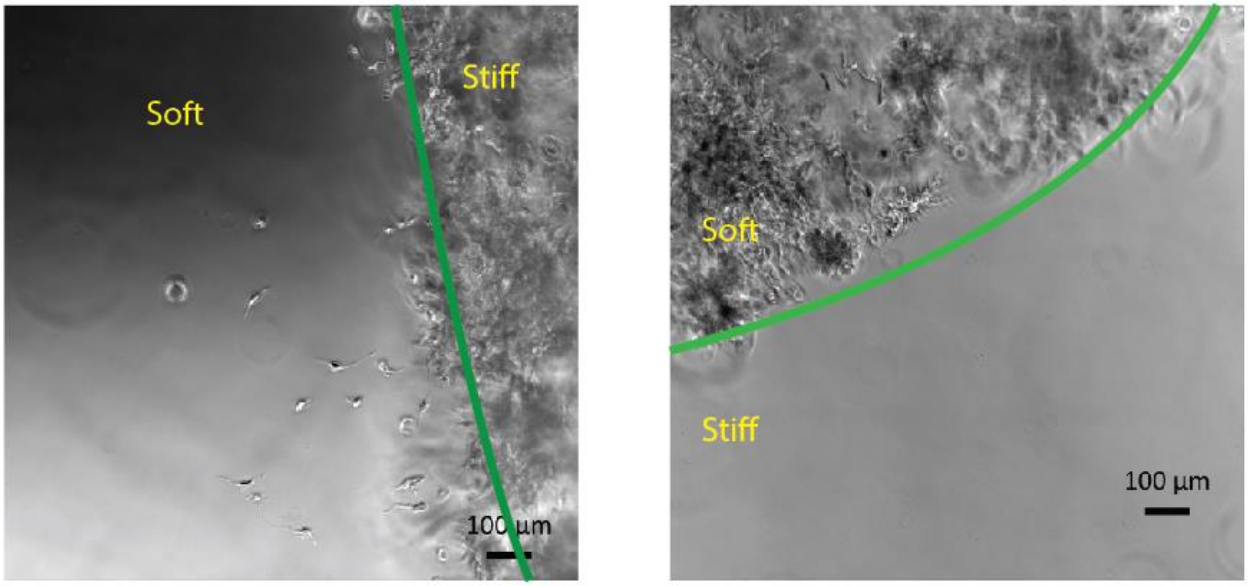

Figure 6.3 Phase contrast image of the encapsulated cells in fusion gel system after 15 days of culture. The soft hydrogel solution consisted of HEPES buffered 0.5%(w/v) HA, 250µM cysteine, 0.09%(w/v) thiolated PEG and 0.36%(w/v) PEG-norbornene plus 0.025%(w/v) LAP in HEPES buffer, and the stiff gel solution had increased thiolated PEG (0.87%(w/v)) and PEG-norborene (0.82%(w/v)) concentrations. The seeding concentration was 1million HK423 cells/mL of gel solution. The borderline of cell-non cell side was labeled with solid green line. The phase contrast image was obtained 4 days after encapsulation.

References

1. Holland, E. C. Glioblastoma multiforme: The terminator. *Proc. Natl. Acad. Sci.* **97,** 6242–6244 (2000).

2. Huse, J. T. & Holland, E. C. Targeting brain cancer: Advances in the molecular pathology of malignant glioma and medulloblastoma. *Nature Reviews Cancer* (2010). doi:10.1038/nrc2818

3. Ostrom, Q. T. *et al.* CBTRUS Statistical Report: Primary brain and other central nervous system tumors diagnosed in the United States in 2010–2014. *Neuro. Oncol.* (2017). doi:10.1093/neuonc/nox158

4. Holland, E. C. *et al.* Combined activation of Ras and Akt in neural progenitors induces glioblastoma formation in mice. *Nat. Genet.* (2000). doi:10.1038/75596

5. Verhaak, R. G. W. *et al.* Integrated Genomic Analysis Identifies Clinically Relevant Subtypes of Glioblastoma Characterized by Abnormalities in PDGFRA, IDH1, EGFR, and NF1. *Cancer Cell* (2010). doi:10.1016/j.ccr.2009.12.020

6. Liu, C. *et al.* Mosaic analysis with double markers reveals tumor cell of origin in glioma. *Cell* (2011). doi:10.1016/j.cell.2011.06.014

7. McLendon, R, Friedman, A, Bigner, D, Van Meir, EG, Brat, DJ, Mastrogianakis, GM, Olson, JJ, et al. Comprehensive genomic characterization defines human glioblastoma genes and core pathways. *Nature* (2008). doi:10.1038/nature07385

8. Singh, S. K. *et al.* Identification of human brain tumour initiating cells. *Nature* (2004). doi:10.1038/nature03128

9. Visvader, J. E. & Lindeman, G. J. Cancer stem cells: Current status and evolving complexities. *Cell Stem Cell* (2012). doi:10.1016/j.stem.2012.05.007

10. Patel, A. P. *et al.* Single-cell RNA-seq highlights intratumoral heterogeneity in primary glioblastoma. *Science (80-.).* (2014). doi:10.1126/science.1254257

11. Puchalski, R. B. *et al.* An anatomic transcriptional atlas of human glioblastoma. *Science (80-.).* (2018). doi:10.1126/science.aaf2666

12. Zamecnik, J. The extracellular space and matrix of gliomas. *Acta Neuropathologica* **110,** 435–442 (2005).

13. Bernstein, J. J. & Woodard, C. A. Glioblastoma cells do not intravasate into blood vessels. *Neurosurgery* **36,** 124–132 (1995).

14. Bellail, A. C., Hunter, S. B., Brat, D. J., Tan, C. & Van Meir, E. G. Microregional extracellular matrix heterogeneity in brain modulates glioma cell invasion. *International Journal of Biochemistry and Cell Biology* **36,** 1046–1069 (2004).

15. Charles, N. A., Holland, E. C., Gilbertson, R., Glass, R. & Kettenmann, H. The brain tumor microenvironment. *Glia* **59,** 1169–1180 (2011).

16. Xiao, W., Sohrabi, A. & Seidlits, S. K. Integrating the glioblastoma microenvironment into engineered experimental models. *Futur. Sci. OA* **3,** FSO189 (2017).

17. Day, A. J. & Prestwich, G. D. Hyaluronan-binding proteins: Tying up the giant. *Journal of Biological Chemistry* **277,** 4585–4588 (2002).

18. Wiranowska, M., Tresser, N. & Saporta, S. The effect of interferon and anti-CD44

antibody on mouse glioma invasiveness in vitro. *Anticancer Res.* **18,** 3331–3338 (1998).

19. Jadin, L. *et al.* Hyaluronan expression in primary and secondary brain tumors. *Ann. Transl. Med.* **3,** 80 (2015).

20. Gilg, A. G. *et al.* Targeting hyaluronan interactions in malignant gliomas and their drug-resistant multipotent progenitors. *Clin. Cancer Res.* **14,** 1804–1813 (2008).

21. Misra, S., Hascall, V. C., Markwald, R. R. & Ghatak, S. Interactions between hyaluronan and its receptors (CD44, RHAMM) regulate the activities of inflammation and cancer. *Front. Immunol.* **6,** 201 (2015).

22. Park, J. B., Kwak, H.-J. J. & Lee, S.-H. H. Role of hyaluronan in glioma invasion. *Cell Adh. Migr.* **2,** 202–207 (2008).

23. Delpech, B., Laquerriere, A., Maingonnat, C., Bertrand, P. & Freger, P. Hyaluronidase is more elevated in human brain metastases than in primary brain tumours. *Anticancer Res.* **22,** 2423–2427 (2002).

24. Varga, I. *et al.* Expression of invasion-related extracellular matrix molecules in human glioblastoma versus intracerebral lung adenocarcinoma metastasis. *Zentralbl. Neurochir.* **71,** 173–180 (2010).

25. Zhang, H., Kelly, G., Zerillo, C., Jaworski, D. M. & Hockfield, S. Expression of a cleaved brain-specific extracellular matrix protein mediates glioma cell invasion in vivo. *J. Neurosci.* **18,** 2370–2376 (1998).

26. Xu, Y., Stamenkovic, I. & Yu, Q. CD44 attenuates activation of the hippo signaling

pathway and is a prime therapeutic target for glioblastoma. *Cancer Res.* **70,** 2455–2464 (2010).

27. Herishanu, Y. *et al.* CD44 signaling via PI3K/AKT and MAPK/ERK pathways protects CLL cells from spontaneous and drug induced apoptosis through MCL-1. *Leuk. Lymphoma* **52,** 1758 (2011).

28. Koochekpour, S., Pilkington, G. J. & Merzak, A. Hyaluronic acid/CD44H interaction induces cell detachment and stimulates migration and invasion of human glioma cells in vitro. *Int. J. cancer* **63,** 450–454 (1995).

29. Chopra, A. *et al.* Augmentation of integrin-mediated mechanotransduction by hyaluronic acid. *Biomaterials* **35,** 71–82 (2014).

30. Kim, Y. & Kumar, S. CD44-mediated adhesion to hyaluronic acid contributes to mechanosensing and invasive motility. *Mol. Cancer Res.* **12,** 1416–1429 (2014).

31. Guo, W. & Giancotti, F. G. Integrin signalling during tumour progression. *Nat. Rev. Mol. Cell Biol.* **5,** 816–826 (2004).

32. Bello, L. *et al.* αvβ3 and αvβ5 integrin expression in glioma periphery. *Neurosurgery* **49,** 380–390 (2001).

33. Chamberlain, M. C., Cloughsey, T., Reardon, D. A. & Wen, P. Y. A novel treatment for glioblastoma: integrin inhibition. *Expert Rev. Neurother.* **12,** 421–435 (2012).

34. Winkler, F. *et al.* Imaging glioma cell invasion in vivo reveals mechanisms of dissemination and peritumoral angiogenesis. *Glia* **57,** 1306–1315 (2009).

35. Watkins, S. *et al.* Disruption of astrocyte–vascular coupling and the blood–brain barrier by invading glioma cells. *Nat. Commun.* **5,** 4196 (2014).

36. Wade, A. *et al.* Proteoglycans and their roles in brain cancer. *FEBS J.* **280,** 2399–2417 (2013).

37. Arslan, F. *et al.* The role of versican isoforms V0/V1 in glioma migration mediated by transforming growth factor-β2. *Br. J. Cancer* **96,** 1560 (2007).

38. Hu, B., Kong, L. L., Matthews, R. T. & Viapiano, M. S. The proteoglycan brevican binds to fibronectin after proteolytic cleavage and promotes glioma cell motility. *J. Biol. Chem.* **283,** 24848–24859 (2008).

39. Phillips, J. J. *et al.* Heparan sulfate sulfatase SULF2 regulates PDGFRα signaling and growth in human and mouse malignant glioma. *J. Clin. Invest.* **122,** 911–922 (2012).

40. Hoelzinger, D. B., Demuth, T. & Berens, M. E. Autocrine factors that sustain glioma invasion and paracrine biology in the brain microenvironment. *J. Natl. Cancer Inst.* **99,** 1583–1593 (2007).

41. Zhu, V. F., Yang, J., LeBrun, D. G. & Li, M. Understanding the role of cytokines in Glioblastoma Multiforme pathogenesis. *Cancer Lett.* **316,** 139–150 (2012).

42. Furnari, F. B., Cloughesy, T. F., Cavenee, W. K. & Mischel, P. S. Heterogeneity of epidermal growth factor receptor signalling networks in glioblastoma. *Nat. Rev. Cancer* **15,** 302–310 (2015).

43. Tsatas, D., Kanagasundaram, V., Kaye, A. & Novak, U. EGF receptor modifies

cellular responses to hyaluronan in glioblastoma cell lines. *J. Clin. Neurosci.* **9,** 282–288 (2002).

44. Ramnarain, D. B. *et al.* Differential gene expression analysis reveals generation of an autocrine loop by a mutant epidermal growth factor receptor in glioma cells. *Cancer Res.* **66,** 867–874 (2006).

45. Park, M.-J. *et al.* PTEN suppresses hyaluronic acid-induced matrix metalloproteinase-9 expression in U87MG glioblastoma cells through focal adhesion kinase dephosphorylation. *Cancer Res.* **62,** 6318–6322 (2002).

46. Reynés, G. *et al.* Circulating markers of angiogenesis, inflammation, and coagulation in patients with glioblastoma. *J. Neurooncol.* **102,** 35–41 (2011).

47. Bruna, A. *et al.* High TGFβ-Smad activity confers poor prognosis in glioma patients and promotes cell proliferation depending on the methylation of the PDGF-B gene. *Cancer Cell* **11,** 147–160 (2007).

48. Dieterich, L. C. *et al.* Transcriptional profiling of human glioblastoma vessels indicates a key role of VEGF-A and TGFβ2 in vascular abnormalization. *J. Pathol.* **228,** 378–390 (2012).

49. Wick, W., Platten, M. & Weller, M. Glioma cell invasion: regulation of metalloproteinase activity by TGF-β. *J. Neurooncol.* **53,** 177–185 (2001).

50. Martinez, F. O. & Gordon, S. The M1 and M2 paradigm of macrophage activation: time for reassessment. *F1000Prime Rep.* **6,** (2014).

51. Tewari, R., Choudhury, S. R., Ghosh, S., Mehta, V. S. & Sen, E. Involvement of

TNFα-induced TLR4–NF-κB and TLR4–HIF-1α feed-forward loops in the regulation of inflammatory responses in glioma. *J. Mol. Med.* **90,** 67–80 (2012).

52. Yoshida, S. *et al.* Involvement of interleukin-8, vascular endothelial growth factor, and basic fibroblast growth factor in tumor necrosis factor alpha-dependent angiogenesis. *Mol. Cell. Biol.* **17,** 4015–4023 (1997).

53. Méndez, O. *et al.* Knock down of HIF-1α in glioma cells reduces migration in vitro and invasion in vivo and impairs their ability to form tumor spheres. *Mol. Cancer* **9,** 133 (2010).

54. Powell, J. D. & Horton, M. R. Threat matrix. *Immunol. Res.* **31,** 207–218 (2005).

55. Sugahara, K. N. *et al.* Tumor cells enhance their own CD44 cleavage and motility by generating hyaluronan fragments. *J. Biol. Chem.* **281,** 5861–5868 (2006).

56. Wu, M. *et al.* A novel role of low molecular weight hyaluronan in breast cancer metastasis. *FASEB J.* **29,** 1290–1298 (2015).

57. Hagemann, C., Anacker, J., Ernestus, R.-I. & Vince, G. H. A complete compilation of matrix metalloproteinase expression in human malignant gliomas. *World J. Clin. Oncol.* **3,** 67 (2012).

58. Le, D. M. *et al.* Exploitation of astrocytes by glioma cells to facilitate invasiveness: a mechanism involving matrix metalloproteinase-2 and the urokinase-type plasminogen activator–plasmin cascade. *J. Neurosci.* **23,** 4034–4043 (2003).

59. Brooks, P. C. *et al.* Localization of matrix metalloproteinase MMP-2 to the surface of invasive cells by interaction with integrin αvβ3. *Cell* **85,** 683–693 (1996).

60. Li, Q. *et al.* Comparative analysis of matrix metalloproteinase family members reveals that MMP9 predicts survival and response to temozolomide in patients with primary glioblastoma. *PLoS One* **11,** e0151815 (2016).

61. Lakka, S. S. *et al.* Inhibition of cathepsin B and MMP-9 gene expression in glioblastoma cell line via RNA interference reduces tumor cell invasion, tumor growth and angiogenesis. *Oncogene* **23,** 4681 (2004).

62. Yu, Q. & Stamenkovic, I. Cell surface-localized matrix metalloproteinase-9 proteolytically activates TGF-β and promotes tumor invasion and angiogenesis. *Genes Dev.* **14,** 163–176 (2000).

63. Platten, M., Wick, W. & Weller, M. Malignant glioma biology: Role for TGF-β in growth, motility, angiogenesis, and immune escape. *Microsc. Res. Tech.* **52,** 401–410 (2001).

64. Bouchonville, N. *et al.* AFM mapping of the elastic properties of brain tissue reveals kPa μm− 1 gradients of rigidity. *Soft Matter* **12,** 6232–6239 (2016).

65. DuFort, C. C., Paszek, M. J. & Weaver, V. M. Balancing forces: architectural control of mechanotransduction. *Nat. Rev. Mol. cell Biol.* **12,** 308 (2011).

66. Lamontagne, C.-A. & Grandbois, M. PKC-induced stiffening of hyaluronan/CD44 linkage; local force measurements on glioma cells. *Exp. Cell Res.* **314,** 227–236 (2008).

67. Cuddapah, V. A., Robel, S., Watkins, S. & Sontheimer, H. A neurocentric perspective on glioma invasion. *Nat. Rev. Neurosci.* **15,** 455–465 (2014).

68. Sharili, A. S. & Connelly, J. T. Nucleocytoplasmic shuttling: a common theme in mechanotransduction. (2014).

69. Netti, P. A., Berk, D. A., Swartz, M. A., Grodzinsky, A. J. & Jain, R. K. Role of extracellular matrix assembly in interstitial transport in solid tumors. *Cancer Res.* **60,** 2497–2503 (2000).

70. Chauvet, D. *et al.* In vivo measurement of brain tumor elasticity using intraoperative shear wave elastography. *Ultraschall der Medizin-European J. Ultrasound* **37,** 584–590 (2016).

71. G. Gritsenko, P., Ilina, O. & Friedl, P. Interstitial guidance of cancer invasion. *J. Pathol.* **226,** 185–199 (2012).

72. Munson, J. M. & Shieh, A. C. Interstitial fluid flow in cancer: implications for disease progression and treatment. *Cancer Manag. Res.* **6,** 317 (2014).

73. Iliff, J. J. *et al.* A paravascular pathway facilitates CSF flow through the brain parenchyma and the clearance of interstitial solutes, including amyloid β. *Sci. Transl. Med.* **4,** 147ra111-147ra111 (2012).

74. Pogoda, K. *et al.* Compression stiffening of brain and its effect on mechanosensing by glioma cells. *New J. Phys.* **16,** 75002 (2014).

75. Kingsmore, K. M. *et al.* Interstitial flow differentially increases patient-derived glioblastoma stem cell invasion via CXCR4, CXCL12, and CD44-mediated mechanisms. *Integr. Biol.* **8,** 1246–1260 (2016).

76. Gielen, P. R. *et al.* Connexin43 confers Temozolomide resistance in human

glioma cells by modulating the mitochondrial apoptosis pathway. *Neuropharmacology* **75,** 539–548 (2013).

77. Péglion, F. & Etienne-Manneville, S. N-cadherin expression level as a critical indicator of invasion in non-epithelial tumors. *Cell Adh. Migr.* **6,** 327–332 (2012).

78. Camand, E., Peglion, F., Osmani, N., Sanson, M. & Etienne-Manneville, S. N-cadherin expression level modulates integrin-mediated polarity and strongly impacts on the speed and directionality of glial cell migration. *J Cell Sci* jcs-087668 (2012).

79. Shinoura, N. *et al.* Expression of N-cadherin and α-catenin in astrocytomas and glioblastomas. *Br. J. Cancer* **72,** 627 (1995).

80. Lee, Y., Lee, J.-K., Ahn, S. H., Lee, J. & Nam, D.-H. WNT signaling in glioblastoma and therapeutic opportunities. *Lab. Investig.* **96,** 137 (2016).

81. Lathia, J. D., Mack, S. C., Mulkearns-Hubert, E. E., Valentim, C. L. L. & Rich, J. N. Cancer stem cells in glioblastoma. *Genes Dev.* **29,** 1203–1217 (2015).

82. Hitomi, M. *et al.* Differential connexin function enhances self-renewal in glioblastoma. *Cell Rep.* **11,** 1031–1042 (2015).

83. Velpula, K. K. *et al.* Glioma stem cell invasion through regulation of the interconnected ERK, integrin α6 and N-cadherin signaling pathway. *Cell. Signal.* **24,** 2076–2084 (2012).

84. Hardee, M. E. & Zagzag, D. Mechanisms of glioma-associated neovascularization. *Am. J. Pathol.* **181,** 1126–1141 (2012).

85. Soda, Y. *et al.* Transdifferentiation of glioblastoma cells into vascular endothelial cells. *Proc. Natl. Acad. Sci.* **108,** 4274–4280 (2011).

86. Cheng, L. *et al.* Glioblastoma stem cells generate vascular pericytes to support vessel function and tumor growth. *Cell* **153,** 139–152 (2013).

87. Calabrese, C. *et al.* A perivascular niche for brain tumor stem cells. *Cancer Cell* **11,** 69–82 (2007).

88. Infanger, D. W. *et al.* Glioblastoma stem cells are regulated by interleukin-8 signaling in a tumoral perivascular niche. *Cancer Res.* (2013).

89. Pietras, A. *et al.* Osteopontin-CD44 signaling in the glioma perivascular niche enhances cancer stem cell phenotypes and promotes aggressive tumor growth. *Cell Stem Cell* **14,** 357–369 (2014).

90. Schneider, S. W. *et al.* Glioblastoma cells release factors that disrupt blood-brain barrier features. *Acta Neuropathol.* **107,** 272–276 (2004).

91. Lathia, J. D. *et al.* Laminin alpha 2 enables glioblastoma stem cell growth. *Ann. Neurol.* **72,** 766–778 (2012).

92. Lathia, J. D. *et al.* Integrin alpha 6 regulates glioblastoma stem cells. *Cell Stem Cell* **6,** 421–432 (2010).

93. M Heddleston, J. *et al.* Glioma stem cell maintenance: the role of the microenvironment. *Curr. Pharm. Des.* **17,** 2386–2401 (2011).

94. Li, Z. *et al.* Hypoxia-inducible factors regulate tumorigenic capacity of glioma stem cells. *Cancer Cell* **15,** 501–513 (2009).

95. Clara, C. A. *et al.* Angiogenesis and expression of PDGF-C, VEGF, CD 105 and HIF-1α in human glioblastoma. *Neuropathology* **34,** 343–352 (2014).

96. Rath, B. H., Wahba, A., Camphausen, K. & Tofilon, P. J. Coculture with astrocytes reduces the radiosensitivity of glioblastoma stem-like cells and identifies additional targets for radiosensitization. *Cancer Med.* **4,** 1705–1716 (2015).

97. Grodecki, J. *et al.* Glioma-astrocyte interactions on white matter tract-mimetic aligned electrospun nanofibers. *Biotechnol. Prog.* **31,** 1406–1415 (2015).

98. Hambardzumyan, D., Gutmann, D. H. & Kettenmann, H. The role of microglia and macrophages in glioma maintenance and progression. *Nat. Neurosci.* **19,** 20 (2016).

99. Wang, S.-C., Hong, J.-H., Hsueh, C. & Chiang, C.-S. Tumor-secreted SDF-1 promotes glioma invasiveness and TAM tropism toward hypoxia in a murine astrocytoma model. *Lab. Investig.* **92,** 151 (2012).

100. Wesolowska, A. *et al.* Microglia-derived TGF-β as an important regulator of glioblastoma invasion—an inhibition of TGF-β-dependent effects by shRNA against human TGF-β type II receptor. *Oncogene* **27,** 918 (2008).

101. Westphal, M. & Meissner, H. Establishing human glioma-derived cell lines. in *Methods in cell biology* **57,** 147–165 (Elsevier, 1998).

102. Allen, M., Bjerke, M., Edlund, H., Nelander, S. & Westermark, B. Origin of the U87MG glioma cell line: Good news and bad news. *Sci. Transl. Med.* **8,** 354re3-

354re3 (2016).

103. Lee, J. *et al.* Tumor stem cells derived from glioblastomas cultured in bFGF and EGF more closely mirror the phenotype and genotype of primary tumors than do serum-cultured cell lines. *Cancer Cell* **9,** 391–403 (2006).

104. Huszthy, P. C. *et al.* In vivo models of primary brain tumors: pitfalls and perspectives. *Neuro. Oncol.* **14,** 979–993 (2012).

105. Zheng, X. *et al.* Proteomic analysis for the assessment of different lots of fetal bovine serum as a raw material for cell culture. Part IV. Application of proteomics to the manufacture of biological drugs. *Biotechnol. Prog.* **22,** 1294–1300 (2006).

106. Sarkaria, J. N. *et al.* Use of an Orthotopic Xenograft Model for Assessing the Effect of Epidermal Growth Factor Receptor Amplification on Glioblastoma Radiation Response Cancer Therapy : Preclinical Epidermal Growth Factor Receptor Amplification on Glioblastoma Radiation Respon. *Clin. Cancer Res.* **12,** 2264–71 (2006).

107. Wakimoto, H. *et al.* Maintenance of primary tumor phenotype and genotype in glioblastoma stem cells. *Neuro. Oncol.* **14,** 132–144 (2011).

108. Sarkaria, J. N. *et al.* Identification of molecular characteristics correlated with glioblastoma sensitivity to EGFR kinase inhibition through use of an intracranial xenograft test panel. *Mol. Cancer Ther.* **6,** 1167–1174 (2007).

109. Chaichana, K., Zamora-Berridi, G., Camara-Quintana, J. & Quiñones-Hinojosa, A. Neurosphere assays: growth factors and hormone differences in tumor and

nontumor studies. *Stem Cells* **24,** 2851–2857 (2006).

110. Hubert, C. G. *et al.* A three-dimensional organoid culture system derived from human glioblastomas recapitulates the hypoxic gradients and cancer stem cell heterogeneity of tumors found in vivo. *Cancer Res.* (2016). doi:10.1158/0008-5472.CAN-15-2402

111. Oh, T. *et al.* Immunocompetent murine models for the study of glioblastoma immunotherapy. *J. Transl. Med.* **12,** 107 (2014).

112. Joo, K. M. *et al.* Patient-Specific Orthotopic Glioblastoma Xenograft Models Recapitulate the Histopathology and Biology of Human Glioblastomas In Situ. *Cell Rep.* **3,** 260–273 (2013).

113. Oh, Y. T. *et al.* Translational validation of personalized treatment strategy based on genetic characteristics of glioblastoma. *PLoS One* **9,** e103327 (2014).

114. Maes, W. & Van Gool, S. W. Experimental immunotherapy for malignant glioma: lessons from two decades of research in the GL261 model. *Cancer Immunol. Immunother.* **60,** 153–160 (2011).

115. Tivnan, A., Heilinger, T., Lavelle, E. C. & Prehn, J. H. M. Advances in immunotherapy for the treatment of glioblastoma. *J. Neurooncol.* **131,** 1–9 (2017).

116. Hambardzumyan, D., Parada, L. F., Holland, E. C. & Charest, A. Genetic modeling of gliomas in mice: new tools to tackle old problems. *Glia* **59,** 1155–1168 (2011).

117. Heyer, J., Kwong, L. N., Lowe, S. W. & Chin, L. Non-germline genetically

engineered mouse models for translational cancer research. *Nat. Rev. Cancer* **10,** 470 (2010).

118. Umesh, V., Rape, A. D., Ulrich, T. A. & Kumar, S. Microenvironmental stiffness enhances glioma cell proliferation by stimulating epidermal growth factor receptor signaling. *PLoS One* **9,** e101771 (2014).

119. Grundy, T. J. *et al.* Differential response of patient-derived primary glioblastoma cells to environmental stiffness. *Sci. Rep.* **6,** 23353 (2016).

120. Pathak, A. & Kumar, S. Independent regulation of tumor cell migration by matrix stiffness and confinement. *Proc. Natl. Acad. Sci.* **109,** 10334–10339 (2012).

121. Ulrich, T. A., de Juan Pardo, E. M. & Kumar, S. The mechanical rigidity of the extracellular matrix regulates the structure, motility, and proliferation of glioma cells. *Cancer Res.* **69,** 4167–4174 (2009).

122. Rape, A. D. & Kumar, S. A composite hydrogel platform for the dissection of tumor cell migration at tissue interfaces. *Biomaterials* **35,** 8846–8853 (2014).

123. Heffernan, J. M., Overstreet, D. J., Le, L. D., Vernon, B. L. & Sirianni, R. W. Bioengineered scaffolds for 3D analysis of glioblastoma proliferation and invasion. *Ann. Biomed. Eng.* **43,** 1965–1977 (2015).

124. Lees, J. G. *et al.* Role of dynamin in elongated cell migration in a 3D matrix. *Biochim. Biophys. Acta (BBA)-Molecular Cell Res.* **1853,** 611–618 (2015).

125. Rao, S. S. *et al.* Mimicking white matter tract topography using core–shell electrospun nanofibers to examine migration of malignant brain tumors.

Biomaterials **34,** 5181–5190 (2013).

126. Johnson, J. *et al.* Quantitative analysis of complex glioma cell migration on electrospun polycaprolactone using time-lapse microscopy. *Tissue Eng. Part C Methods* **15,** 531–540 (2009).

127. Rape, A. D., Zibinsky, M., Murthy, N. & Kumar, S. A synthetic hydrogel for the high-throughput study of cell–ECM interactions. *Nat. Commun.* **6,** 8129 (2015).

128. Ananthanarayanan, B., Kim, Y. & Kumar, S. Elucidating the mechanobiology of malignant brain tumors using a brain matrix-mimetic hyaluronic acid hydrogel platform. *Biomaterials* **32,** 7913–7923 (2011).

129. Fraley, S. I. *et al.* A distinctive role for focal adhesion proteins in three-dimensional cell motility. *Nat. Cell Biol.* **12,** 598 (2010).

130. Vartanian, A. *et al.* GBM's multifaceted landscape: highlighting regional and microenvironmental heterogeneity. *Neuro. Oncol.* **16,** 1167–1175 (2014).

131. Pedron, S., Becka, E. & Harley, B. A. C. Regulation of glioma cell phenotype in 3D matrices by hyaluronic acid. *Biomaterials* **34,** 7408–7417 (2013).

132. Florczyk, S. J. *et al.* Porous chitosan-hyaluronic acid scaffolds as a mimic of glioblastoma microenvironment ECM. *Biomaterials* **34,** 10143–10150 (2013).

133. Jiglaire, C. J. *et al.* Ex vivo cultures of glioblastoma in three-dimensional hydrogel maintain the original tumor growth behavior and are suitable for preclinical drug and radiation sensitivity screening. *Exp. Cell Res.* **321,** 99–108 (2014).

134. Jin, S.-G. *et al.* The effect of hyaluronic acid on the invasiveness of malignant

glioma cells: comparison of invasion potential at hyaluronic acid hydrogel and matrigel. *J. Korean Neurosurg. Soc.* **46,** 472 (2009).

135. Sarkar, S., Nuttall, R. K., Liu, S., Edwards, D. R. & Yong, V. W. Tenascin-C stimulates glioma cell invasion through matrix metalloproteinase-12. *Cancer Res.* **66,** 11771–11780 (2006).

136. Coquerel, B. *et al.* Elastin-derived peptides: Matrikines critical for glioblastoma cell aggressiveness in a 3-D system. *Glia* **57,** 1716–1726 (2009).

137. Logun, M. T. *et al.* Glioma cell invasion is significantly enhanced in composite hydrogel matrices composed of chondroitin 4-and 4, 6-sulfated glycosaminoglycans. *J. Mater. Chem. B* **4,** 6052–6064 (2016).

138. Rao, S. S. *et al.* Glioblastoma behaviors in three-dimensional collagen-hyaluronan composite hydrogels. *ACS Appl. Mater. Interfaces* **5,** 9276–9284 (2013).

139. Pedron, S., Becka, E. & Harley, B. A. Spatially gradated hydrogel platform as a 3D engineered tumor microenvironment. *Adv. Mater.* **27,** 1567–1572 (2015).

140. Wang, C., Tong, X., Jiang, X. & Yang, F. Effect of matrix metalloproteinase-mediated matrix degradation on glioblastoma cell behavior in 3D PEG-based hydrogels. *J. Biomed. Mater. Res. Part A* **105,** 770–778 (2017).

141. Wang, C., Tong, X. & Yang, F. Bioengineered 3D brain tumor model to elucidate the effects of matrix stiffness on glioblastoma cell behavior using PEG-based hydrogels. *Mol. Pharm.* **11,** 2115–2125 (2014).

142. Azagarsamy, M. A. & Anseth, K. S. Bioorthogonal click chemistry: an

indispensable tool to create multifaceted cell culture scaffolds. (2012).

143. Fairbanks, B. D., Schwartz, M. P., Bowman, C. N. & Anseth, K. S. Photoinitiated polymerization of PEG-diacrylate with lithium phenyl-2, 4, 6-trimethylbenzoylphosphinate: polymerization rate and cytocompatibility. *Biomaterials* **30,** 6702–6707 (2009).

144. Ulrich, T. A., Jain, A., Tanner, K., MacKay, J. L. & Kumar, S. Probing cellular mechanobiology in three-dimensional culture with collagen–agarose matrices. *Biomaterials* **31,** 1875–1884 (2010).

145. Cha, J., Kang, S.-G. & Kim, P. Strategies of mesenchymal invasion of patient-derived brain tumors: microenvironmental adaptation. *Sci. Rep.* **6,** 24912 (2016).

146. Kievit, F. M. *et al.* Proliferation and enrichment of CD133+ glioblastoma cancer stem cells on 3D chitosan-alginate scaffolds. *Biomaterials* **35,** 9137–9143 (2014).

147. Pedron, S. *et al.* Spatially graded hydrogels for preclinical testing of glioblastoma anticancer therapeutics. *MRS Commun.* **7,** 442–449 (2017).

148. Hachet, E., Van den Berghe, H., Bayma, E., Block, M. R. & Auzély-Velty, R. Design of biomimetic cell-interactive substrates using hyaluronic acid hydrogels with tunable mechanical properties. *Biomacromolecules* **13,** 1818–1827 (2012).

149. Shu, X. Z., Liu, Y., Luo, Y., Roberts, M. C. & Prestwich, G. D. Disulfide cross-linked hyaluronan hydrogels. *Biomacromolecules* **3,** 1304–1311 (2002).

150. Zustiak, S. P. *et al.* Three-dimensional matrix stiffness and adhesive ligands affect cancer cell response to toxins. *Biotechnol. Bioeng.* **113,** 443–452 (2016).

151. Shikanov, A., Smith, R. M., Xu, M., Woodruff, T. K. & Shea, L. D. Hydrogel network design using multifunctional macromers to coordinate tissue maturation in ovarian follicle culture. *Biomaterials* **32,** 2524–2531 (2011).

152. Kim, H.-D. *et al.* Epidermal growth factor–induced enhancement of glioblastoma cell migration in 3D arises from an intrinsic increase in speed but an extrinsic matrix-and proteolysis-dependent increase in persistence. *Mol. Biol. Cell* **19,** 4249–4259 (2008).

153. Nie, T., Baldwin, A., Yamaguchi, N. & Kiick, K. L. Production of heparin-functionalized hydrogels for the development of responsive and controlled growth factor delivery systems. *J. Control. release* **122,** 287–296 (2007).

154. Coniglio, S. J. *et al.* Microglial stimulation of glioblastoma invasion involves epidermal growth factor receptor (EGFR) and colony stimulating factor 1 receptor (CSF-1R) signaling. *Mol. Med.* **18,** 519 (2012).

155. Kenig, S., Alonso, M. B. D., Mueller, M. M. & Lah, T. T. Glioblastoma and endothelial cells cross-talk, mediated by SDF-1, enhances tumour invasion and endothelial proliferation by increasing expression of cathepsins B, S, and MMP-9. *Cancer Lett.* **289,** 53–61 (2010).

156. Chen, Z. *et al.* In vitro angiogenesis by human umbilical vein endothelial cells (HUVEC) induced by three-dimensional co-culture with glioblastoma cells. *J. Neurooncol.* **92,** 121–128 (2009).

157. Yang, N. *et al.* A co-culture model with brain tumor-specific bioluminescence

demonstrates astrocyte-induced drug resistance in glioblastoma. *J. Transl. Med.* **12,** 278 (2014).

158. Coniglio, S., Miller, I., Symons, M. & Segall, J. E. Coculture Assays to Study Macrophage and Microglia Stimulation of Glioblastoma Invasion. *J. Vis. Exp. JoVE* (2016).

159. Seidlits, S. K. *et al.* The effects of hyaluronic acid hydrogels with tunable mechanical properties on neural progenitor cell differentiation. *Biomaterials* **31,** 3930–3940 (2010).

160. Brown, J. A. *et al.* Metabolic consequences of inflammatory disruption of the blood-brain barrier in an organ-on-chip model of the human neurovascular unit. *J. Neuroinflammation* **13,** 306 (2016).

161. Wang, Y. I., Abaci, H. E. & Shuler, M. L. Microfluidic blood–brain barrier model provides in vivo-like barrier properties for drug permeability screening. *Biotechnol. Bioeng.* **114,** 184–194 (2017).

162. Haar, C. P. *et al.* Drug resistance in glioblastoma: A mini review. *Neurochem. Res.* **37,** 1192–1200 (2012).

163. Löscher, W. & Potschka, H. Drug resistance in brain diseases and the role of drug efflux transporters. *Nat. Rev. Neurosci.* **6,** 591–602 (2005).

164. Eramo, A. *et al.* Chemotherapy resistance of glioblastoma stem cells. *Cell Death Differ.* **13,** 1238–1241 (2006).

165. Holohan, C., Schaeybroeck, S. Van, Longley, D. B. & Johnston, P. G. Cancer

drug resistance : an evolving paradigm. *Nat. Publ. Gr.* **13,** 714–726 (2013).

166. Fink, D., Aebi, S. & Howell, S. B. The role of DNA mismatch repair in drug resistance. *Clin. Cancer Res.* **4,** 1–6 (1998).

167. Nabors, L. B. *et al.* Two cilengitide regimens in combination with standard treatment for patients with newly diagnosed glioblastoma and unmethylated MGMT gene promoter: Results of the open-label, controlled, randomized phase II CORE study. *Neuro. Oncol.* **17,** 708–717 (2015).

168. Liu, G. *et al.* Analysis of gene expression and chemoresistance of CD133+ cancer stem cells in glioblastoma. *Mol. Cancer* **5,** (2006).

169. Dean, M., Fojo, T. & Bates, S. Tumour stem cells and drug resistance. *Nat. Rev. Cancer* **5,** 275–284 (2005).

170. Singh, A. & Settleman, J. EMT, cancer stem cells and drug resistance: An emerging axis of evil in the war on cancer. *Oncogene* **29,** 4741–4751 (2010).

171. Tanaka, K. *et al.* Oncogenic EGFR signaling activates an mTORC2–NF-κB pathway that promotes chemotherapy resistance. *Cancer Discov.* **1,** 524–538 (2011).

172. Nathanson, D. A. *et al.* Targeted therapy resistance mediated by dynamic regulation of extrachromosomal mutant EGFR DNA. *Science (80-.).* **343,** 72–76 (2014).

173. Shepherd, F. A. *et al.* Erlotinib in Previously Treated Non–Small-Cell Lung Cancer. *N. Engl. J. Med.* **353,** 123–132 (2005).

174. de Vries, N. A. *et al.* Restricted brain penetration of the tyrosine kinase inhibitor erlotinib due to the drug transporters P-gp and BCRP. *Invest. New Drugs* **30,** 443–449 (2012).

175. Mellinghoff, I. K. *et al.* Molecular Determinants of the Response of Glioblastomas to EGFR Kinase Inhibitors. *N. Engl. J. Med.* **353,** 2012–2024 (2005).

176. Akhavan, D. *et al.* De-repression of PDGFRβ transcription promotes acquired resistance to EGFR tyrosine kinase inhibitors in glioblastoma patients. *Cancer Discov.* **3,** 534–537 (2013).

177. Nagane, M., Levitzki, A., Gazit, A., Cavenee, W. K. & Huang, H.-J. S. Drug resistance of human glioblastoma cells conferred by a tumor-specific mutant epidermal growth factor receptor through modulation of Bcl-XL and caspase-3-like proteases. *Proc. Natl. Acad. Sci.* **95,** 5724–5729 (1998).

178. Nagane, M. *et al.* A common mutant epidermal growth factor receptor confers enhanced tumorigenicity on human glioblastoma cells by increasing proliferation and reducing apoptosis. *Cancer Res.* **56,** 5079–5086 (1996).

179. Akiyama, S. K., Olden, K. & Yamada, K. M. Fibronectin and integrins in invasion and metastasis. *Cancer Metastasis Rev.* **14,** 173–189 (1995).

180. Uhm, J. H., Dooley, N. P., Kyritsis, A. P., Rao, J. S. & Gladson, C. L. Vitronectin, a glioma-derived extracellular matrix protein, protects tumor cells from apoptotic death. *Clin. Cancer Res.* **5,** 1587–1594 (1999).

181. Rizzardi, A. E. *et al.* Quantitative comparison of immunohistochemical staining

measured by digital image analysis versus pathologist visual scoring. *Diagn. Pathol.* **7,** (2012).

182. Unlu, G., Levic, D. S., Melville, D. B. & Knapik, E. W. Trafficking mechanisms of extracellular matrix macromolecules: Insights from vertebrate development and human diseases. *Int. J. Biochem. Cell Biol.* **47,** 57–67 (2014).

183. Yang, C. *et al.* The high and low molecular weight forms of hyaluronan have distinct effects on CD44 clustering. *J. Biol. Chem.* **287,** 43094–43107 (2012).

184. Stern, R., Asari, A. A. & Sugahara, K. N. Hyaluronan fragments: an information-rich system. *Eur. J. Cell Biol.* **85,** 699–715 (2006).

185. Lokeshwar, V. B. & Selzer, M. G. Differences in hyaluronic acid-mediated functions and signaling in arterial, microvessel, and vein-derived human endothelial cells. *J. Biol. Chem.* **275,** 27641–27649 (2000).

186. Riddles, P. W., Blakeley, R. L. & Zerner, B. Ellman's reagent: 5, 5′-dithiobis (2-nitrobenzoic acid)—a reexamination. *Anal. Biochem.* **94,** 75–81 (1979).

187. Leach, J. B. & Schmidt, C. E. Characterization of protein release from photocrosslinkable hyaluronic acid-polyethylene glycol hydrogel tissue engineering scaffolds. *Biomaterials* **26,** 125–135 (2005).

188. Laks, D. R. *et al.* Large-scale assessment of the gliomasphere model system. *Neuro. Oncol.* **18,** 1367–1378 (2016).

189. Mai, W. X. *et al.* Cytoplasmic p53 couples oncogene-driven glucose metabolism to apoptosis and is a therapeutic target in glioblastoma. *Nat. Med.* 1342–1351

(2017). doi:10.1038/nm.4418

190. Langmead, B. & Salzberg, S. L. Fast gapped-read alignment with Bowtie 2. *Nat. Methods* **9,** 357–359 (2012).

191. Li, B. & Dewey, C. N. RSEM: accurate transcript quantification from RNA-Seq data with or without a reference genome. *BMC Bioinformatics* **12,** 323 (2011).

192. Miroshnikova, Y. A. *et al.* Tissue mechanics promote IDH1-dependent HIF1α-tenascin C feedback to regulate glioblastoma aggression. *Nat. Cell Biol.* **18,** 1336–1345 (2016).

193. Georges, P. C., Miller, W. J., Meaney, D. F., Sawyer, E. S. & Janmey, P. A. Matrices with compliance comparable to that of brain tissue select neuronal over glial growth in mixed cortical cultures. *Biophys. J.* **90,** 3012–3018 (2006).

194. Pedron, S. & Harley, B. A. C. Impact of the biophysical features of a 3D gelatin microenvironment on glioblastoma malignancy. *J. Biomed. Mater. Res. Part A* **101,** 3404–3415 (2013).

195. Chen, J. E., Pedron, S. & Harley, B. A. C. The Combined Influence of Hydrogel Stiffness and Matrix-Bound Hyaluronic Acid Content on Glioblastoma Invasion. *Macromol. Biosci.* **17,** (2017).

196. Mao, P. *et al.* Mesenchymal glioma stem cells are maintained by activated glycolytic metabolism involving aldehyde dehydrogenase 1A3. *Proc. Natl. Acad. Sci.* **110,** 8644–8649 (2013).

197. E Taylor, T., B Furnari, F. & K Cavenee, W. Targeting EGFR for treatment of

glioblastoma: molecular basis to overcome resistance. *Curr. Cancer Drug Targets* **12,** 197–209 (2012).

198. Xiao, W. *et al.* Brain-Mimetic 3D Culture Platforms Allow Investigation of Cooperative Effects of Extracellular Matrix Features on Therapeutic Resistance in Glioblastoma. *Cancer Res.* **78,** 1358–1370 (2018).

199. Telmer, P. G., Tolg, C., McCarthy, J. B. & Turley, E. A. How does a protein with dual mitotic spindle and extracellular matrix receptor functions affect tumor susceptibility and progression? *Commun. Integr. Biol.* **4,** 182–185 (2011).

200. Chopra, A. *et al.* Augmentation of integrin-mediated mechanotransduction by hyaluronic acid. *Biomaterials* **35,** 71–82 (2014).

201. Fraley, S. I., Feng, Y., Giri, A., Longmore, G. D. & Wirtz, D. Dimensional and temporal controls of three-dimensional cell migration by zyxin and binding partners. *Nat. Commun.* **3,** 719 (2012).

202. Reardon, D. A. *et al.* Cilengitide: an RGD pentapeptide αvβ3 and αvβ5 integrin inhibitor in development for glioblastoma and other malignancies. *Futur. Oncol.* **7,** 339–354 (2011).

203. Brandes, A. A., Franceschi, E., Tosoni, A., Hegi, M. E. & Stupp, R. Epidermal growth factor receptor inhibitors in neuro-oncology: hopes and disappointments. *Clin. Cancer Res.* **14,** 957–960 (2008).

204. Shinojima, N. *et al.* Prognostic value of epidermal growth factor receptor in patients with glioblastoma multiforme. *Cancer Res.* **63,** 6962–6970 (2003).

205. Stupp, R. *et al.* Radiotherapy plus Concomitant and Adjuvant Temozolomide for Glioblastoma. *New Engl. J. Med.* **352,** 987–996 (2005).

206. Chowdhary, S. A., Ryken, T. & Newton, H. B. Survival outcomes and safety of carmustine wafers in the treatment of high-grade gliomas: a meta-analysis. *J. Neurooncol.* **122,** 367–382 (2015).

207. Stupp, R. *et al.* Radiotherapy plus Concomitant\nand Adjuvant Temozolomide for Glioblastoma. *N. Engl. J. Med.* (2005). doi:10.1056/NEJMoa043330

208. Chakravarti, A. *et al.* Temozolomide-mediated radiation enhancement in glioblastoma: A report on underlying mechanisms. *Clin. Cancer Res.* **12,** 4738–4746 (2006).

209. Roos, W. P. *et al.* Apoptosis in malignant glioma cells triggered by the temozolomide-induced DNA lesion O6-methylguanine. *Oncogene* **26,** 186 (2007).

210. Hegi, M. E. *et al.* MGMT Gene Silencing and Benefit from Temozolomide in Glioblastoma. *N. Engl. J. Med.* **352,** 997–1003 (2005).

211. Perazzoli, G. *et al.* Temozolomide resistance in glioblastoma cell lines: Implication of MGMT, MMR, P-glycoprotein and CD133 expression. *PLoS One* **10,** (2015).

212. Gutenberg, A. *et al.* MGMT promoter methylation status and prognosis of patients with primary or recurrent glioblastoma treated with carmustine wafers. *Br. J. Neurosurg.* **27,** 772–778 (2013).

213. Gaspar, N. *et al.* MGMT-independent temozolomide resistance in pediatric glioblastoma cells associated with a PI3-kinase-mediated HOX/stem cell gene

signature. *Cancer Res.* **70,** 9243–9252 (2010).

214. Playford, M. P. & Schaller, M. D. The interplay between Src and integrins in normal and tumor biology. *Oncogene* **23,** 7928 (2004).

215. Mitra, S. K. & Schlaepfer, D. D. Integrin-regulated FAK-Src signaling in normal and cancer cells. *Curr. Opin. Cell Biol.* **18,** 516–523 (2006).

216. Bourguignon, L. Y. W., Zhu, H., Shao, L. & Chen, Y.-W. CD44 interaction with c-Src kinase promotes cortactin-mediated cytoskeleton function and hyaluronic acid-dependent ovarian tumor cell migration. *J. Biol. Chem.* **276,** 7327–7336 (2001).

217. Guo, Q. *et al.* Influence of c-Src on hypoxic resistance to paclitaxel in human ovarian cancer cells and reversal of FV-429. *Cell Death Dis.* **8,** e3178 (2018).

218. Shor, A. C. *et al.* Dasatinib inhibits migration and invasion in diverse human sarcoma cell lines and induces apoptosis in bone sarcoma cells dependent on Src kinase for survival. *Cancer Res.* **67,** 2800–2808 (2007).

219. Du, J. *et al.* Bead-based profiling of tyrosine kinase phosphorylation identifies SRC as a potential target for glioblastoma therapy. *Nat. Biotechnol.* **27,** 77 (2009).

220. Katsumi, A., Orr, A. W., Tzima, E. & Schwartz, M. A. Integrins in Mechanotransduction. *J. Biol. Chem.* **279,** 12001–12004 (2004).

221. Kim, Y. & Kumar, S. CD44-Mediated Adhesion to Hyaluronic Acid Contributes to Mechanosensing and Invasive Motility. *Mol. Cancer Res.* **12,** 1416–1429 (2014).

222. Lee, S. Y. Temozolomide resistance in glioblastoma multiforme. *Genes Dis.* **3,**

198–210 (2016).

223. Xiao, W., Ehsanipour, A., Sohrabi, A. & Seidlits, S. K. Hyaluronic-Acid Based Hydrogels for 3-Dimensional Culture of Patient-Derived Glioblastoma Cells. *J. Vis. Exp.* e58176 (2018). doi:10.3791/58176

224. Huveldt, D. *et al.* Targeting Src Family Kinases Inhibits Bevacizumab-Induced Glioma Cell Invasion. *PLoS One* (2013). doi:10.1371/journal.pone.0056505

225. Ahluwalia, M. S., Groot, J. de, Liu, W. M. & Gladson, C. L. Targeting SRC in glioblastoma tumors and brain metastases: Rationale and preclinical studies. *Cancer Lett.* **298,** 139–149 (2010).

226. Fujisaki, T. *et al.* CD44 stimulation induces integrin-mediated adhesion of colon cancer cell lines to endothelial cells by up-regulation of integrins and c-Met and activation of integrins. *Cancer Res.* **59,** 4427–4434 (1999).

227. Lu, K. V. *et al.* Fyn and Src Are Effectors of Oncogenic Epidermal Growth Factor Receptor Signaling in Glioblastoma Patients. *Cancer Res.* **69,** 6889–6898 (2009).

228. Karni, R., Jove, R. & Levitzki, A. Inhibition of pp60(c-Src) reduces Bcl-X(L) expression and reverses the transformed phenotype of cells overexpressing EGF and HER-2 receptors. *Oncogene* **18,** 4654 (1999).

229. Bhattacharya, S., Ray, R. M. & Johnson, L. R. Integrin beta3-mediated Src activation regulates apoptosis in IEC-6 cells via Akt and STAT3. *Biochem. J.* **397,** 437–447 (2006).

230. Adams, J. M. & Cory, S. The Bcl-2 apoptotic switch in cancer development and

therapy. *Oncogene* **26,** 1324 (2007).

231. Morin, P. J. Drug resistance and the microenvironment: Nature and nurture. *Drug Resist. Updat.* **6,** 169–172 (2003).

232. Sethi, T. *et al.* Extracellular matrix proteins protect small cell lung cancer cells against apoptosis: a mechanism for small cell lung cancer growth and drug resistance in vivo. *Nat. Med.* **5,** 662 (1999).

233. Edmondson, R., Broglie, J. J., Adcock, A. F. & Yang, L. Three-Dimensional Cell Culture Systems and Their Applications in Drug Discovery and Cell-Based Biosensors. *Assay Drug Dev. Technol.* **12,** 207–218 (2014).

234. Ravi, M., Paramesh, V., Kaviya, S. R., Anuradha, E. & Paul Solomon, F. D. 3D cell culture systems: Advantages and applications. *J. Cell. Physiol.* **230,** 16–26 (2015).

235. Wang, K. *et al.* Culture on 3D Chitosan-Hyaluronic Acid Scaffolds Enhances Stem Cell Marker Expression and Drug Resistance in Human Glioblastoma Cancer Stem Cells. *Adv. Healthc. Mater.* **5,** 3173–3181 (2016).

236. Mammoto, T. *et al.* Role of Collagen Matrix in Tumor Angiogenesis and Glioblastoma Multiforme Progression. *Am. J. Pathol.* **183,** 1293–1305 (2013).

237. Serres, E. *et al.* Fibronectin expression in glioblastomas promotes cell cohesion, collective invasion of basement membrane in vitro and orthotopic tumor growth in mice. *Br. Dent. J.* (2014). doi:10.1038/onc.2013.305

238. Lam, C. R. I. *et al.* A 3D biomimetic model of tissue stiffness interface for cancer

drug testing. *Mol. Pharm.* (2014). doi:10.1021/mp500059q

239. Ponta, H., Sherman, L. & Herrlich, P. A. CD44: From adhesion molecules to signalling regulators. *Nat. Rev. Mol. Cell Biol.* **4,** 33 (2003).

240. Lee, J.-L., Wang, M.-J., Sudhir, P.-R. & Chen, J.-Y. CD44 engagement promotes matrix-derived survival through the CD44-SRC-integrin axis in lipid rafts. *Mol. Cell. Biol.* **28,** 5710–5723 (2008).

241. Formisano, L. *et al.* Epidermal growth factor-receptor activation modulates Src-dependent resistance to lapatinib in breast cancer models. *Breast Cancer Res.* **16,** R45 (2014).

242. Stupp, R. *et al.* Cilengitide combined with standard treatment for patients with newly diagnosed glioblastoma with methylated MGMT promoter (CENTRIC EORTC 26071-22072 study): a multicentre, randomised, open-label, phase 3 trial. *Lancet Oncol.* **15,** 1100–1108 (2014).

243. Lassman, A. B. *et al.* Phase 2 trial of dasatinib in target-selected patients with recurrent glioblastoma (RTOG 0627). *Neuro. Oncol.* **17,** 992–998 (2015).

244. Agarwal, S. *et al.* Active efflux of Dasatinib from the brain limits efficacy against murine glioblastoma: broad implications for the clinical use of molecularly targeted agents. *Mol. Cancer Ther.* **11,** 2183–92 (2012).